Universidade de Brasília
Instituto de Geociências

GEOLOGIA DO DEPÓSITO AURÍFERO DO CAIAMAR, *GREENSTONE BELT* DE GUARINOS: UM RARO DEPÓSITO ASSOCIADO À EPISIENITO SÓDICO

VINICIUS GOMES RODRIGUES

Dissertação de mestrado em Geologia nº **279**

Orientador

Prof. Dr. Hardy Jost

Banca Examinadora

Hardy Jost

Nilson Francisquini Botelho

José Affonso Brod

Valmir da Silva Souza (suplente)

BRASÍLIA

2011

SUMÁRIO

Lista de Figuras

PARTE 1

PARTE II

Lista de Tabelas e Anexos

PARTE 1

PARTE 2

ANEXOS

RESUMO

O depósito aurífero do Caimar se situa no Brasil Central e está hospeado por um episienito sódico derivado da alteração hidrotermal de uma intrusão de gabro Neoproterozóica em rochas supracrustais Paleoprotezóicas de baixo grau metamórfico do greenstone belt de Guarinos. A alteração hidrotermal do gabro resultou na formação de zonas externa, intermediária, interna e de episienito, cada qual caracterizado por paragêneses minerais próprias. A mineralização aurífera ocorre como *stockwork* bem como disseminação no episienito e na zona interna e está associada com arsenopirita. A principal associação mineral do episienito consiste de albita, quartzo e rara biotita, ilmenita, magnetita e arsenopirita disseminada. Do gabro ao episienito houve progressivo ganho de Na_2O. Em detalhe, do gabro à zona externa, a alteração resultou em ganho de Na_2O, SiO_2, MnO, K_2O, P_2O_5, Sr e Zr, perda de MgO, CaO, Fe_2O_3, TiO_2, Ba, Co, V e Ni, com Rb, Y e ETR imóveis. Da zona externa para a intermediária, a alteração resultou em ganho de K_2O, Na_2O, SiO_2, P_2O_5, Ba, Rb, Y, Zr e ETRL, com Al_2O_3 e ETRP imóveis. A maxima alteração potássica ocorreu na zona intermediária, como indicado pelo contínuo aumento nas proporções de biotita. Da zona intermediária para a interna houve ganho de CaO, Fe_2O_2 e MgO devido à formação de ankerita, e parte do Fe_2O_3 representado pela arsenopirita disseminada, bem como de TiO_2, P_2O_5, V e Sr, e perda de K_2O, MnO, Zr e Rb, com SiO_2, Al_2O_3, Y, Ni, ETRL permanecendo imóveis. Da zona interna ao episienito ganho máximo ocorreu com Na_2O, seguido de Al_2O_3, Zr, Y e ETRL e significativa perda de MgO, CaO, K_2O, Fe_2O_3, TiO_2, MnO, Ba, Sr, Rb, Co e V, com SiO_2, Ni e ETRP permanecendo imóveis. A alteração hidrotermal crescente resultou em progressivo aumento nas proporções ETR em direção ao episienito, com enriquecimento em ETRL comparativamente aos ETRP. Evidências geológicas, geoquímicas, mineralógicas e petrográficas sugerem que a origem do episienito esteja relacionada à ação de processos metassomáticos por circulação de fluidos tardios através da seqüência vulcanossedimentar do *greenstone belt* e provavelmente derivaram de uma intrusão em profundidade como sugerem dados geofísicos. A mineralização aurífera ocorreu em pelo menos duas fases, uma precoce representada pela associação ouro-arsenopirita que ocorre disseminada na zona interna e no episienito e outra tardia formada durante a abertura de fraturas que alojaram o *stockwork*. A estatística de amostras da zona de minério indica que sua assinatura geoquímica é dada pela associação Au-S-Se-Sb-Ag-Te-As, em ordem decrescente de correlação. A investigação de isótopos de enxofre de várias amostras de sulfetos mostram que a arsenopirita disseminada no episienito tem $\delta^{34}S$ entre 2,67‰ e -3,25‰, sugestivo de fonte magmática durante formação do episienito, enquanto nas demais amostras $\delta^{34}S$ variou de -5,20‰ a -8,82‰, indicativo de fonte local, como os filitos carbonosos. Dados geocronológicos U-Pb em zircão indicam que a idade do episienito é de 729 ± 15 Ma.

Palavras-chave: Ouro, episienito sódico, Caiamar, Guarinos, greenstone belt, Goiás

ABSTRACT

The Caiamar gold deposit is located in Central Brazil and hosted by a sodic episyenite derived by hydrothermal alteration of a Neoproterozoic gabbro that intruded low-grade metamorphic supracrustal rocks of the Paleoproterozoic Guarinos greenstone belt. Hydrothermal alteration of the gabbro leads to the formation of outer, intermediate, inner and an episyenite zoned, each characterized by particular mineral paragenesis. Gold mineralization occurs as a stockwork as well as dissemination in the episyenite and in the inner alteration zone, and is always associated with arsenopyrite. The main mineralogical association of the episyenite consists of albite, quartz and rare biotite, ilmenite, magnetite and disseminated arsenopyrite. From the gabbro to the episyenite a progressive gain in Na_2O took place. In detail, from the gabbro to the outer zone, alteration resulted in gain of Na_2O, SiO_2, MnO, K_2O, P_2O_5, Sr and Zr, with losses of MgO, CaO, Fe_2O_3, TiO_2, Ba, Co, V and Ni, with, Rb, Y and HREE remaining immobile. From the outer to the intermediary zone, alteration resulted in gain of K_2O, Na_2O, SiO_2, P_2O_5, Ba, Rb, Y, Zr and LREE, with Al_2O_3 and HREE remaining immobile. Maximum potassium alteration occurs at the intermediary zone indicated by continuous increase in the amount of biotite. From the intermediary to the inner zone, alteration resulted in gain of CaO, Fe_2O_2 and MgO, due to due to the deposition of ankerite, and part of Fe_2O_3 represented by disseminated arsenopyrite, as well a of TiO_2, P_2O_5, V and Sr, and loss of K_2O, MnO, Zr and Rb, with SiO_2, Al_2O_3, Y, Ni, LREE and HREE remaining immobile. From the inner zone to the episyenite maximum gains occurred with Na_2O, followed by Al_2O_3, Zr, Y and LREE, with massive loss of MgO, CaO, K_2O, Fe_2O_3, TiO_2, MnO, Ba, Sr, Rb, Co and V, with SiO_2, Ni and HREE remaining immobile. Increasing hydrothermal alteration resulted in progressive enrichment in REE towards the episyenite, without significant changes in their signature, except for more pronounced enrichment in LREE, as compared to HREE. Geological, geochemical, mineralogical and petrographic evidence suggest that the origin of the sodic episyenite can be related to the action of metassomatic processes by circulation of later fluids through the volcanosedimentary sequence of the greenstone belt and probably derived from a hidden intrusion as indicated by geophysical dada. Gold mineralization took place in at least two phases, an early phase is represented by the gold-arsenopyrite association that occurs in the inner alteration zone and within the episyenite as disseminations, and a later formed during an open system responsible for the mineralized stockwork. The statistics of chip-samples of the ore zone indicates that its geochemical signature is given by the association Au-S-Se-Sb-Ag-Te-As, in decreasing order of correlation. Investigation of the sulfur isotopes from several samples show that arsenopyrite disseminated in the episyenite have $\delta^{34}S$ between 2,67‰ and -3,25‰, suggesting that sulfur was provided by an igneous source during the formation of the episyenite, whilst the $\delta^{34}S$ of the other samples varies from -5,20‰ to -8,82‰, indicating a local sulfur source, such as the carbonaceous phyllites. Geochronological U-Pb zircon data indicate that the age of the episyenite is 729 ± 15 Ma.

Key-words: Gold, sodic episyenite, Caiamar, Guarinos, greenstone belt, Goiás

AGRADECIMENTOS

Meus agradecimentos a todos quantos contribuíram para esta dissertação de mestrado:

Ao Instituto de Geociências da Universidade de Brasília (IG/UnB);

Aos Professores Doutores Farid Chemale Jr. e Bernard Buhm, do Laboratório de Geocronologia do Instituto de Geociências da Universidade de Brasília, pela geração de dados geocronológicos e de isótopos de enxofre;

À Prof.ª Drª Juliana Charão Marques, do Laboratório de Geocronologia do Instituto de Geociências da Universidade Federal do Rio Grande do Sul;

À Área de Balística Forense do Instituto Nacional de Criminalística do Departamento de Polícia Federal, em Brasília, pelas análises de cristais de granada por EDS em Microscópio Eletrônico de Varredura (MEV).

Ao Conselho Nacional de Desenvolvimento Científico e Tecnológico – CNPq, pelo auxilio financeiro para as etapas de campo e análises químicas de rocha parciais mediante a Taxa de Bancada do Prof. Dr. Hardy Jost, orientador (Proc. #304764/2007-6);

A Yamana Gold Inc. pela oportunidade de cursar e concluir o Mestrado, bem como pelo total acesso aos dados de campo, sondagens, análises químicas de rocha e pela oportunidade de coordenar o projeto Caiamar durante o ano de 2009 e 2010;

Aos grandes e valiosíssimos amigos que fiz durante as jornadas de campo nestes quatro anos trabalhando na Yamana. Marcelo, Thiago e Gustavo, vocês serão meus amigos do peito pelo resto da minha vida. Obrigado pelas noites intermináveis regadas a bons rótulos e as discussões geológicas de alto nível, onde aprendi e continuo aprendendo com vocês o desafio de fazer uma exploração moderna e agressiva objetivando levar para os rincões deste país, de tamanho continental, um pouco de trabalho e esperança para os mais simples. A humildade e simplicidade abriram e abrem todas as portas que precisamos. Mais uma vez, obrigado por esta lição de vida;

Aos amigos de longa data, Leandro, Gustavo Alves, Marcelo Rocha, Diego, Ram e Maytê. Vocês nunca me faltaram e, dentro de suas possibilidades, ouviram minhas preocupações, amarguras, tristeza, além, é claro, de dividir inúmeros momentos de felicidade. Hoje não são mais amigos do peito, mas sim verdadeiros irmãos de coração;

Ao Amigo e orientador Professor Doutor Hardy Jost pelas sugestões, apoio, hospitalidade e pelas inúmeras conversas geológicas nos deliciosos *happy hours*, onde eu apenas ouvia e tentava absorver pelo menos uma pequena parte do seu vasto conhecimento. Mestre, a tua humildade e paciência são de extrema raridade e, acredito, dentre todo o aprendizado, estes conceitos foram a maior lição que aprendi contigo. À tua esposa Mary, por ter nos aturado nas intermináveis horas de discussão geológica e providenciado o meu suporte durante as estadias na sua residência.

Aos meus irmãos Rose, André, Ju e Pila pelo simples fato de serem meus irmãos de sangue e por não me esquecerem nunca. Também dentro das vossas possibilidades, ouviram e foram pacientes durante as minhas ausências. Ao tio Gatto, pela eterna amizade e carinho e as minhas sobrinhas Isa, Lari e Mari, por serem tão amorosas;

Agradeço aos meus pais, Alvanir, Zueli e Zenil pelo amor, apoio incondicional durante todos os momentos de minha vida e por sempre acreditarem em mim. Todo o empenho foi e sempre será pensando em vocês e só por vocês;

A Deus, que trilha meu caminho e me faz cruzar com estas adoráveis pessoas acima mencionadas;

E por fim, à mãe natureza por me ensinar a cada dia muito mais sobre a deliciosa viagem que é essa Ciência chamada Geologia.

Dedicatória

Ao meu irmão Eduardo Gatto (in memoriam), por continuar a me inspirar com seus ensinamentos o amor pela vida e por nossa família. Esse é mais um passo pra ti, meu irmão!

PARTE 1

INTRODUÇÃO

Terrenos do tipo *greenstone belt* do Neoarqueano e Paleoproterozóico contêm importantes depósitos de Ouro de dimensões e volume variados, responsáveis por grande parte das 23.000 a 25.000 t da produção histórica mundial do metal, excluído os depósitos Sul-Africanos de Witwatersrand (Groves *et al*. 2005). Ambientes semelhantes ocorrem no Centro-Oeste do Brasil, reunidos no Bloco Arqueano-Paleoproterozóico de Goiás, e desde a sugestão de Danni & Ribeiro (1978) de que a região consistiria de típica associação granito-*greenstone belt*, o interesse econômico e científico pela mesma cresceu exponencialmente. A produção de Ouro na região iniciou com os Bandeirantes no século XVIII e prosseguiu por atividade garimpeira até meados de 1970 quando a exploração mineral por empresas resultou na descoberta de importantes depósitos nos *greenstone belts* da região. Dentre estes, o de Crixás hospeda a sexta maior reserva de Ouro do Brasil (~80 t Au, média 5 g/t) e onde se localiza o maior distrito do tipo *gold-only* do Brasil Central, explorado desde o início da década de 1980 pela Mineração Serra Grande S.A., hoje *joint venture* da AngloGold Ashanti Brasil Mineração S.A. e Kinross Brasil Ltda. Exploração mineral realizada pela Yamana Gold Inc. resultou na descoberta e viabilização do depósito Jordino (37,25 t Au, média 5,14 g/t) localizado no *greenstone belt* de Pilar de Goiás, cujas instalações da mina estão previstas para iniciar em 2011. O potencial do *greenstone belt* de Guarinos, no entanto, é o menos conhecido e hospeda, até o momento, apenas dois depósitos de pequeno porte, um no extremo sul (Maria Lázara), no passado objeto de atividade garimpeira, e outro no extremo norte (Caiamar), cuja exploração iniciou na época dos Bandeirantes e, a partir da década de 1990, foi objeto de extração parcial pela Mineração Serra Formosa S.A. e é, hoje, propriedade da Yamana Gold Inc.

GEOLOGIA REGIONAL E LOCAL

O *greenstone belt* de Guarinos é parte do Bloco Arqueano-Paleoproterozóico de Goiás (Pimentel *et al*. 2000), o qual foi amalgamado à porção sudoeste da Faixa Brasília, Província Tocantins, durante o Neoproterozóico. Possui cerca de 16.000 km^2 e está tectonicamente envolto por rochas de origem e idade variadas (Fig. 1). Ao norte limita-se com o Arco Magmático de Mara Rosa, de idade entre 850 e 560 Ma (Pimentel *et al.*1997). No noroeste está truncado pelo Lineamento Transbrasiliano, o qual consiste da mega-estrutura colisional N30^{o}E do limite nordeste da Faixa Brasília com a Faixa Araguaia e que, na região do bloco arqueano, está parcialmente coberta por sedimentos modernos da planície aluvial do Rio Araguaia. No sudoeste está em contato com uma cunha aberta para norte e composta de ortognaisses do bloco Fazenda Nova, de idade Sm-Nd 2,61 a 2,25 Ga (Mota-Araújo & Pimentel 2002), limitados a leste por um dos ramos do lineamento transcorrente sinistral Moiporá-Novo Brasil, e que separa o bloco arqueano do Arco Magmático de Arenópolis, de idade 940 a 630 Ma (Pimentel *et al.* 2000). No sul se limita com quartzitos, metaconglomerados e xistos da Seqüência Serra Dourada, sotopostos, a sul, a rochas metavulcano-sedimentares de idade Rb-Sr em rocha total de 1977 ± 55 Ma, e idade Sm-Nd (T_{DM}) de *ca*. 2,2 Ga (Pimentel *et al.* 1996). No sudeste está sotoposto a rochas metassedimentares do Grupo Araxá, cuja população de zircão detrítico dominante data de 666 a 682 Ma, com idade mínima de 638 ± 11 Ma dada pela

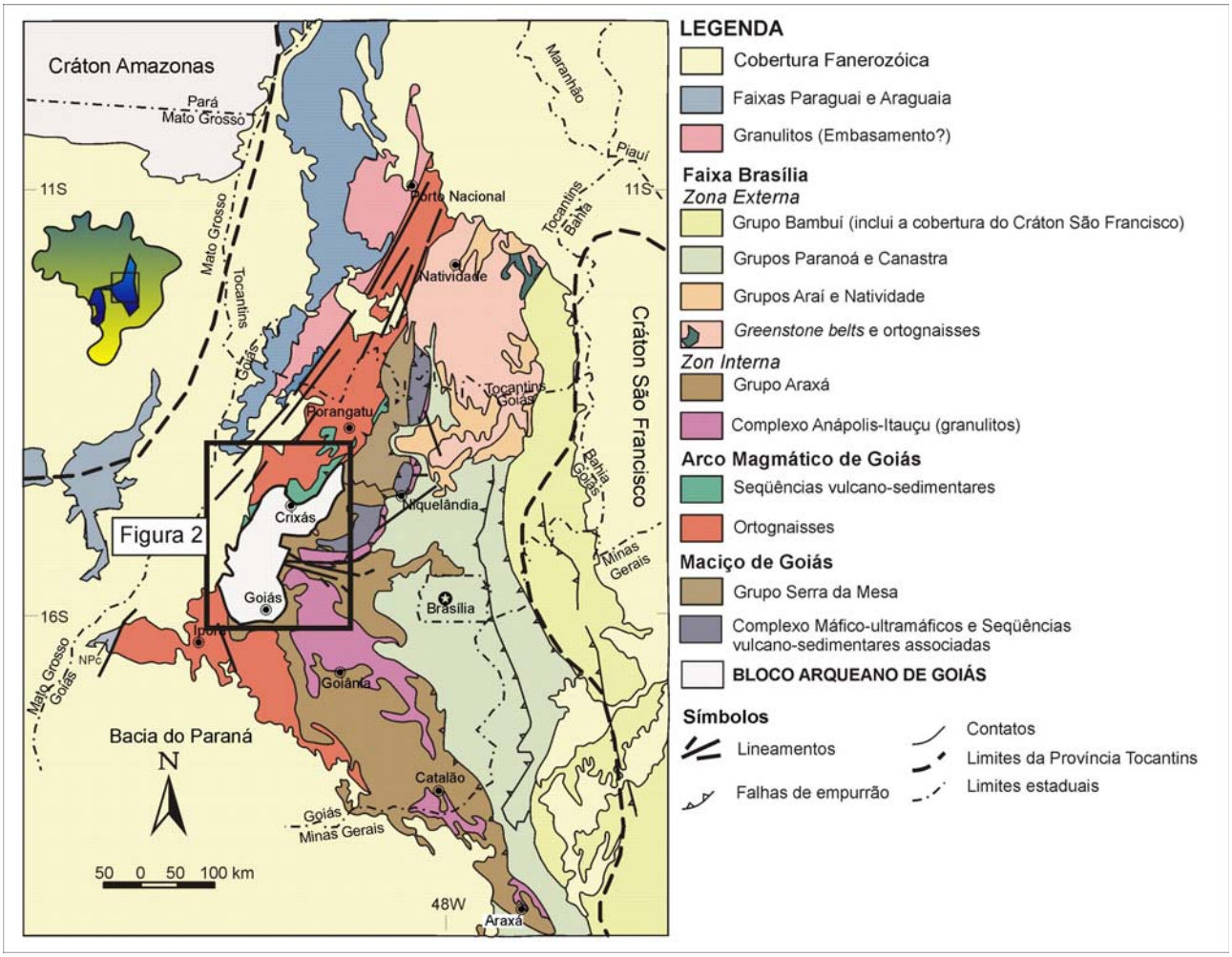

Figura 1 – Mapa geológico da Faixa Brasília e enquadramento do Bloco Arqueano-Paleoproterozóico na mesma. Modificado de Pimentel et al. (2000).

de cristalização de um tonalito intrusivo (Piuzana *et al*. 2003). Ao leste e nordeste ocorrem rochas metassedimentares do Grupo Serra da Mesa de idade-modelo Sm-Nd T_{DM} de 1,9 a 2,3 Ga (Pimentel *et al.* 2001).

Os principais componentes do bloco arqueano-paleoproterozóico compreendem seis complexos de ortognaisses que separam cinco *greenstone belts* (Fig. 2). Os complexos de ortognaisses da metade norte do bloco compreendem, de leste para oeste, os da Anta, Caiamar, Moquém e Hidrolina e, na metade sul, de norte para sul, Caiçara e Uvá (Fig. 2). Estes diferem no arranjo estrutural, conteúdo litológico, proporções de protólitos de características composicionais e cronológicas distintas que permitem reuni-los em dois grupos. O dominante consiste de protólitos batolíticos juvenis de tonalito, granodiorito e granito com zircão de idade U-Pb SHRIMP e TIMS entre 2,95 Ga e 2,80 Ga (Pimentel *et al*. 2003, Jost *et al.* 2005, Queiroz *et al*. 2008) e zircão herdado e idade-modelo Sm-Nd (T_{DM}) em rocha total entre 3,00 a 3,2 Ga (Queiroz 2000, Pimentel *et al.* 1996, 2003, Potrel *et al.* 1998, Jost *et al.* 2005), indicativo de influência de crosta mais antiga. Representantes deste grupo compreendem os complexos da Anta, Caiamar, Hidrolina, parte do complexo Uvá e provavelmente o complexo Caiçara. O grupo subordinado consiste de intrusões tabulares de granodiorito, monzogranito e granito de filiação crustal e idade U-Pb SHRIMP e TIMS em zircão entre 2,70 e 2,76 Ga (Jost *et al.* 2005, Queiroz *et al*. 2008) ao qual

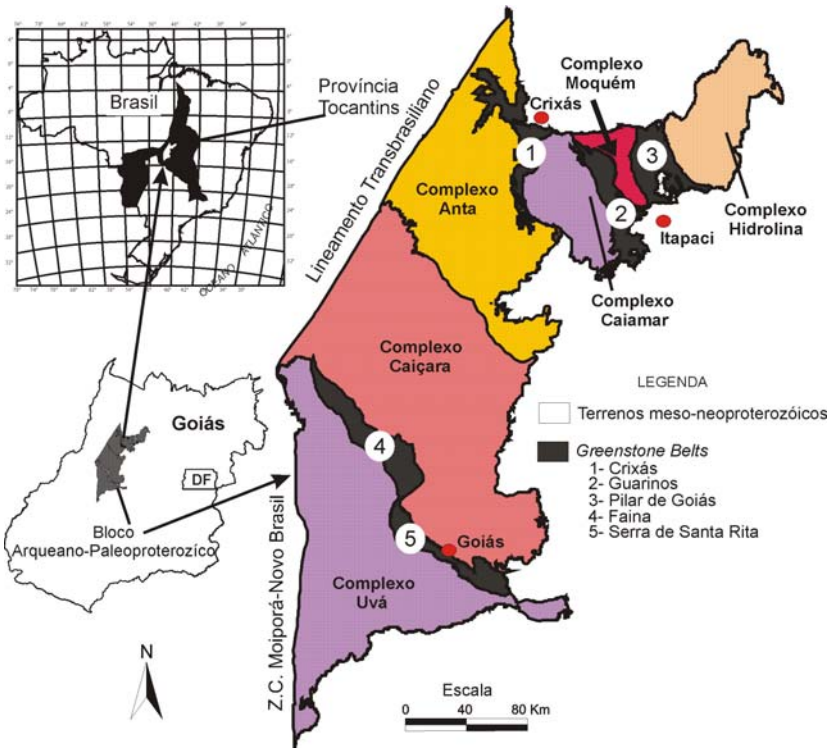

Figura 2 – Subdivisão do Bloco Arqueano-Paleoproterozóico de Goiás. Modificado de Pimentel et al. (.2002).

pertence parte dos complexos Moquém e Uva. A geometria tabular dos corpos mais jovens sugere que as intrusões ocorreram por empilhamento tectônico durante as fases finais da orogênese arqueana em cerca de 2,7 Ga, provável idade da cratonização arqueana do bloco.

Dentre os *greenstone belt*s três situam-se na metade norte, estão orientados segundo NS, possuem em média cerca de 40 km de comprimento e 6 km de largura e são designados, de oeste para leste, de Crixás, Guarinos e Pilar de Goiás. Dois situam-se na metade sul, estão justapostos por falha direcional N30ºE, estão orientados segundo N60ºW, em conjunto totalizam cerca de 150 km de comprimento, com cerca de 6 km de largura média e são designados, de noroeste para sudeste, de Faina e Serra de Santa Rita. O contato dos *greenstone belts* com os gnaisses adjacentes são tectônicos o que, somado à existência de *klippen* nos gnaisses indica que são alóctones.

Os registros estratigráficos dos *greenstone belts* são semelhantes e compreendem seções inferiores de metakomatiitos seguidos de metabasaltos toleiíticos com proporções variadas de formações ferríferas e manganesíferas, e seções superiores de rochas metassedimentares com características peculiares a cada faixa (Jost & Oliveira 1991, Resende *et al.* 1999). Apenas os komatiitos de Crixás foram datados e geraram idades isocrônicas Sm-Nd de 2.825 ± 98 Ma e Pb/Pb em rocha total de 2.728 ± 140 Ma (Arndt *et al.* 1989) e Sm-Nd em rocha total de 3,00 ± 0.07 Ga (Fortes *et al.* 2003). A ausência de dados geocronológicos das rochas vulcânicas dos demais *greenstone belts* restringe a correlação destas com as de Crixás. Por outro lado, dados geocronológicos Sm-Nd da seção metassedimentar de Crixás obtidos por Fortes *et al.* (2003) indicaram área-fonte situada entre 2,5 Ga e 2,3 Ga, por provável mistura de detritos de fonte paleoproterozóica e arqueana. A datação U-Pb SHRIMP em zircão detrítico de metagrauvaca de Crixás por Tassinari *et al*. (2006) registrou que os cristais de

zircão mais jovens possuem idade de 2.212 ± 36 Ma e a datação U-Pb LA-ICP-MS de zircão de amostras de metagrauvaca por Jost *et al*. (2008) gerou o intervalo de 3.354 ± 40 Ma a 2.209 ± 28 Ma. Em zircão de formação ferrífera da base do pacote sedimentar de Guarinos, Jost *et al*. (2008) obtiveram uma população com idade concordante LA-ICP-MS de 2.627 ± 19 Ma e outra com intercepto superior de 2.232 ± 39 Ma e, em rochas calcissilicáticas de Pilar de Goiás, a idade-modelo Sm-Nd de ~2,2 Ga. Nos *greenstone belts* de Serra de Santa Rita e Faina, Resende *et al*. (1999) obtiveram idades-modelo Sm-Nd das seções metassedimentares entre 3,0 Ga e 2,7 Ga, sugestivo de área-fonte mais homogeneamente arqueana, em contraste com as idades-modelo de Crixás. Estes dados indicam que, a par das seções vulcânicas de Crixás, Faina e Serra de Santa Rita poderem ser arqueanas, as sedimentares são, talvez em grande parte, paleoproterozóicas.

Dados geocronológicos adicionais revelam que, após a cratonização, o bloco foi palco de eventos do Paleoproterozóico registrados por:

(i) enxame de diques máficos nos complexos Caiçara e da Anta e que correspondem a uma fase de distensão crustal em torno de 2.5 a 2.3 Ga (Tomazzoli 1997, Costa 2003);

(ii) enxame de diques máficos e intrusão diorítica de idade U-Pb SHRIMP em zircão de 2.146 ± 1.6 Ma (Jost *et al.* 1993) alojados em lineamento transcorrente que corta a porção sul do Complexo Hidrolina (Danni *et al.* 1986);

(iii) *sills* e *stocks* de albita-granito intrusivos nos pacotes sedimentares dos *greenstone belts* de norte e hospedados em falhas de empurrão de vergência norte (Jost *et al.* 1992), de idade U-Pb SHRIMP em zircão de 2.145 ± 12 Ma (Queiroz 2000);

(iv) mineralização aurífera hospedada por zonas de cisalhamento de baixo ângulo em Pilar de Goiás e que também controlaram intrusões graníticas com zircão de idade U-Pb SHRIMP de 2.145 ± 12 Ma (Queiroz 2000), e zircão de zona de alteração hidrotermal da Mina III, Crixás, de idade U-Pb SHRIMP com intercepto superior de 2.165 ± 47 Ma (Tassinari *et al.* 2006), bem como de diques máficos que cortam a mineralização de Crixás e que geraram a idade de 2,170 ± 17 Ma (Jost *et al*. 2010) e

(v) metamorfismo epidérmico em 2.011 ± 15 Ma (Queiroz 2000) detectado por U-Pb SHRIMP em titanita dos gnaisses Crixás-Açu, do Complexo Caiamar, e idade K-Ar de 2.006 ± 45 Ma no enxame de diques máficos dos complexos da Anta e Caiçara (Tomazolli 1997);

Assim, após a cratonização, o bloco arqueano acolheu o registro de um ciclo completo de abertura e fechamento de orógeno durante o Rhyaciano, mas a sua distribuição sugere que o mesmo se desenvolveu em posição marginal à faixa móvel. Entre o final do Rhyaciano e Neoproterozóico, a região permaneceu intacta e como parte de uma área estável de posição geográfica incerta.

GEOLOGIA DO *GREENSTONE BELT* DE GUARINOS

O *greenstone belt* de Guarinos situa-se no extremo norte do Bloco Arqueano-Paleoproterozóico de Goiás, está orientado segundo NS e tem geometria triangular irregular com vértice voltado para norte com cerca

de 40 km de comprimento e 6 km de largura media (Fig. 3). Seus limites são tectônicos e no norte está em contato com rochas do Arco Magmático de Mara Rosa, de idade neoproterozóica (Viana *et al*. 1995), no oeste com ortognaisses do Complexo Caiamar, no leste com o Complexo Moquém, ambos de idade arqueana (Queiroz *et al*. 2008) e no sul com rochas do Grupo Araxá, também do Neoproterozóico (Piuzana *et al*. 2003).

Com as rochas do arco magmático o contato é a Zona de Cisalhamento Mandinópolis, a qual sobrepõe as rochas metavulcânicas e ortognaisses do arco ao bloco Arqueano-Paleoproterozóico por cavalgamento com vergência para sul (Jost *et al*. 2001). A natureza tectônica do contato com as rochas dos complexos Caiamar e Moquém resulta do soerguimento dos gnaisses em meio às rochas supracrustais de Crixás e Guarinos e de Guarinos e Pilar de Goiás, respectivamente (Jost *et al.*1994a, 1994b, 1995). Já o contato do Grupo Araxá com o *greenstone belt* é uma rampa lateral resultante do transporte deste para leste (Jost *et al*. 1995).

Estratigrafia

A primeira proposta estratigráfica para o *greenstone belt* de Guarinos, extensiva aos de Crixás e Pilar de Goiás, foi apresentada por Danni & Ribeiro (1978), sob a denominação de Grupo Pilar de Goiás. O grupo foi subdividido por Sabóia (1979) nas formações Córrego Aladaginho, Rio Vermelho e Ribeirão das Antas, para reunir os metakomatiitos, metabasaltos e as rochas metassedimentares, respectivamente. Ao revisar os conteúdos litológicos das três faixas, Jost & Oliveira (1991) propuseram considerá-las como entidades independentes e, assim, propuseram os grupos Crixás, Guarinos e Pilar de Goiás, cada qual com unidades estratigráficas formais.

O Grupo Guarinos foi subdividido, da base para o topo, nas formações Serra do Cotovelo e Serra Azul, para reunir, respectivamente, metakomatiitos e metabasaltos, e as formações São Patricinho, Aimbé e Cabaçal para designar as associações litológicas específicas de rochas metassedimentares. Posteriormente, Jost *et al.* (1995) subdividiram a Formação Cabaçal em um Membro Inferior e outro Superior, cujo contato foi interpretado como possivel discordância erosiva, em vista do contraste litológico entre ambos os membros, o inferior de filitos carbonosos e o superior de metagrauvacas. Por outro lado, Jost & Fortes (2001) dividiram o *greenstone belt* em dois conjuntos litológicos justapostos por falha transcorrente NW-SE meridiana à faixa. A porção de oeste conteria as formações Serra Azul, São Patricinho, Aimbé e Cabaçal e, a de leste, intercalações entre as formações Serra Azul e Cabaçal. O mapeamento de detalhe 1:10.000 e os resultados de sondagens para fins exploratórios na faixa realizados pela equipe da Yamana Gold Inc. levaram Jost *et al*. (2011) a rever as propostas de Jost & Oliveira (1991) e Jost *et al*. (1995) no tocante à Formação Cabaçal e a subdividiram nos membros Inferior, Intermediário e Superior e criaram a Formação Mata Preta (Fig. 4) em substituição ao Membro Superior da Formação Cabaçal de Jost *et al*. (1995).

A Formação Serra do Cotovelo tem espessura inferior a 100 m e sua área de ocorrência mais expressiva situa-se no extremo sul do *greenstone belt*, com exposições esporádicas na porção noroeste sob a forma de cunhas e lentes em metabasaltos da Formação Serra Azul, nas imediações do contato com rochas do Complexo Caiamar (Fig. 3). A unidade consiste de metakomatiitos (Fig. 5A) transformados em xistos com proporções vari-

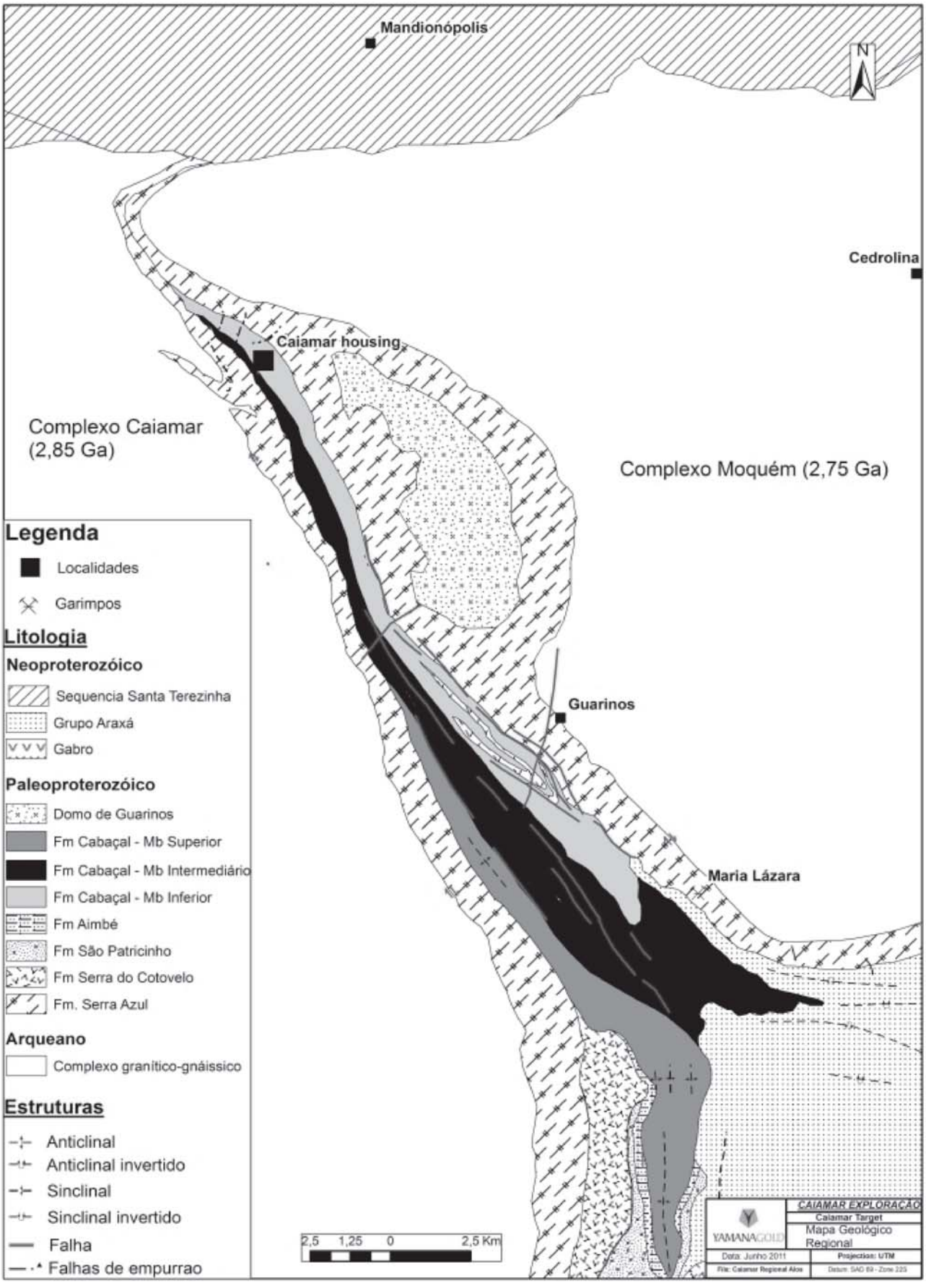

Figura 3 – Mapa geológico do greenstone belt de Guarinos e entorno.

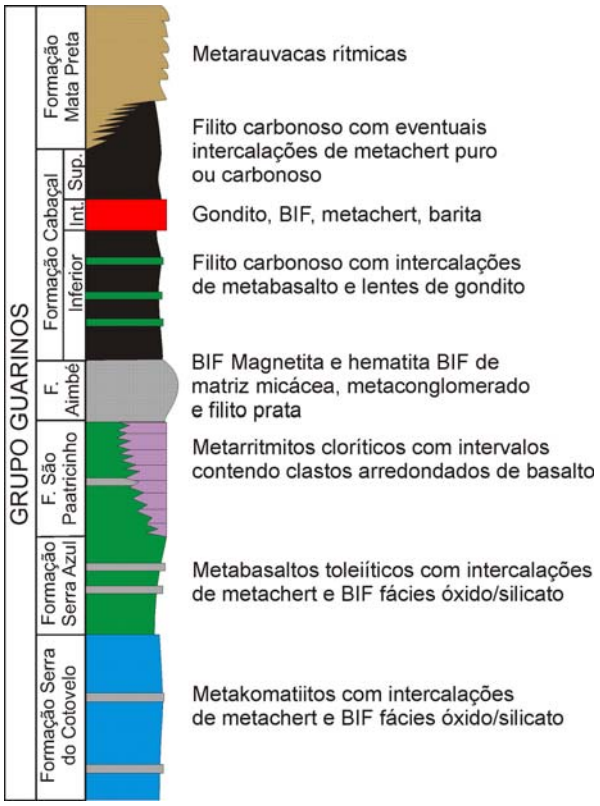

Figura 4 – Coluna estratigráfica do greenstone belt e Guarinos segundo Jost et al. (2011).

adas de talco, clorita, carbonato, serpentina e actinolita. As rochas desta unidade não possuem texturas e estruturas vulcânicas preservadas, o que dificulta interpretá-las como vulcânicas, exceto pela presença de intercalações de espessura métrica de formações ferríferas da fácies óxido.

A Formação Serra Azul tem cerca de 600 m de espessura e está disposta em duas faixas de 500 m e 1 km de largura coalescentes para a extremidade norte e que contornam, pelo leste e oeste, o núcleo dominado pelas rochas metassedimentares (Fig. 3). A unidade é composta de metabasaltos (Fig. 5B) que, segundo Jost *et al*. (1999), ocorrem em duas variedades química e petrograficamente distintas. A mais abundante compreende metabasaltos toleiíticos (<8% MgO), finos, foliados a maciços, com locais restos de almofadas e amígdalas, e ocorrem em camadas de espessura métrica a hectométrica, por vezes contínuas por dezenas de quilômetros segundo a direção. São compostos de proporções variadas de ferro-actinolita e albita, subordinadamente clorita, epidoto, quartzo, opacos e local granada. A outra variedade, rara, consiste de basaltos komatiíticos (>18% MgO), ocorre em lentes de espessura métrica em meio a primeira e é composta de proporções similares de Fe-actinolita e Mg-clorita, com magnetita acessória. Formações ferríferas e manganesíferas ocorrem como intercalações, ainda que raras, de espessura métrica, maciças a bandadas. As formações ferríferas são da fácies óxido, com magnetita e/ou hematita, por vezes grunerita, e as manganesíferas, compostas por espessartita e quartzo, estão em geral oxidadas para um complexo de hidróxidos de manganês.

A Formação São Patricinho tem uma espessura entre 30 e 100 m, é descontínua, aflora apenas nas porções meridionais do *greenstone belt* (Fig. 3) onde está em contato ora tectônico e ora brusco com os metabasaltos da Formação Serra Azul. As rochas desta unidade compreendem clorita xistos, clorita-quartzo xistos e

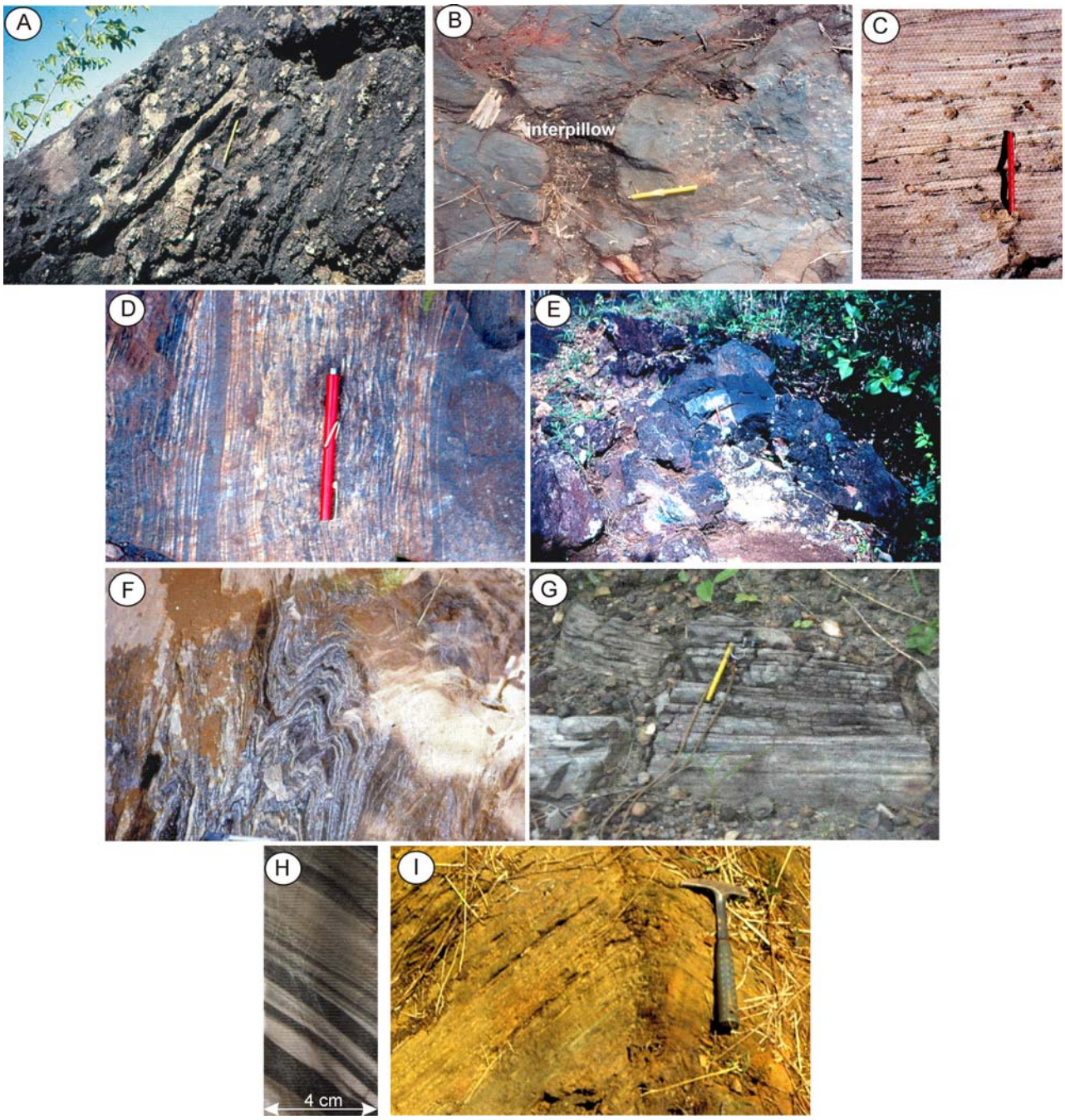

Figura 5 – Afloramentos de litótipos característicos das unidades estatigráficas do greenstone belt de Guarinos. A – Metakomatiito da Formação Serrra do Cotovelo transformado em talco xisto dobrado. B – Metabasalto com almofada, interpillow e vesículas da Formação Serra Azul. C – Metarritmito da Formação São Patricinho com clastos arredondados de basalto. D – Formação ferrífera bandada da fácies hematita com abundante mica branca da Formação Aimbé. E – Conduto exalativo marcado por parede de turmalinito da Formação Aimbé. F – Filito carbonosso típico dos membros inferior e superior da Formação Cabaçal. G – Barita maciça com estratificação cruzada de baixo ângulo do Membro Intermediário associada a gondito, BIF e metachert da Formação Cabaçal. H – Testemunho de sondagem que registra a interdigitação de filito carbonoso da Formação Cabaçal (leitos pretos) com metagruvaca da Formação Mata Preta (leitos brancos). I - Afloramento de metagrauvaca da Formação Mata Preta.

clorita-sericita-quartzo xistos, em geral rítmicos e, por vezes, conglomeráticos, verticalmente granoclassificados e com grânulos e seixos arredondados a subarredondados de quartzo e basalto (Fig. 5C). A abundância de Mg-clorita, ilmenita, rutilo e de clastos de basalto nos ritmitos sugere que a sua carga detrítica deve ter derivado dos basaltos da Formação Serra Azul e depositada sob correntes de turbidez.

A Formação Aimbé tem espessura média de 70 m, ocorre apenas na metade sul do *greenstone belt* (Fig. 3) e é caracterizada por rochas metassedimentares detríticas, formações ferríferas e metahidrotermalitos (Resende 1994, Resende & Jost 1994, 1995), sobrepostos simultaneamente às formações Serra Azul e São Patricinho, em contato interpretado por Resende & Jost (1994) como provável discordância. As fácies detríticas ocorrem em lentes de até 10 m de espessura situadas na base da formação e compreendem metaconglomerados e muscovita xistos. Os metaconglomerados são oligomíticos, suportados por matriz, com grânulos, seixos e blocos de quartzo leitoso e *chert* com pirita, magnetita ou hematita em matriz foliada de quartzo, sericita, hematita, magnetita e clorita. Os muscovita xistos ocorrem no topo dos metaconglomerados e são compostos por mica branca com subordinados cristais microscópicos de especularita. As formações ferríferas são as diagnósticas da unidade, se estendem por cerca de 30 km de modo contínuo com espessura média da ordem de 80 m. São compostas por uma fácies basal com magnetita que passa gradualmente para uma de topo com hematita. Ambas podem ser maciças, laminadas ou bandadas (Fig. 5D) e a sua característica reside na presença de matriz de mica branca, com menos de 5% de quartzo, o que as distingue de outras ocorrências similares na área. Os metahidrotermalitos situam-se na base da formação em lentes com centenas de metros de comprimento e de 20 a 40 m de largura, engastadas nas rochas das formações Serra Azul e São Patricinho. São compostas por condutos de descarga exalativa (Fig. 5E) circundados por auréolas de alteração hidrotermal que, das posições proximais para as distais, compreendem protólitos metamorfizados para (a) cloritóide-clorita-magnetita-muscovita xisto, (b) clorita-muscovita-magnetita xisto, e (c) sericita xisto com proporções subordinadas de quartzo, clorita e turmalina.

A Formação Cabaçal tem espessura estimada em cerca de 400 m (Jost & Oliveira 1991) e seu contato com a Formação Aimbé é transicional, dado pela alternância entre litótipos de ambas as unidades ao longo de um curto intervalo. A unidade foi redefinida por Jost *et al*. (2001) e consiste de rochas metassedimentares reunidas em três membros. O Inferior consiste de filitos carbonosos (Fig. 5F) com níveis centimétricos de arenitos finos e rítmicos e prováveis esteiras algais, alternados com intervalos decamétricos de metabasalto, por vezes transformados em magnetita-clorita xistos por alteração subaquosa, e locais lentes de formação ferrífera e gondito. O Membro Intermediário tem espessura variável entre 2 a 10 m, é relativamente continuo de sul a norte no *greenstone belt* e composto de gondito, formação ferrífera, metachert e barita maciça estratificada (Fig. 5G). No sul predominam gonditos que dão lugar, para norte, a formações ferríferas. O Membro Superior é composto por filitos carbonosos com eventuais lentes de metachert, metachert carbonoso e sericita filito.

A Formação Mata Preta (Fig. 3), como definida por Jost *et al*. (2001), se interdigita lateralmente com a Formação Cabaçal (Fig. 5H), tem espessura indeterminada, pois em afloramentos está estruturalmente sotoposta e, em testemunhos de sondagem, lateralmente interdigitada com a Formação Cabaçal. A unidade é representada

por metagrauvacas (Fig. 5I) homogêneas, médias a finas e compostas por proporções variadas de quartzo, plagioclásio, mica branca, biotita, opacos e, por vezes, granada. As variações texturais e composicionais indicam que os protólitos eram arenitos e siltitos impuros, e argilitos. Relíquias de estruturas primárias compreendem estratificação e laminação plano-paralela rítmica e cruzada, estruturas de corte-e-preenchimento e em chama, sugestivos de deposição por correntes de turbidez e fluxo de detritos. Entretanto, não se descarta a possibilidade de que alguns intervalos maciços sejam de tufos félsicos.

Geocronologia

Os primeiros resultados geocronológicos de rochas supracrustais de Guarinos foram obtidos por Jost *et al.* (2008) por datação U-Pb LA-ICP-MS de cristais de zircão de amostras das fácies magnetita da Formação Aimbé. Os cristais analisados ocorrem associados à matriz de mica branca interpretada como provável cinza vulcânica (Resende 1994). Foram obtidas duas populações, uma com idade concordante de 2.627 ± 19 Ma e outra com intercepto superior de 2.232 ± 36 Ma.

Dados U-Pb LA-ICP-MS obtidos por Jost *et al*. (2011) em zircão detrítico da Formação São Patricinho, sotoposta à Formação Aimbé, geraram a idade de 2.180 ± 36 Ma. Os cristais são internamente homogêneos, sem zonas de crescimento, típicos de rochas máficas, o que, somado à abundância de rutilo no concentrado de minerais pesados e à presença de fragmentos de basalto nos ritmitos da unidade sugerem, segundo Jost *et al.* (1995), que a unidade derivou da erosão dos basaltos da Formação Serra Azul com a qual está em contato lateral. Os autores também apresentam dados isotópicos de zircão detrítico de uma amostra de metagrauvaca do limite sul de ocorrência da Formação Mata Preta e na qual os mais jovens forneceram a idade U-Pb de 2.176 ± 11 Ma.

Se considerados os erros analíticos das amostras pode-se interpretar que as três unidades são contemporâneas. Contudo, se desconsiderado o erro, é possível reconhecer discreto decréscimo da idade entre os basaltos da Formação Serra Azul, retratada nos cristais de zircão da Formação São Patricinho, e a área-fonte das grauvacas da Formação Mata Preta. Por outro lado, estes dados revelam que o *greenstone belt* de Guarinos não é Arqueano mas Paleoproterozóico, especificamente do Rhyaciano.

Estrutura

A partir do mapeamento da metade norte do *greenstone belt* de Guarinos, Jost *et al*. (1995) concluem que o seu arcabouço estrutural se caracteriza por pelo menos dois estágios principais de deformação. Ao primeiro atribuem a formação de dobras com superfície axial marcada por xistosidade (Sn) da fácies xisto verde paralela ao acamamento (So), sugestivo de dobras apertadas a isoclinais. Por interferência do segundo estágio, Sn/ /So foi dobrada em uma sucessão de antiformes e sinformes com superfície axial de direção média N15°W e mergulho médio de 35° ora para SW ora para NE. Os autores descrevem que na porção sudoeste da faixa a

formação ferrífera da Formação Aimbé é marco estrutural e, de oeste para leste (Fig. 3), desenha uma antiforme seguida de sinforme, ambas simétricas, com ângulo interflancos médio de 45°. A sinforme dá, para leste, lugar a uma antiforme apertada e inversa, de superfície axial suavemente curvilínea, direção N15°W a norte, que passa para N70°W a sul e de mergulho médio de 40°SW.

Para norte, a dobra normal de sudoeste dá lugar a sucessivas antiformes e sinformes apertadas e inversas. Ao nordeste, Sn//So descreve trajetória que contorna o corpo do Trondhjemito Santo Antônio em antiforme alongada (Domo de Guarinos) (Fig. 3). Nos quadrantes de sul, oeste e norte do entorno do trondhjemito, a foliação mergulha com ângulos médios inferiores a 20°SW e no de leste a 40°SW, o que indica que a estrutura está adernada para leste.

Na porção norte, a sucessão estratigráfica e a estruturação do *greenstone belt* fooram delaminadas por falhas de direção média N10°W, mergulho da ordem de 30°SW e contém uma lineação de estiramento ora horizontal paralela à direção da foliação milonítica, ora com duplo caimento máximo de 15° para NW e SE. Indicadores cinemáticos, em particular dobras de arrasto, registram que as falhas são direcionais e que, no oeste são sinistrais e, no leste, dextrais. Jost *et al*. (1995) interpretam estas falhas como possíveis rampas laterais de escamas de empurrão. O sistema nasce no extremo norte como falha principal que, para sul, desfia em diversos ramos que abrem para sudeste. As falhas estão confinadas ao *greenstone belt*, pois são truncadas pelas rampas de empurrão do Arco Magmático no norte e do Grupo Araxá no sul. De sul para norte, o sistema interrompe a continuidade das formações Aimbé e São Patricinho e reduz a expressão das formações Cabaçal e Mata Preta. As falhas se manifestam por milonitos e ultramilonitos, venulações de quartzo e locais blocos decamétricos imbricados de granada-sillimanita-quartzito e gnaisses graníticos, indicativos do envolvimento de rochas mais profundas e exóticas. Algumas falhas alojam intrusões menores do que *stocks,* por vezes tabulares, de gabro e granodiorito, uma das quais aloja o depósito do Caiamar, bem como veios com arsenopirita, pirita, calcopirita e ouro, como nos garimpos Maria Lázara, extremo sudeste do *greenstone belt*.

Por outro lado, Jost *et al*. (1995) e Resende (1994) descrevem que a disposição da Formação Aimbé em relação às demais unidade e as estruturas sedimentares primárias reliquiares de metagrauvacas da Formação Mata Preta revelam que a sucessão estratigráfica de Guarinos está invertida.

Ambiente Tectônico

A revisão sobre a origem, composição e ambiente tectônico de *greenstone belts* realizada por Hunter & Stowe (1997) registra que as rochas vulcânicas desses ambientes podem derivar de *rifts* continentais (p. ex. Henderson 1981), arcos de ilha (Folinsbee *et al.* 1968, Langford & Morin 1976), bacias de *back-arc* (Tarney *et al.* 1976) e ofiolitos (De Witt & Stern 1980). Os exemplos descritos em De Wit & Ashwall (1997) permitem concluir que *greenstone belts* não se explicam por um modelo tectônico universal, que cada caso deve ser analisado individualmente e que há exemplos que podem ser explicados por apenas um ambiente tectônico quanto pela convergência de mais de um ambiente. O entendimento do ambiente de Guarinos, tanto quanto os demais *gre-*

enstone belts de Goiás, está em estágio embrionário e carece de investigações detalhadas. Há, no entanto, dados esparsos na literatura sobre a assinatura geoquímica das rochas supracrustais de Guarinos que permitem especular sobre um modelo a partir da sucessão estratigráfica e das características geoquímicas de suas rochas (Fig. 6).

Dados litogeoquímicos dos komatiitos dos cinco *greenstone belts* de Goiás apresentados e discutidos por Kuyumjian & Jost (2006) sugerem que em nenhum dos casos o vulcanismo resultou de regime compressivo. Os autores não abordam o regime crustal responsável pelos komatiitos de Guarinos, mas os interpretam como empobrecidos em Alumínio e derivados de magmas gerados por plumas de profundidades inferiores a 200 km, em contraste com os de Crixás, gerados a partir de manto empobrecido e profundidades superiores. Sugerem que a diferença entre ambos os komatiitos pode ser explicada tanto por plumas distintas sincrônicas quanto diacrônicas. Um primeiro ensaio sobre o ambiente tectônico dos basaltos de Guarinos realizado por Jost *et al*. (1999) sugere que a sua assinatura geoquímica é compatível com toleiitos modernos de ambiente de *back-arc.*

A passagem da seção vulcânica para a sedimentar iniciou com turbiditos da Formação São Patricinho derivados da erosão dos basaltos da Formação Serra Azul, o que sugere o desenvolvimento de uma calha limitada por falhas, as quais canalizaram os fluídos hidrotermais responsáveis pelas formações ferríferas da Formação Aimbé. Estas foram gradualmente soterradas pelo ingresso de ambiente euxênico representado por pelitos ricos em matéria orgânica do Membro Inferior da Formação Cabaçal, durante cuja deposição ocorreu episódica atividade vulcânica basáltica e locais exalações que geraram lentes ricas em manganês, ferro e chert. A sedimentação pelítica foi temporariamente suprimida por atividade exalativa e deposição da associação gondi-

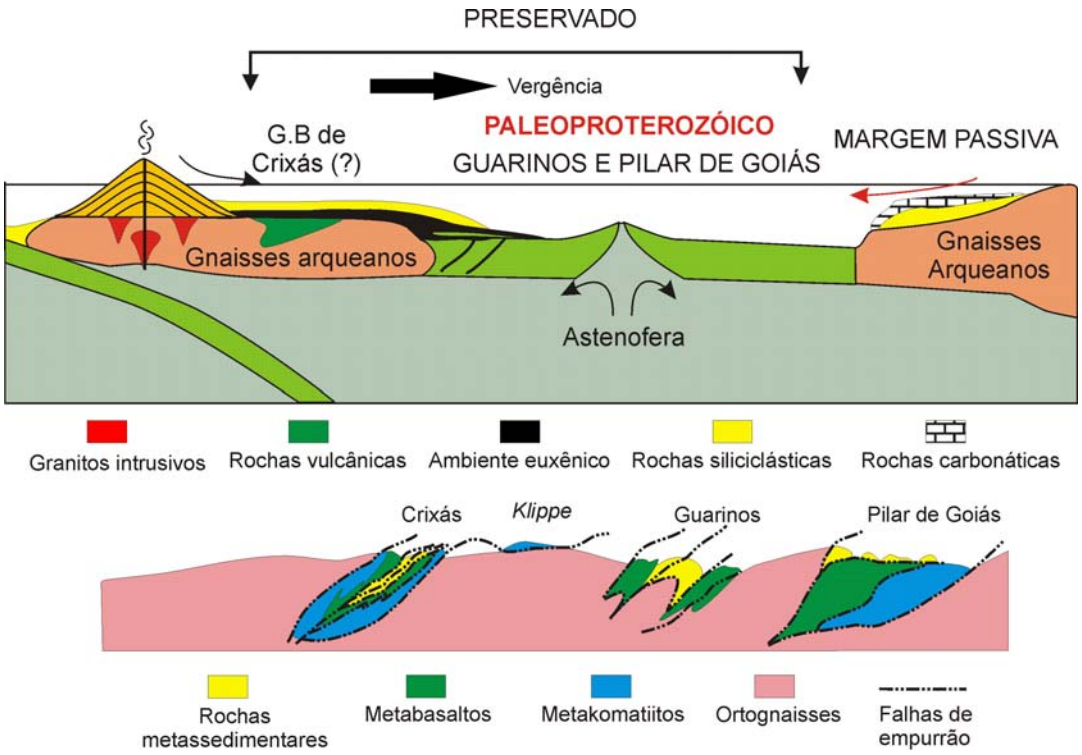

Figura 6 – Esquema de evolução estimada para os greenstone belts da porção norte do Bloco Arqueano-Paleoproterozóico de Goiás.

to-BIF-barita-chert do Membro Intermediário da Formação Cabaçal, o qual, no norte, é contínuo, mas, no sul se expressa como rosário de lentes de gondito. O Membro Intermediário é seguido da reativação do ambiente euxênico e deposição do Membro Superior. A Formação Cabaçal contém, portanto, dois ciclos sedimentares separados por período de atividade exalativa que se estendeu por toda a bacia.

A partir de determinado instante, ainda incerto, a sedimentação euxênica foi acompanhada pelo ingresso da carga clástica arenosa imatura representada pelas grauvacas da Formação Mata Preta. A sua deposição foi gradual no início da fase de bacia e passou a predominar no final e, assim, com progressivo sufocamento das condições euxênicas, o que sugere erosão da área-fonte em soerguimento progressivo. O estado de preservação dos grãos de plagioclásio e ortoclásio e de fragmentos de rocha do arcabouço das grauvacas indica que a área-fonte foi submetida a intemperismo de incipiente a moderado (Jost *et al*. 1996), rápida erosão e transporte de massa. O predomínio de granoclassificação vertical e as estruturas primárias das grauvacas sugerem que a sua deposição ocorreu sob regime de correntes de turbidez e as alternâncias de litótipos ora grosso e ora fino, bem como com pelitos carbonosos em distintas posições estratigráficas sugerem que a deposição ocorreu sob variados níveis de energia. Dados geoquímicos obtidos por Jost *et al.* (1996) mostram que a proveniência da carga clástica da maioria das amostras pode ser explicada mediante área-fonte dominada por rochas básicas e félsicas. Os dados geocronológicos de zircão detrítico das formações São Patricinho, Aimbé e Mata Preta indicam que a área-fonte continha rochas do Arqueano e do Rhyaciano, as primeiras interpretadas como de um continente ao qual se ancorou um arco magmático, fonte das últimas.

O evento euxênico representado pela Formação Cabaçal provavelmente resultou de progressiva ascensão do nível de mar controlada por uma flutuação eustática de primeira ordem da crosta terrestre e geração de Eventos Oceânicos Anóxicos, ou AOEs (*Anoxic Oceanic Events*) no conceito de Schlanger & Jenkyns (1976). AOEs são marcadores bioestratigráficos temporais no Globo Terrestre e representam lapsos de circulação de correntes oceânicas, carência de Oxigênio, aquecimento global, emissão de gases de efeito estufa e extinções em massa. Dados mundiais mostram que os OAEs se instalaram rapidamente após importantes anomalias positivas de $\delta^{13}C$ em dolomitos. No Paleoproterozóico, estas ocorreram em escala global entre 2,33 e 2,06 Ga (Bekker *et al*. 2006, dentre outros). Segundo Barley *et al*. (2005), a amalgamação de fragmentos continentais durante o Paleoproterozóico resultou na formação de um supercontinente em cerca de 2.4 Ga, com retorno a baixos níveis do mar e relativa qüiescência tectônica seguida de fragmentação em 2,32 a 2,22 Ga. Segundo Kopp *et al*. (2005), três glaciações globais ocorreram neste tempo, dentre as quais a geocronologicamente melhor determinada ocorreu entre 2,22 e 2,06 Ga, denominada de evento Lomagundi. Quando folhelhos pretos são comparados com a espessura preservada de várias regiões (Isley & Abbott 1999), uma série temporal mostra a presença de três picos de ocorrência no Paleoproterozóico, situados em 2,0 Ga, 1,85 Ga e 1,7 Ga. Segundo Condie *et al.* (2000, 2001), há uma boa correlação entre a ocorrência de folhelhos e o evento de superpluma de 1,9 a 1,7 Ga, com pico menor em 2.0 Ga. Assim, os metapelitos carbonosos da Formação Cabaçal combinados com os dados geocronológicos de zircão magmático da Formação Serra Azul, cristais detríticos das demais unidades e as anomalias de $d^{13}C$ de dolomitos dos *greenstone belts* da região compatíveis com o Evento Loma-

gundi (Santos *et al.* 2008, Jost *et al.* 2008) indicam que a deposição dos pelitos carbonosos da Formação Cabaçal resultou de um AOEs durante o Rhyaciano. Logo, a seção vulcânica e os litotipos sedimentares subseqüentes podem ter se desenvolvido durante o evento de superpluma do entorno de 2,0 Ga proposta por Condie *et al.* (2000, 2001). O estágio de bacia foi seguido de atividade tectônica, com fechamento, compressão e deformação do provável ambiente de *back-arc*, com retomada estrutural e reciclagem isotópica no Neoproterozóico, quando da amalgamação do Bloco Arqueano na Faixa Brasília.

TIPOLOGIAS DE DEPÓSITOS AURÍFEROS DA PORÇÃO NORTE DO BLOCO ARQUEANO-PALEOPROTEROZÓICO DE GOIÁS

Os depósitos auríferos da porção norte da região compreendem três tipos distintos, isto é, sulfeto maciço, veios de quartzo e minério disseminado.

Sulfeto maciço aurífero ocorre em dois corpos em Crixás e compreendem a Zona Superior, exaurida, e o Corpo Palmeiras, estruturalmente mais elevado. A Zona Superior consistiu de um conjunto de lentes com 0,5 a 2,5 m de largura e de 50 a 200 m de comprimento que se estendiam até 400 m segundo o *plunge*, da superfície até cerca de 450m de profundidade. As lentes situavam-se próximo ao contato de metabasalto com xistos carbonosos. O detalhamento da Zona Superior foi realizado por Fortes (1996) e os primeiros dados sobre o Corpo Palmeiras, a partir de um furo de sondagem antes de sua exposição em galeria, por Almeida (2006). Ambos os corpos contêm até 95% de pirrotita e/ou arsenopirita e quantidades subordinadas de magnetita, ilmenita, bornita e calcopirita, em rara ganga de quartzo, plagioclásio, siderita, sericita, biotita, mica branca, epidoto e rutilo e, eventuais veios pegmatóides com quartzo, feldspatos, biotita, arsenopirita e ouro (Fig. 7A). O Ouro ocorre livre e associado com arsenopirita. A alteração hidrotermal resultou em uma sucessão de halos que, de posições distais para as proximais compreendem um externo de dolomito, um intermediário de clorita xistos e um interno de sericita xistos. A alteração por sulfetação se manifesta de modo incipiente desde o halo externo até o interno como disseminações de arsenopirita e pirrotita. A alteração potássica é discreta nos três halos, mas pode ser pronunciada no interno, como indica a substituição progressiva de mica branca por biotita e magnetita próximo aos corpos mineralizados, o que sugere a presença de um fluido tardio mais rico em potássio e ferro. A presença de granada sintectônica, cloritóide pós-tectônico e de magnetita euédrica indicam que as paragêneses minerais dos halos de alteração são produtos de metamorfismo. Estudos geoquímicos realizados por Fortes (1996) e Oliver *et al*. (2005) mostram que a alteração hidrotermal associada ao sulfeto maciço resultou da interação dos fluidos com basaltos. A origem dos corpos de sulfeto maciço é ainda incerta, se resultante de canalização de fluidos ao longo de falhas de empurrão, ou se originalmente do tipo VMS associado aos basaltos. A interpretação de sua gênese é dificultada pelo estado de deformação do contexto estratigráfico de Crixás, a desordem da seqüência de litótipos hospedeiros e conseqüente dificuldade de recomposição paleogeográfica, bem como pela exaustão da Zona Superior.

O veio de quartzo é o principal corpo de minério aurífero remanescente de Crixás (Fig. 7B). É descon-

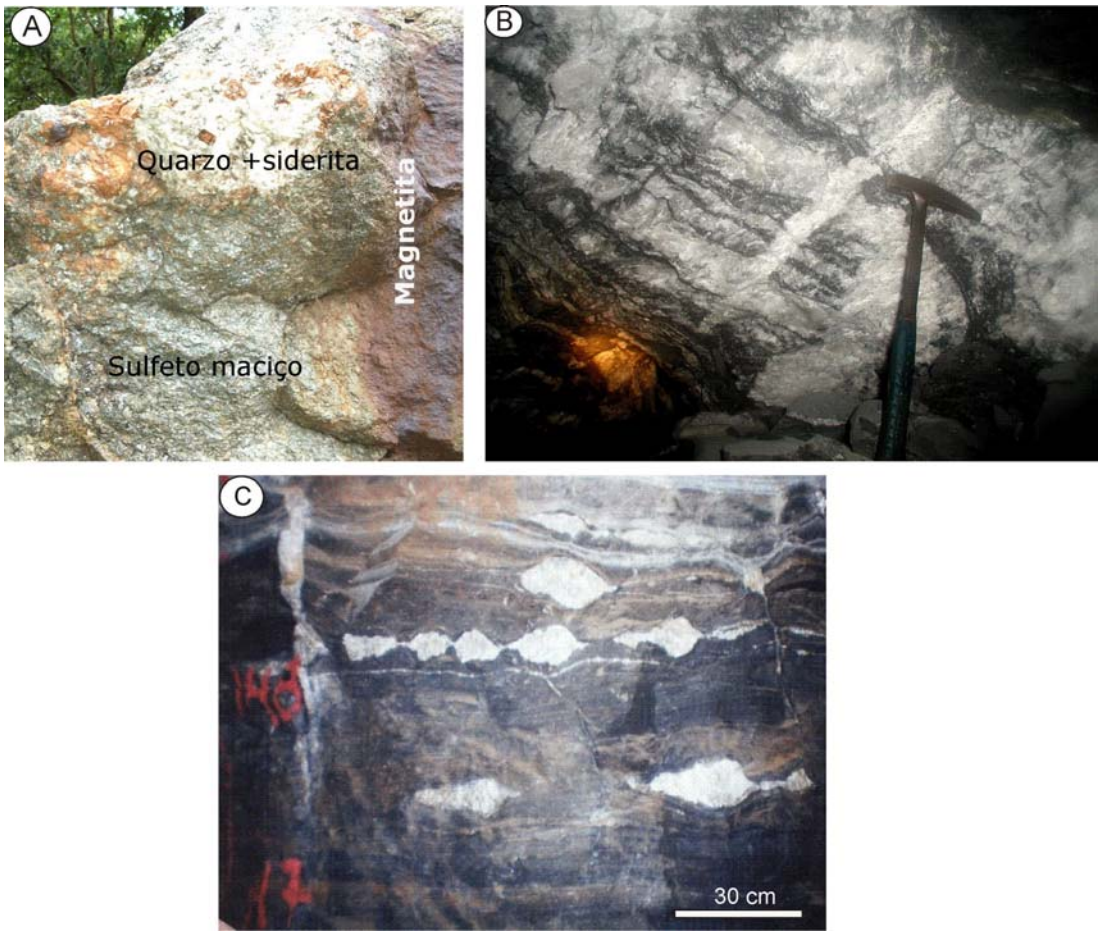

Figura 7 – Exemplos de exposições dos principais tipos de depósitos auríferos da porção norte do Bloco Arqueano-Paleoproterozóico de Goiás. A – Sulfeto maciço da Zona Superior de Crixás. B – Veio de quartzo da Zona Inferior de Crixás. C – Minério disseminado com venulação de quartzo boudinado da Mina Nova, Crixás.

tínuo, com 0,5 a 5,0 m de largura, 500 m de comprimento e se estende até cerca de 1.500 m segundo o *plunge*, desde a superfície até mais de 700 m de profundidade. O veio se situa em uma zona de alto *strain* que marca o contato entre xistos carbonosos sobrepostos a metagrauvacas, cerca de 120 m abaixo das lentes de sulfeto maciço da Zona Superior. O ouro ocorre disseminado ou como preenchimento de fraturas, em grãos de menos de 0,1 mm até 2 mm. Componentes menores compreendem pirrotita, arsenopirita, mica branca, material carbonoso, plagioclásio, carbonato e clorita. Os xistos carbonosos encaixantes foram pouco reativos com as soluções hidrotermais, motivo pelo qual a alteração correspondente foi débil e se manifesta pela local lixiviação de material carbonoso e transformação da rara biotita em mica branca sugestivo de alteração fílica localmente acompanhada de sulfetação dada por arsenopirita e pirrotita disseminadas.

O depósito do tipo disseminado ocorre em corredores de alto *strain* em filitos carbonosos e é representado por corpos mineralizados de Crixás (Zona Intermediária, Mina Nova, Forquilha, Corpos IV e V, Pequizão e Cajueiro) e de Pilar de Goiás (Jordino, Ogó, Três Buracos). Em Guarinos, a mineralização exposta em cinco garimpos está hospedada em zona de alto *strain* em metabasaltos com intercalações de filito carbonoso e formação ferrífera. A título de exemplo, na Mina Nova, em Crixás, a zona rica em ouro tem, em média, 1,5 m de largura,

cerca de 200 m de comprimento e se estende por mais de 1000 m de profundidade. Os intervalos ricos em ouro se caracterizam pela presença de venulações auríferas com quartzo, quartzo-carbonato ou quartzo-albita-biotita-carbonato, centimétricas a decimétricas, paralelas à foliação, dobradas e/ou boudinadas, por vezes transversais (Fig. 7C), como descrito por Fortes (1996), Portocarrero (1996), Petersen (2003) e Jost (2004) em Crixás, por Pulz (1990) em Guarinos e Pulz (1995) em Pilar de Goiás. As venulações mesoscópicas são, por exemplo, no Corpo Forquilha, acompanhadas por enxame de microvenulações descontínuas com amplo espectro composicional, cujo arranjo sugere micro-brechação hidráulica durante a mineralização. O filito carbonoso encaixante também é, em geral, aurífero e com disseminações de pirita, pirrotita e arsenopirita. Constituintes menores compreendem, em Crixás, calcopirita, bornita e pentlandita, e em Guarinos, compostos de Au-Te-Bi e em Pilar de Goiás de galena e esfalerita. Como no modelo em veio de quartzo, os intervalos de filito carbonoso mineralizado também foram pouco reativos às soluções hidrotermais, mas a sua resposta varia entre os corpos de minério. No garimpo Maria Lázara, Guarinos, situado em metabasaltos, a alteração hidrotermal pode alcançar até 50 m, de forma simétrica a partir do intervalo com veios de quartzo e carbonato auríferos e se manifesta por um halo externo de cloritização e carbonatação, um intermediário de biotitização e um interno de alteração fílica (Pulz 1990, 1995). O ouro ocorre na forma nativa e maldonita (Au_2Bi) associados à arsenopirita e pirrotita e traços de esfalerita, monazita, pirita, calcopirita, galena, molibdenita, prata nativa, joesita-B (Bi_4Te_2S), csilovaita (Bi_2TeS_2), bismutinita e bismuto nativo (Pulz *et al*. 1991). Em Pilar de Goiás não há, até o presente, descrições petrográficas dos estilos de alteração hidrotermal. No garimpo da Cachoeira do Ogó, Pulz (1995) descreve que o Ouro ocorre livre e como electrum, associado com arsenopirita, pirita, pirrotita, esfalerita, galena e calcopirita.

Até o presente eram desconhecidas tipologias adicionais, mas a avaliação do depósito do Caiamar pela Yamana Gold Inc. revelou que o mesmo está hospedado em um corpo de episienito sódico resultante da alteração hidrotermal de uma intrusão de gabro, o que gerou uma nova tipologia de depósito aurífero da região, mundialmente rara, objeto deste estudo.

O DEPÓSITO AURÍFERO DO CAIMAR

Localização

A área de estudo situa-se no noroeste do Estado de Goiás (Fig. 8), a aproximados 350 km de Brasília e 250 km de Goiânia. A partir de Brasília, o acesso é feito pela rodovia BR-060 rumo sudoeste até Anápolis, por cerca de 150 km onde se localiza o entroncamento com a rodovia BR-153 (Belém-Brasília). De Goiânia, segue-se rumo nordeste até Anápolis, por cerca de 60 km, onde se acessa a rodovia Belém-Brasília. De Anápolis percorre-se 199 km pela BR-153 rumo norte até o entroncamento com a rodovia GO-154, que de onde se prossegue para as cidades de Itapaci, Pilar de Goiás e Santa Terezinha de Goiás. De Itapaci segue-se até Pilar de Goiás, por cerca de 20 km, de onde se toma rumo oeste por estrada de terra ate a cidade de Guarinos, que dista 18 km. O trajeto de Guarinos ate o projeto Caiamar é feito pela GO-336, de Itapaci para Crixás. A partir GO-336

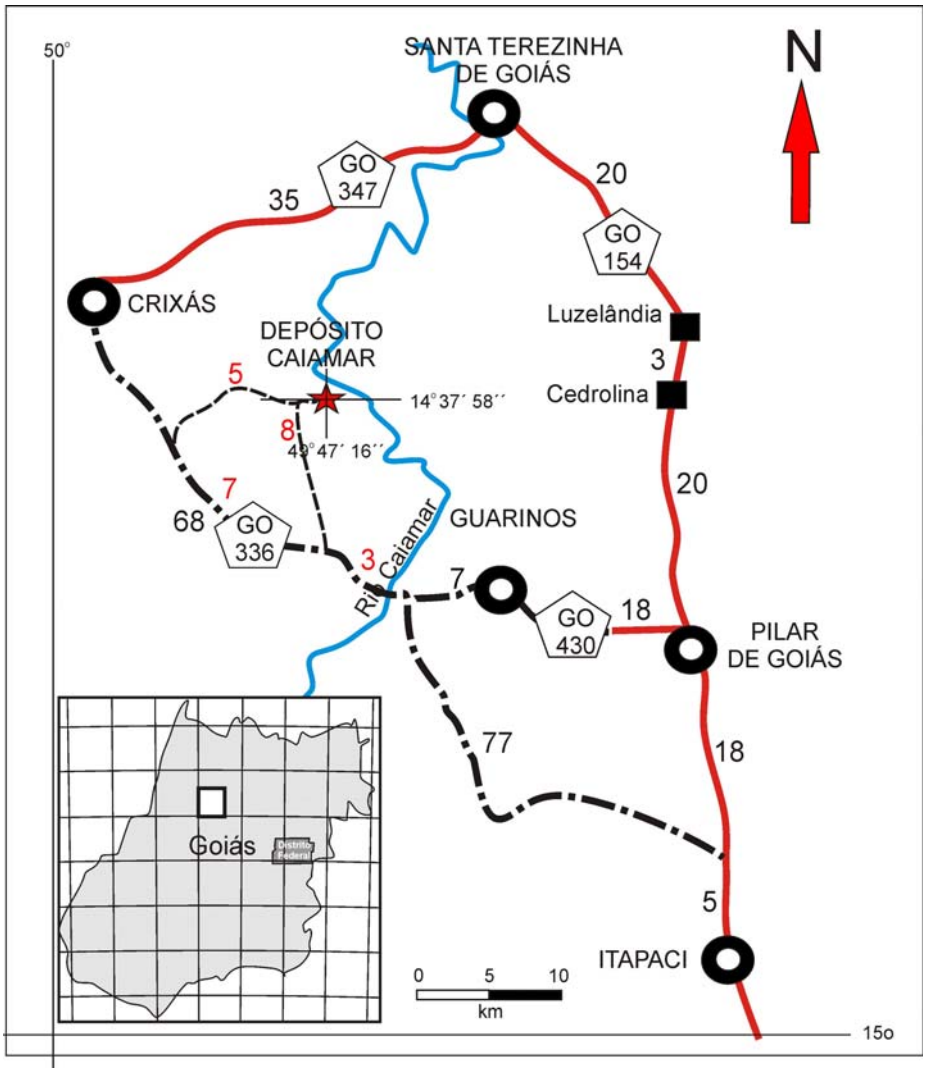

Figura 8 – Localização do depósito do Caiamar.

há dois acessos até a área do projeto, por vias vicinais. Um dista 8 km rumo norte e o outro cerca de 5 km rumo leste.

Objetivos

O presente estudo visa descrever as características do depósito Caiamar, interpretar a sua gênese, enquadrá-lo no arcabouço geológico do *greenstone belt* de Guarinos e definir o modelo de depósito ao qual a mineralização está relacionada. O depósito está associado a uma intrusão de gabro a partir da qual foram gerados halos de alteração hidrotermal até um episienito sódico mineralizado, cujos detalhes constam do artigo da Parte 2 desta dissertação.

Métodos

Com vistas ao entendimento das características da intrusão de gabro e seus halos de alteração hidro-

termal realizou-se mapeamento geológico na escala 1:10.000 associado à descrição detalhada de testemunhos de 129 sondagens e mapeamento de duas galerias na escala 1:500 onde melhor estão expostos os corpos mineralizados. Para o presente estudo, selecionou-se a sondagem CA-87 como referência por conter a maior espessura de testemunhagem contínua interceptada ortogonalmente à estruturação local. A partir da primeira ocorrência de gabro, em contato com filito carbonoso a 62,05 m de profundidade, a sucessão litológica de interesse se estende até 152,20 m, onde se situa contato com metapelito perfazendo, assim, cerca de 90 m representativos. Ao longo desta seção foram coletadas 13 amostras inicialmente interpretadas como de gabro, 9 do halo de alteração hidrotermal externo, 21 do intermediário e duas do estreito halo interno, localizadas nas profundidades indicadas na Tabela 1. O sienito sódico foi amostrado nas sondagens CA-81 e CA-81C, que o cortam segundo o mergulho e de onde foram coletadas 8 e 9 amostras, respectivamente, nas profundidades indicadas na Tabela 2, adicionada a três amostras da pilha de estoque de minério. Os métodos de estudo compreenderam a interpretação de resultados de sondagem, amostragem para estudos petrográficos, análises químicas de rocha total, de isótopos de Enxofre e geocronológicas. Em amostras selecionadas de gabro e dos halos de alteração hidrotermal foram analisados cristais de granada com vistas à identificação da espécie.

As 63 amostras foram analisadas sob microscópio petrográfico convencional por luz transmitida e refletida nas de minério, para identificar os constituintes minerais maiores, menores e traços e suas variações ao longo da seção por análise química de rocha total. A preparação e análise química das amostras foram realizadas pela Divisão Mineral do ALS Laboratory Group, Vancouver, Canadá. As amostras tinham em média 150 g, foram britadas, moídas, pulverizadas em moinho com panela de ágata, quarteadas e separada uma alíquota de 2 g de polpa. As polpas foram fundidas com Tetraborato de Lítio e analisadas por ICP-AES. A Perda ao Fogo foi obtida a partir de 2 g de polpa aquecida em forno a 1000 ^{o}C.

As análises de isótopos de Enxofre foram realizadas pelo Dr. Bernard Buhn no Laboratório de Estudos Geocronológicos, Geodinâmicos e Ambientais do Instituto de Geociências da Universidade de Brasília, por MC-ICP-MS. As amostras foram analisadas comparativamente ao padrão representado por uma amostra de pirita do laboratório. O tamanho dos *spots* analisados foi de 100 mm.

Dados geocronológicos foram obtidos pelo método U-Pb por meio de LA-ICP-MS em frações de cristais de zircão do episienito pela Profa. Dra. Juliana Charão Marques no Laboratório de Geocronologia da Universidade Federal do Rio Grande do Sul.

Os elementos maiores de cristais de granada foram determinados em microscópio eletrônicos de varredura (MEV) acoplado a sistema de análise de raios-X por espectrometria de energia dispersiva (EDS) com emprego do software INCA, em aumento de 10.000x. O equipamento é da marca FEI, modelo Quanta 200-3D e pertence à Área de Balística Forense do Instituto Nacional de Criminalística do Departamento de Polícia Federal, em Brasília.

Tabela 1 – A – Sucessão de litótipos da sondagem CA-87 e profundidades de amostragem para estudos petrográficos e análise química.

Amostra	Profundidade	Litótipos
	62,05	Filito Carbonoso
1	62,40-62,50	Gabro
2	63,10-63,20	
3	64,10-64,20	
4	64,80-64,90	
5	65,95-66,05	Zona externa
6	66,60-66,70	
7	67,50-67,60	
8	68,80-68,90	
9	69,80-69,90	
10	71,20-71,30	
11	72,50-72,60	
12	73,40-73,50	
13	74,90-75,00	
14	76,50-76,60	
15	77,80-77,90	
16	79,60-79,70	
17	80,80-80,90	
18	81,80+81,90	Zona intermediária
19	82,95-83,15	
20	84,30-84,40	
21	86,25-86,35	
22	87,70-87,85	
23	89,15-89,30	
24	91,50-91,70	
25	93,80-94,00	
26	95,80-95,95	
27	97,70-97,90	
28	99,50-99,70	
29	100,20-100,35	Z. externa
30	101,30-101,40	Z. interm.
	102,00-105,60	
31	105,70-105,85	Z. interm.
32	110,50-110,75	Zona externa
33	112,40-112,60	
34	115,20-115,40	
35	123,80-124,00	Z. interm.
	124,65-139,55	
36	140,15-140,35	Z. interm.
37	141,50-141,70	Zona interna
38	143,30-143,35	
39	144,50-144,70	
40	145,50-145,70	
41	146,10-146,30	
	146,38-147,68	Episienito
42	147,95-148,20	Zona interna
43	149,10-149,30	
44	150,50-150,70	
45	151,40-151,55	
	152,20	Metapelito

Tabela 2 - Profundidades de amostragem dos intervalos com episienito sódico nas sondagens CA-81 e CA-812C.

Amostra	Sondagem	Profundidade
81A	CA-081	62,25-62,45
81B		74,30-74,45
81C		75,50-75,75
81D		76,55-76,75
81E		77,50-77,70
81F		80,90-81,10
81G		83,30-83,50
81H		97,70-97,90
81CA	CA-081C	5,90-6,10
81CB		7,00-7,20
81CC		8,50-8,70
81CD		9,50-9,70
81CE		10,50-10,70
81CF		11,70-11,90
81CG		19,50-19,70
81CH		22,60-22,80
81CI		27,30-27,50
CAX		PILHA
CAB	DUPLICATA	81CF
CAC	DUPLICATA	81D

REFERÊNCIAS

Almeida B.S. 2006. *Mineralização aurífera, alteração hidrotermal e indicadores prospectivos do Corpo Palmeiras, greenstone belt de Crixás, Goiás*. Trabalho de Conclusão do Curso, IG/UFRGS, 88 p.

Arndt N.T., Teixeira N.A., White, W.M. 1989. Bizarre geochemistry of komatiites from the Crixás Greenstone Belt. *Contr. Mineral. Petrol.*, **101**:187-197.

Barley M.E., Bekker A., Krapez B. 2005. Late Archean to Early Paleoproterozoic global tectonics, environmental change and the rise of atmospheric oxygen. *Earth Planet. Scie. Letters,* **238**:156–171

Bekker A., Karhu J.A., Kaufman A.J. 2006. Carbon isotope record for the onset of the Lomagundi carbon isotope excursion in the Great Lakes area, North America. *Prec. Res.*, **148**:145-180

Condie K.A., D. Des Marais D.J., Abbott D. 2001. Precambrian superplumes and supercontinents: A record in black shales, carbon isotopes, and paleoclimates?, *Prec. Res*., **106**:239-260.

Condie K.A., Des Marais D.J., Abbott D. 2000. Geologic evidence for a mantle superplume event at 1.9 Ga, Geochemistry, geophysics, and geosystems, 1, *Geochemical Earth Reference Model (GERM) Special Issue*, Paper number 2000GC000095.

Costa P.C.C. 2003. *Petrologia, geoquímica e geocronologia dos diques máficos da região de Crixás-Goiás, porção centro-oeste do Estado de Goiás*. Tese de Doutorado, Instituto de Geociências, Universidade de São Paulo, 151 pg.

Danni J.C.M. & Ribeiro C.C. 1978. Caracterização estratigráfica da sequência vulcano-sedimentar de Pilar de Goiás e de Guarinos, Goiás. *In*: SBG, Congr. Brás. Geol., 30, Recife, *Anais,* 582-596.

Danni J.C.M., Jost H., Winge M., Andrade G.F. 1986. Aspectos da evolução dos terrenos granito-greenstone: exemplo da região de Hidrolina, Goiás. *In*: SBG, Congr. Bras. Geol., 34, Goiânia. *Anais,* 2:570-584.

De Wit M. & Ashwall L.D. 1997. *Greenstone belts*. Oxford University Press, 809 pg.

De Witt M.J. & Stern C.R. 1980. The 3000 Ma ophiolite complex from the Barberton greenstone belt, South Africa: Archean oceanic crust and its geotectonic implications. 2nd. Intern. Archean Symp., Perth, *Abstracts*, 85-87.

Folinsbee R.E., Baadsgaard H., Cumming G.L., Gree D.C. 1968. A very ancient island arc. *Am. Geoph. Union Monograph*, **12**:441-448.

Fortes P.T.F.O. 1996. *Metalogênese dos depósitos auríferos Mina III, Mina Nova e Mina Inglesa, greenstone belt de Crixás, GO*. Tese de Doutorado, Instituto de Geociências, Universidade de Brasília, 176 p.

Fortes P.T.F.O., Pimentel M.M., Santos R.V., Junges S.L. 2003. Sm-Nd studies at Mina III gold deposit, Crixás greenstone belt, Central Brazil: implications for the depositional age of the upper metasedimentary rocks and associated Au mineralization. *J. South Am. Earth Sci.,* **16**:503-512.

Groves D.E., Condie K.C., Goldfarb R.J., Hronsansky J.M.A., Vierlreicher R.M. 2005. Secular changes in global tectonic processes and their influence on the temporal distribution of gold-bearing mineral deposits. *Econ. Geol*., **100**:203-224

Henderson J.B. 1981. Archaaean basin evolution in the Slave Province, Canada. *In*: A. Kroner (ed.) *Precambrian Plate Tectonics*. Elsevier, pp. 211-235

Hunter D.R. & Stowe C.W. 1997.A historical review of the origin, composition, and setting of Archean greenstone belts (pre-1980). *In*: M.J. de Wit & L.D. Ashwal (eds.) *Greenstone belts*. Oxford University Press, pg. 5-30.

Isley A.E. Abbott D. H. 1999. Plume-related mafic volcanism and the deposition of banded iron-formation. *J. Geoph. Res*., **104**:15461-15477.

Jost H. 1995. Alguns aspectos da geoquímica de metabasaltos do greenstone belt de Guarinos, Goiás. *In*: SBGq, Congr. Bras. Geoqui., 5, *Anais em CD-ROM*, 4 pg.

Jost H. 2004. Diagnóstico da alteração hidrotermal dos corpos Palmeiras e Forquilha da Mina III, Crixás. Anglo-Gold Ashanti, Relatório de Consultoria. 52 pgs. (inédito).

Jost H. & Oliveira A.M. 1991. Stratigraphy of the greenstone belts, Crixás region, Goiás, Central Brazil. *J. South Am. Earth Sci.,* **4**:201 -214.

Jost H. & Fortes P.T.F.O . 2001. Gold deposits and occurrences of the Crixás Gold Field, central Brazil. *Mineral. Depos.*, **36**:358-376.

Jost H., Oliveira A.M., Vargas M.C. 1992. Petrography, geochemistry, and structural control of trondhjemitic intrusions in greenstone belts of the Crixás region, Central Brazil. SBG, Congresso Brasileiro de Geologia, 37, São Paulo, *Resumos Expandidos*, 1:43-44.

Jost H., Carmelo A.C., Menezes P.R. 1994a. Litologias, relações de contato e estruturas do Bloco do Caiamar, Crixás, Goiás. *In*: SBG, Simp. Geol. Centro-Oeste,4, Brasília, *Resumos Expandidos*, p. 18-20.

Jost H., Brod J.A., Kuyumjian R.M. 1999. Aspectos Geoquímicos de metabasaltos do Greenstone Belt de Guarinos, Goiás. *Rev. Bras. Geoci.*, **29**:449-451.

Jost H., Theodoro S.M.C.H., Figueiredo A.M.G., Boaventura G.R. 1996. Propriedades geoquímicas e proveniência de rochas metassedimentares detríticas arquanas dos greenstone belts de Crixás e Guarinos, Goiás. *Rev. Bras. Geoc*. **26**:151-166.

Jost H., Sial A.N., Bennel M.R., Ferreira V.P. 2008. Carbon isotopes in dolostones of the Goiás State greenstone belts, Central Brazil. *In*: SBG, Congr. Bras. Geol., 44, Curitiba, *Boletim de Resumos*, pg.687.

Jost H., Vargas M.C., Fuck R.A., Kuyumjian R.M., Pires A.C.B. 1994b. Relações de contato, litologias, geologia estrutural e geofísica do Bloco Arqueano do Moquém, Crixás, Goiás. *In*: SBG, Simp. Geol. Centro-Oeste, 4, Brasília, *Resumos Espandidos*, p. 15-17.

Jost H., Pimentel M.M., Fuck R.A., Danni J.C., Heaman L. 1993. Idade U-Pb do Diorito Posselândia, Hidrolina, Goiás. *Rev. Bras. Geoc.,* **23**:352-355.

Jost H., Dussin I.A., Chemale Jr. F., Tassinari C.C.G., Junges S. 2008. U-Pb and Sm-Nd constraints for the Paleoproterozoic age of the metasedimentary sequences of the Goiás Archean greenstone belts. South Am. Symp. Isotope Geol., 6, San Carlos de Bariloche, Argentina, *Proceedings*, 4 pgs.

Jost H., Chemale Jr. F., Dussin I.A., Tassinari C.C.G., Martins R. 2010. A U–Pb zircon Paleoproterozoic age for the metasedimentary host rocks and gold mineralization of the Crixás greenstone belt, Goiás, Central Brazil. *Ore Geol. Rev.*, **37**:127-139.

Jost H., Fuck R.A., Brod J.A ., Dantas E.L., Meneses P.R., Assad M.L.L., Pimentel M.M., Blum M.L.B., Silva A .M.,

Spigolon A .L.D., Maas M.V.R., Souza M.M., Fernandez B.P., Faultish F.R.L., Macedo Júnior P.M., Schobbenhaus C.N., Almeida L., Silva A.A.C., dos Anjos C.W.D., Santos A.P.M.R., Bubenick A.N., Teixeira A.A., Lima B.E.M., Campos M.O., Barjud R.M., Carvalho D.R., Scislewski L.R., Sarli C.L., Oliveira D.P.L. 2001. Geologia de terrenos arqueanos e proterozóicos da região de Crixás-Cedrolina, Goiás. *Rev. Bras. Geoc.*, **31**:315-328.

Jost H., Fuck R.A., Dantas E.L., Rancan C.C., Rezende D.B., Santos E., Portela J.F., Mattos L., Chiarini M.F.N., Oliveira R.C., Silva S.E. 2005. Geologia e geocronologia do Complexo Uvá, bloco arqueano de Goiás. *Rev. Bras. Geoc.,* **35**:559-572.

Jost H., Kuyumjian R. M., Freitas A.L.S., Costa A.L.L., Nascimento C.T.C., Vasconcelos F.M., Galotti L., Martins M.C.A., Carvalho M.N., Condé V.C. 1995. Geologia da porção norte do Greenstone Belt de Guarinos, GO. *Rev. Bras. Geoc.,* **25**:51-60.

Kopp R.E., Kirschvink J.L., Hilburn I.A., Nash C.Z. 2005. The Paleoproterozoic snowball Earth: A climate disaster triggered by the evolution of oxygenic photosynthesis. National Academy of Sciences of the United States of America, *Proceedings,* **102**:11131-11136.

Kuyumjian R.M. & Jost H., 2006. Low- and high-alumina komatiites of Goiás, Central Brazil. J*. South Am. Earth Sci*., **20**:315-326.

Langford F.F. & Morin J.A. 1976. The development of the Superior Province of northwestern Ontario by merging island arcs. *Amer. J. Sci*., **276**:1023-1034.

Mota-Araújo J.G.M. & Pimentel M.M. 2002. U-Pb ages and Sm-Nd isotopes and structural analysis of the Moiporá-Novo Brasil shear-zone system: the limits between Neoproterozoic Goiás Magmatic Arc and the Archean Uvá Complex, Tocantins Province, Central Brazil. In: South Am. Symp. Isotopic Geology, 4, Salvador, *Short Papers Volume*, pp.: 221-224.

Oliver N., Foster D., Jost H. 2005. Geological, geochemical and isotopic controls on gold mineralisation and implications for mining and exploration in the Crixás greenstone belt. AngloGold Ashanti Ltda., Interim Report, 72 pgs.

Petersen Jr. K.J. 2003. *Estudo das mineralizações dos corpos IV e V da estrutura IV do greenstone belt de Crixás (GO).* Tese de Doutorado, Intituto de Geociências, Universidade de São Paulo, 175 pp.

Pimentel M.M., Dardenne M.A., Fuck R.A., Viana M.G., Junges S.L., Fischel D.P., Seer H.J., Dantas E.L. 2001. Nd isotopes and the provenance of detrital sediments of the Neoproterozoic Brasília Belt, Central Brazil. *J. South Am. Earth Sci.*, **14**:571-585.

Pimentel M.M., Fuck R.A., Del'Rey Silva L.J.H. 1996. Dados Rb-Sr e Sm-Nd da região de Jussara-Goiás-Mossâmedes (GO) e o limite entre terrenos antigos do Macio de Goiás e o Arco Magmático de Goiás. *Rev. Bras. Geoc.*, **26**:61-70.

Pimentel M.M., Whitehouse M.J., Vianna M.G., Fuck R.A., Machado N. 1997. The Mara Rosa arc in the the Tocantins Province: further evidence for Neoproterozoic crustal accretion in central Brazil. *Prec. Res.,* **81**:299-310.

Pimentel M.M., Fuck R.A., Jost H., Ferreira Filho C.F., Araújo S.M. 2000. The basement of the Brasilia Fold Belt

and Goiás Magmatic Arc. In: U.G. Cordani, E.J. Milani, A. Fhomaz Filho, D.A. Campos (eds) *Tectonic Evolution of South America.* 31st International Geological Congress, pp.: 195-230.

Pimentel M.M., Jost H., Fuck R.A., Armstrong R.A., Dantas E.L., Potrel A. 2003. Neoproterozoic anatexis of 2.9 Ga old granitoids in the Goiás-Crixás block, Central Brazil: evidence from new SHRIMP U-Pb data and Sm-Nd isotopes. *Geologia USP*, Sér. Científica, **3**:1-12.

Piuzana D., Pimentel M.M., Fuck R.A., Armstrong R.A. 2003. SHRIMP U Pb and Sm Nd data for the Araxá Group and associated magmatic rocks: constraints for the age of sedimentation and geodynamic context of the southern Brasília Belt, central Brazil. *Prec. Res*., **125**:139-160.

Portocarrero J.L.T., 1996. *Geologia da jazida aurífera Mina Nova, greenstone belt de Crixás, Goiás*. Dissertação de Mestrado, Instituto de Geociências, Universidade de Brasília, 110 pp.

Potrel A., Resende M.G., Jost H. 1998. Transition in acid magmatismo during Archaean: example of the granito-gnaissic basement of the Goiás Massive. *In*: SBG, Congr. Bras. Geol., 40, *Anais*, pg. 69-70

Pulz G.M. 1990. *Geologia do depósito aurífero tipo Maria Lázara (Guarinos, Goiás).* Dissertação de Mestrado, Instituto de Geociências, Universidade de Brasília, 139 p.

Pulz G.M. 1995. *Modelos prospectivos para ouro em Greenstone Belts: O exemplo dos depósitos Maria Lázara, Guarinos e Ogó, Pilar de Goiás.* Tese de Doutoramento, Instituto de Geociências, Universidade de Brasília, 189p.

Pulz G.M., Jost H., Giuliani G., Michel D. 1991. The Archean Maria Lázara gold deposit, Goiás, Brazil: example of Au-Bi-Te-S metallogeny related to shear zones intruded by sinkinematic granitoids. *In*: Symp. BRAZIL GOLD 91. Belo Horizonte, *Proceedings*, Rotterdam, Balkema. p. 385-387.

Queiroz C.L. 2000. *Evolução Tectono-Estrutural dos Terrenos Granito-Greenstone Belt de Crixás, Brasil Central.* Tese de Doutorado, Instituto de Geociências, Universidade de Brasília, Brasília, 209 p.

Queiroz C.L., Jost H., McNaughton N.J., Silva L.C., 2008. U-Pb SHRIMP and Sm-Nd geochronology of granite-gneiss complexes and implications for the evolution of the Central Brazil Achean Terrain. *J. South Am. Earth Sci.*, **26**:100-124.

Resende M.G. & Jost H. 1994. Redefinição da Formação Aimbé, Greenstone Belt de Guarinos, Goiás e sua interpretação paleogeográfica e paleotectônica. SBG, *Bol. Geoc. do Centro-Oeste,* **17**:49-57.

Resende M.G. & Jost, H. 1995. Petrogênese de formações ferríferas e metahidrotermalitos da Formação Aimbé, Grupo Guarinos (Arqueano), Goiás. *Rev. Bras. Geoc.*, **25**:41-50.

Resende M.G. 1994. *Geoquímica e Petrologia da Formação Aimbé, Grupo Guarinos, Goiás*. Dissertação de Mestrado, Instituto de Geociências, Universidade de Brasília, 129 p.

Resende M.G., Jost H., Lima B.E.M., Teixeira A.A. 1999. Proveniência e idades-modelo Sm-Nd de rochas siliciclásticas arqueanas dos greenstone belts de Faina e Santa Rita, Goiás. *Rev. Bras. Geoc.*, **29**:281-290.

Jost H., Rodrigues V.G., Carvalho M.J., Costa R.T.C. 2011. Redefinição estratigráfica do greenstone belt de Guarinos, Goiás. (em revisão final), 25 pgs.

Sabóia L.A. de 1979. Os greenstone belts de Crixás e Goiás, Go. Sociedade Brasileira de Geologia Núcleo

Centro-Oeste, *Boletim Informativo*, 9, pp. 44-72.

Santos R.V., Oliveira C.G., Souza V.H.V., Carvalho M.J., Andrade T.V., Souza H.G.A. 2008. Correlação isotópica baseada em isótopos de Carbono entre os greenstone belts de Goiás. In: SBG, 44 Congresso Brasileiro de Geologia, Curitiba, *Volume de Resumos*, pg. 52.

Schlanger S. & Jenkyns H. 1976. Cretaceous oceanic anoxic events: causes and consequences. *Geologie en Mijnbouw*, **55**:179-184.

Tarney J., Dalziel I.W.D., de Wit M.J. 1976. Maginal basin “Rocas Verdes” complex from S. Chile: a model for Archean greenstone belt formation. *In*: B.F. Windley (ed.) *The early history of Earth*. Wiley, London, pp. 131-146.

Tassinari C.C.G., Jost H., Santos J.C., Nutman A.P., Bennell M.R. 2006. Pb and Nd isotope signatures and SHRIMP U-Pb geochronological evidence of Paleoproterozoic age for Mina III gold mineralization, Crixás District, Central Brazil. South Am. Symp. Isot. Geol., 5, Chile, *Proceedings*, 4 pgs.

Tomazzoli E.R. 1997. *Aspectos geológicos e petrológicos do enxame de diques Morro Agudo de Goiás*. Tese de Doutorado, Instituto de Geociências, Universidade de Brasília, 285 p.

Vargas M.C. 1992. *Geologia das rochas granito-gnáissicas da região de Crixás, Guarinos, Pilar de Goiás e Hidrolina*. Dissertação de Mestrado, Instituto de Geociências, Universidade de Brasília, 167p.

Viana M.G., Pimentel M.M., Whitehouse M.J., Fuck R.A., Machado N. 1995. O arco magmático de Mara Rosa, GO: geoquímica e geocronologia e suas implicações regionais. *Rev. Bras. Geoc.*, **25**:111-123.

PARTE II

THE CAIAMAR SODIUM EPISYENITE GOLD DEPOSIT, GUARINOS GREENSTONE BELT, CENTRAL BRAZIL

Artigo a ser submetido para publicação em periódico internacional

THE CAIAMAR SODIC EPISYENITE GOLD DEPOSIT, GUARINOS *GREENSTONE BELT*, CENTRAL BRAZIL

Vinícius Gomes Rodrigues[1], Hardy Jost[2] & Marcelo Juliano de Carvalho[1]

1 – Yamana Gold Inc., Avenida Principal, nº 250, Qd. 01 Lt. 01 Sala 01 - Centro - 76.370-000, Pilar de Goiás, Goiás. E-mails: vgrodrigues@yamana.com, mcarvalho@yamana.com,
2 – Geoscience Institute, University of Brasília, P.O. Box 04465. 70919-970 Brasília, DF. E-mail: hmc_jost@opendf.com.br

Abstract The Caiamar gold deposit is located in Central Brazil and hosted by a sodic episyenite derived by hydrothermal alteration of a gabbro that intruded low-grade metamorphic supracrustal rocks of the Paleoproterozoic Guarinos greenstone belt. Hydrothermal alteration of the gabbro leads to the formation of an outer, intermediate, inner and an episyenite zone, each characterized by particular mineral paragenesis. Gold mineralization occurs both as a stockwork as well as dissemination in the episyenite and in the inner alteration zone, always associated with arsenopyrite. The main mineralogical association of the episyenite consists of albite, quartz and rare biotite, ilmenite, magnetite and disseminated arsenopyrite. From the gabbro to the episyenite a progressive gain in Na_2O took place. In detail, from the gabbro to the outer zone, alteration resulted in gain of Na_2O, MnO, K_2O, P_2O_5, Sr and Zr, with loss of MgO, CaO, Fe_2O_3, TiO_2, Ba, Co, V and Ni, while SiO_2, Rb, Y and HREE remained immobile. From the outer to the intermediate zone, alteration resulted in gain of K_2O, Na_2O, SiO_2, P_2O_5, Ba, Rb, Y, Zr and LREE, with Al_2O_3 and HREE remaining immobile. Maximum potassium alteration occurs at the intermediate zone indicated by continuous increase in the amount of biotite. From the intermediate to the inner zone, alteration resulted in gain of CaO, Fe_2O_3 and MgO, due to the deposition of ankerite, and part of Fe_2O_3 represented by disseminated arsenopyrite, as well as of TiO_2, P_2O_5, V and Sr, and loss of K_2O, MnO, Zr and Rb, with SiO_2, Al_2O_3, Y, Ni, LREE and HREE remaining immobile. From the inner zone to the episyenite maximum gains occurred in Na_2O, followed by Al_2O_3, Zr, Y and LREE, with massive loss of MgO, CaO, K_2O, Fe_2O_3, TiO_2, MnO, Ba, Sr, Rb, Co and V, with SiO_2, Ni and HREE remaining immobile. Increasing hydrothermal alteration resulted in progressive enrichment in REE towards the episyenite, with pronounced enrichment in LREE, as compared to HREE. Geological, geochemical, mineralogical and petrographic evidence suggest that the origin of the sodic episyenite can be related to the action of metassomatic processes by circulation of later fluids through the volcanosedimentary sequence of the greenstone belt, probably derived from a hidden intrusion as indicated by geophysical data. Gold mineralization took place in at least two phases, an early phase is represented by the gold-arsenopyrite association that occurs in the inner alteration zone and as dissemination within theepisyenite, and a late phase formed during an open system responsible for the mineralized stockwork. The statistics of chip-samples of the ore zone indicates that its geochemical signature is given by the association Au-S-Se-Sb-Ag-Te-As, in decreasing order of correlation. Investigation of the sulfur isotopes from several samples of sulfides show that $ä^{34}S$ of arsenopyrite disseminated in the episyenite lies between 2.67‰ and -3,25‰, suggesting that sulfur was provided by an igneous source during the formation of the episyenite, whilst the $ä^{34}S$ of the other samples varies from -5,20‰ to -8,82‰, indicating a local sedimentary sulfur source. Geochronological U-Pb zircon data yielded a 729 ± 15 Ma age for the episyenite.

Keywords: Caiamar deposit, Central Brazil, Gold, sodic episyenite, geochemistry, geochronology

Introduction

Episyenite (Leroy, 1978) designates udersaturated rocks that resulted from the dissolution of SiO_2 at a mineralization site by hydrothermal alteration followed by potassium or sodium metassomatism. These rocks are more commonly known to host either Uranium (e.g. Leroy, 1978; Ruzicka, 1993; Dahlkamp, 2009), or Tin deposits (e.g. Costi *et al*., 2002; Borges *et al*., 2009), but gold deposits hosted by sodic episyenites are considered as a rare and atypical style of mineralization and seldom described in the literature (e.g. Theodore *et al*., 1987; Thorette *et al*., 1990; Jébrak, 1992; Witt, 1997).

Known gold mineralization in the Archean-Paleoproterozoic low-grade metamorphic greenstone belts of Central Brazil occurs either as massive sulfide deposits, quartz vein or disseminated ore bodies (Yamaoka and Araújo, 1988; Jost and Fortes, 2001), structurally controlled by moderate to low-angle thin-skinned thrust faults hosted by metasedimentary rocks, particularly carbonaceous phyllites, or at the contact between metabasalts and metasedimentary rocks. Recent exploration undertaken by Yamana Gold Inc. in the northern portion of the Archean-Paleoproterozoic crustal segment of Central Brazil lead to the recognition of a Gold deposit hosted by a sodium episyenite derived from hydrothermal alteration of a gabro intrusion and known as the Caiamar deposit, located in the northern portion of the Guarinos greenstone belt (Figure 1). This paper describes the petrographic, geochemical and isotopic characteristics of the gabbro intrusion, its hydrothermal alteration zones and those of the Au-bearing episyenite, as well as geophysical data that lead to a possible intrusion that may have driven the hydrothermal system. Due to the rarity of such a deposit, major emphasis was given to the geochemistry of the alteration zones.

Geologic setting

The Archean-Paleoproterozoic terrain of Central Brazil consists of five low-grade, allochthonous greenstone belts separated by granite-gneiss complexes. The northern part of the terrain includes three N–S-trending greenstone belts designated, from West to the East, as Crixás, Guarinos and Pilar de Goiás (Figure 1). The Guarinos greenstone belt, which hosts the Caiamar Gold deposit, is 40 km long with a 6 km average width, has a North-South triangular shape that gradually narrows towards the North. It is limited to the West by 2.85 Ga tonalite to granodiorite gneisses and to the East by 2.75 Ga granite-granodiorite gneisses (Queiroz *et al*., 2008). To the North it is overlain by thrusted metavolcano-sedimentary sequences that belong to the Mara Rosa Arc and to the south by metasedimentary rocks of the Araxá Group, both of Neoproterozoic (Pimentel et al., 2000).

The first stratigraphic model for the Guarinos greenstone belt was proposed by Danni & Ribeiro (1978), further detailed by Jost and Oliveira (1991) and renaimed as Guarinos Group. The group consists of a lower sequence of metakomatiites followed by tholeiitic metabasalts, and an upper sequence of carbonaceous phyllites,

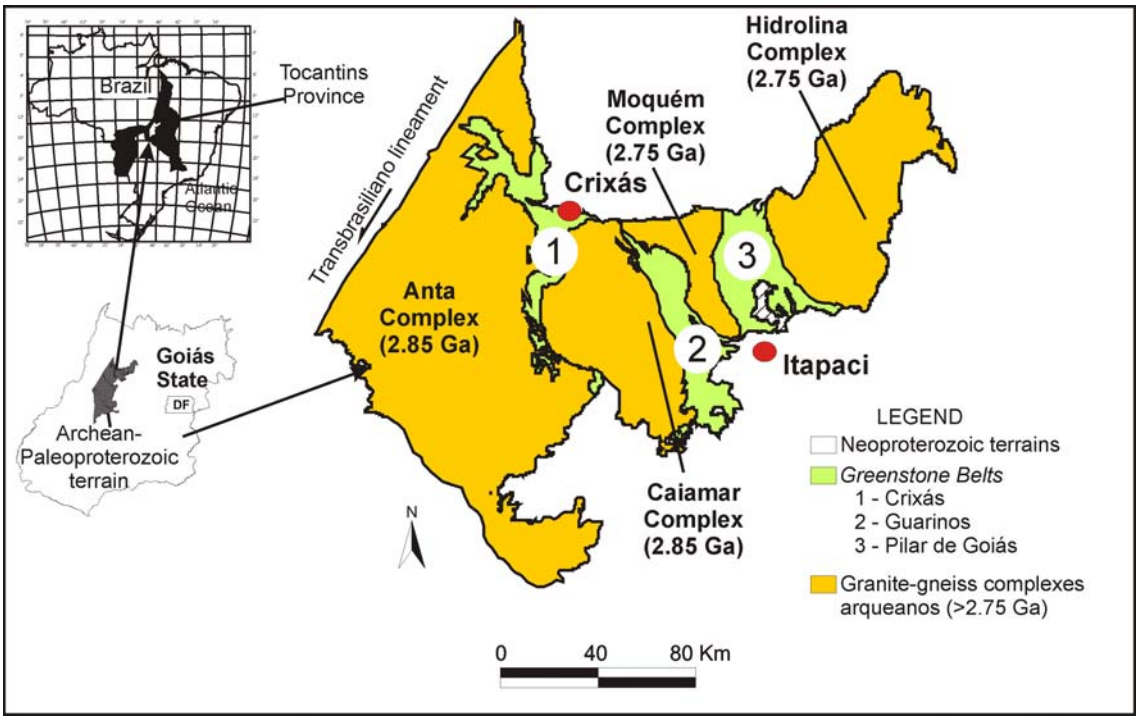

Figure 1 – Location and subdivision of the northern portion of the Archean-Paleoproterozoic terrain of Central Brazil.

metagraywackes, BIF´s and gondites (Figure 2). In outcrop, the metamorphic foliation (Sn) is parallel to the volcanic and sedimentary bedding (So) and the variation in the attitude of Sn//So describes a complex folding system that varies from a branched open antiform and sinform with a vertical axial surface in the South to a westerly dipping, narrow and tight sequence of antiforms and sinforms in the North. In the Northeast, Sn//So contours the Santo Antônio Trondhjemite, around which the structure is a westerly dipping and duble-plunging brachiantiform.

A set of N10°W,30°SW dextral splay-faults cuts the greenstone belt longitudinally. The main fault and its splays are subparallel to slightly diagonal to Sn//So and are responsible for delamination, suppression and repetition of the stratigraphic sequence. The main fault is approximately situated at the middle of the belt within the sedimentary sequence, well marked by high-strain zones, drag-folds and hosts tabular to rounded granodiorite and gabbro intrusions less then 2 sq. km, one of which contains the Caiamar deposit.

In situ zircon U-Pb geochronological data from samples of a magnetite-bearing iron formation obtained by Jost et al. (2008) and from turbidites that underlie and overlie the iron formation by Jost *et al.* (2010, 2011) contained two magmatic populations that differ in age. The youngest and most abundant populations yielded upper intercepts at 2,232 ± 36 Ma, 2,180 ± 30 Ma and 2,176 ± 11 Ma, respectivelly, indicating that the main source-area was Paleoproterozoic. The oldest and more rare population is as old as 3.4 Ga thus indicating that part of the source-area was Archean.

Historical review

The Caiamar deposit was discovered during Brazil's Gold Cycle in the mid XVIII century by Portuguese settlers, by panning active sediments of a creek about 1 km to the East of the deposit. Gold production began in a

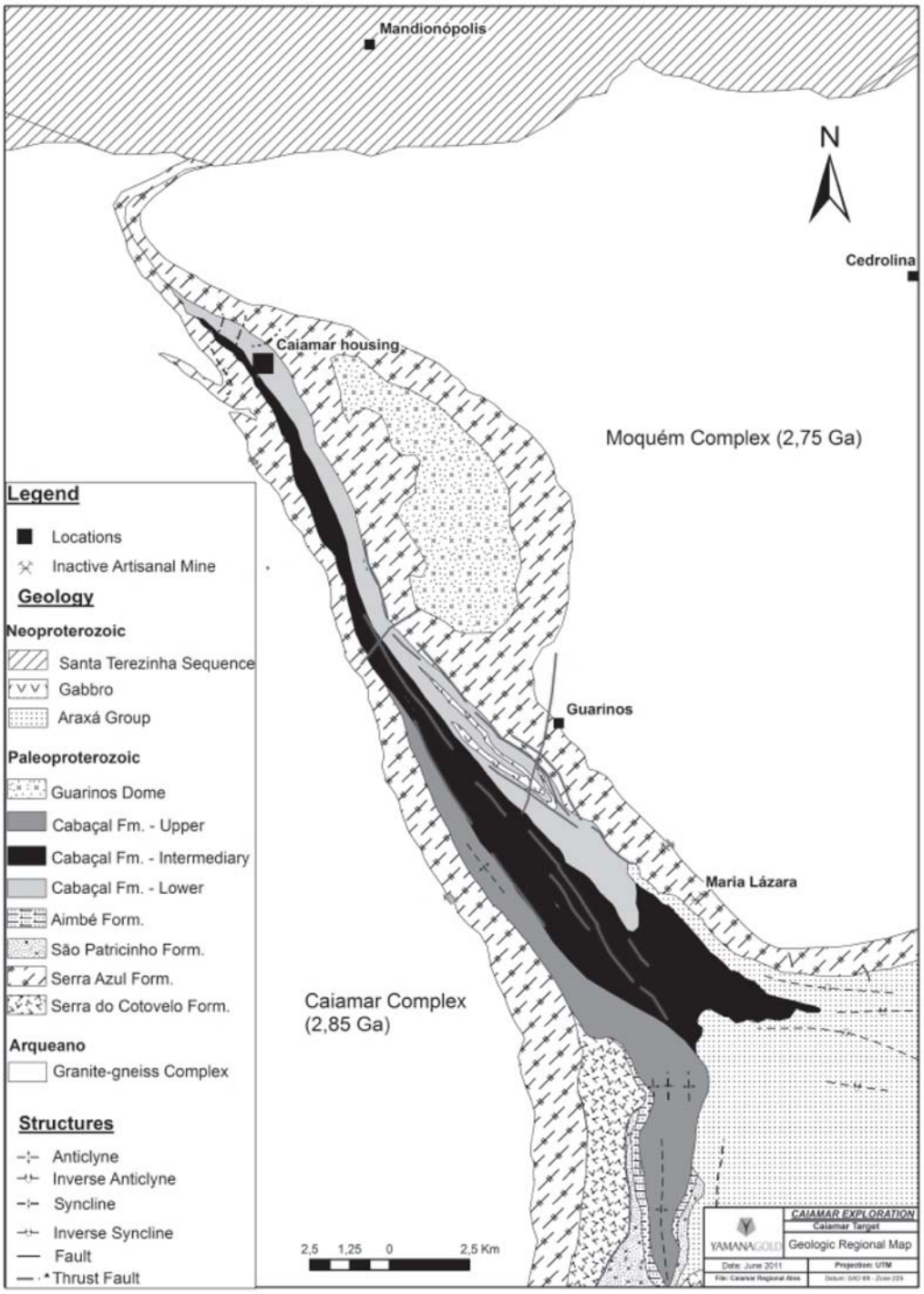

Figure 2 – Geologic sketch of the Guarinos greenstone belt.

local gravel terrace near the primary ore and progressed as open-pit in the oxidation zone and into primary ore. There is no record of production between the end of the XVIII century and the onset of 1990 Mr. Paulo Hertz acquired the exploitation rights, opened a 150-m deep shaft and two galleries in primary ore, one at the 55-m and another at 110-m deep levels. Mineração Serra Formosa Ltd. was then founded and the company drilled a few holes at maximum 200-m deep in an area restricted to the nearness of the portuguese workings, with simultaneous geologic mapping of the galleries and definition of the main ore geometry. During the 1990 the deposit was evaluated by several minin g companies, but the erratic nature of the ore-bodies, the discontinuous Gold grades,

the metal market price at that time and the scarce data did not fulfill the production criteria and aims of those companies. By March 2009, the exploration rights of Mineração Serra Formosa were transferred to Yamana Gold Inc.

Until then, Lacerda (1991) interpreted the deposit as hosted by a NS/45°W sheared biotite gneiss. However, during 2009 and 2010, a 40,586-m drilling program, sampling, assaying and 1:500 geologic mapping program of the galleries was undertaken by Yamana Gold Inc. The drilling program added to petrographic description of samples from one drill-hole taken as reference lead to the recognition that the mineralization is hosted by a sodic episyenite, which is one of the hydrothermal alteration zones of a gabbro intrusion. Updated results show that the so far known resources of the deposits are about 300,000 Oz of Gold, at 5g/t.

Deposit description

The gabbro and its hydrothermal alteration zones occur as a sigmoid-shaped body intruded into a N20°W,30°SW sheared contact between easterly metabasalts and westerly metasedimentary rocks and is parallel to the local structure of the supracrustal rocks (Figure 3). Data from drill-holes and surface mapping indicate that the intrusion is about 4.500-m long and divided into a western section up to 250-m wide and an eastern section 300-m wide, separated by carbonaceous phyllites interpreted as a roof-pendant. The unaltered gabbro (Figure 4A) is 80-m wide and gradually gives place to a 3-m to 15-m outer alteration zone (Figure 4B), which grades into a 50-m intermediate zone characterized by a quartz-biotite-albite schist (Figure 4C) in sharp contact with a 5-m inner zone of arsenopyrite and gold-bearing quartz-biotite-albite-ankerite schist (Figure 4D). The inner zone is in sharp contact with an undeformed Au-bearing sodic episyenite about 1-km long, in the average 2-m wide (Figure 4E) and known at least to 150 m in depth.

Drill-holes CA-87, CA-81 and CA-81C (see Figure 3 for location) were selected for sampling and petrographic studies as well as whole-rock chemical analysis. Amongst the drill-holes, CA-87 crosscuts the sequence orthogonally, was selected as the best lithologic section and used as reference for detailed petrographic studies and whole-rock geochemistry. The drill-hole exposed a sequence of carbonaceous phyllites interlayered with meter-wide metagraywacke until the contact with the gabbro, at 62.05-m deep. The gabbro and its hydrothermal alteration zones extend until 152.20-m, where they are bound by the contact with a metapelite. The mineralized episyenite occurs from 146.38-m to 147.68-m. Two intervals of carbonaceous phyllites occur at 102-m to 105.60-m and 124.65-m to 139.55-m, and are interpreted as roof-pendants due to their partial contact metamorphic recrystallization. Therefore, the representative rock sequence of interest was about 71-m long and subdivided on petrographic criteria into gabbro (20-m), and outer (15-m), intermediate (33-m), and inner (3-m) hydrothermal alteration zones, followed by a 2-m wide sodic spisyenite. Along this section, 11 samples of gabbro, 10 of the outer zone, 15 of the intermediate zone and 9 of the inner zone, all free of veinlets, were collected for detailed studies, thus representing about 1 sample for each 1.5-m of drill-core (Figure 5). The mineralized sodic episyenite was sampled on drill-holes CA-81 and CA-81C, both along plunge, and from where 8 and 9 samples were respectively

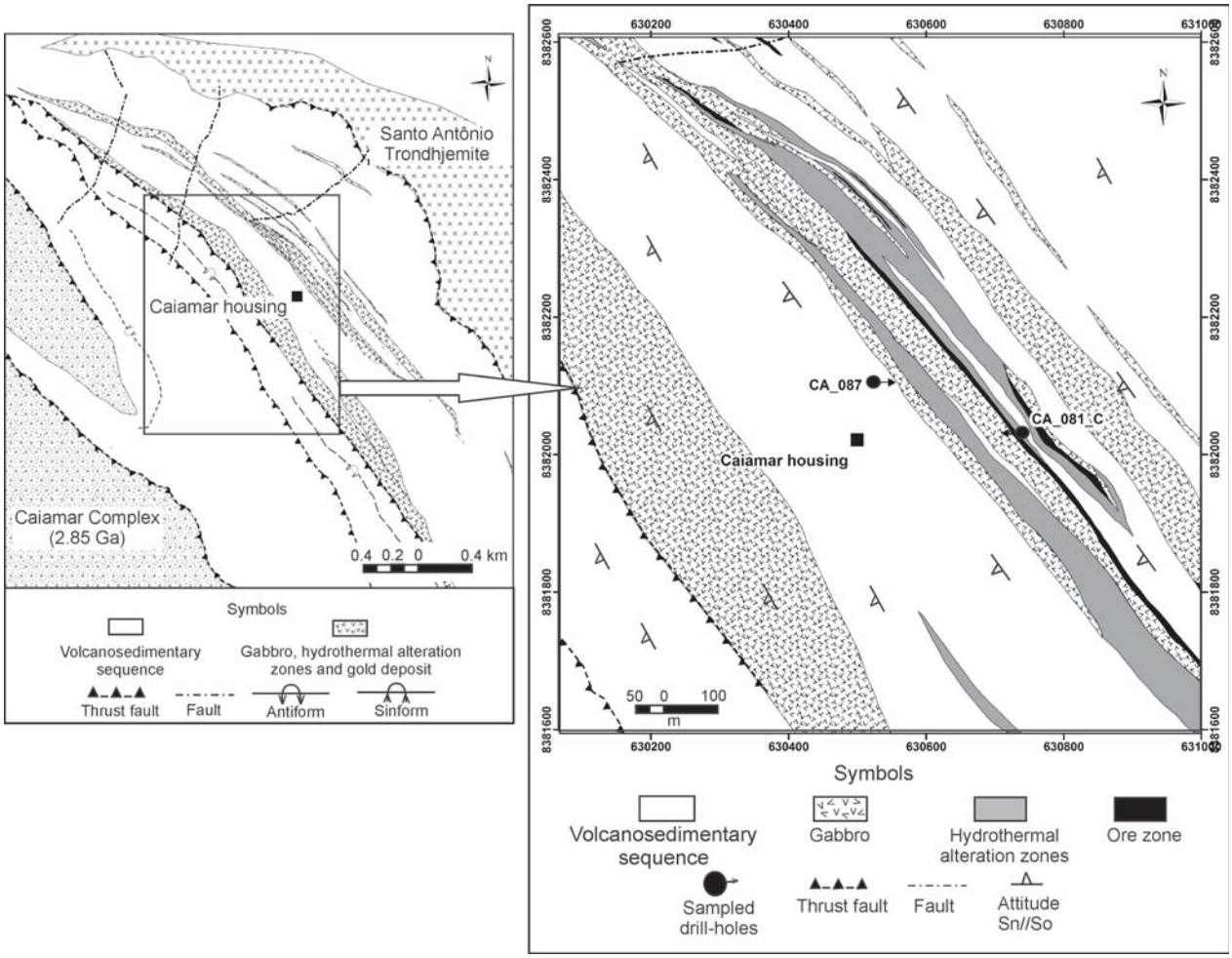

Figure 3 – Detailed geologic map around the Caiamar deposit.

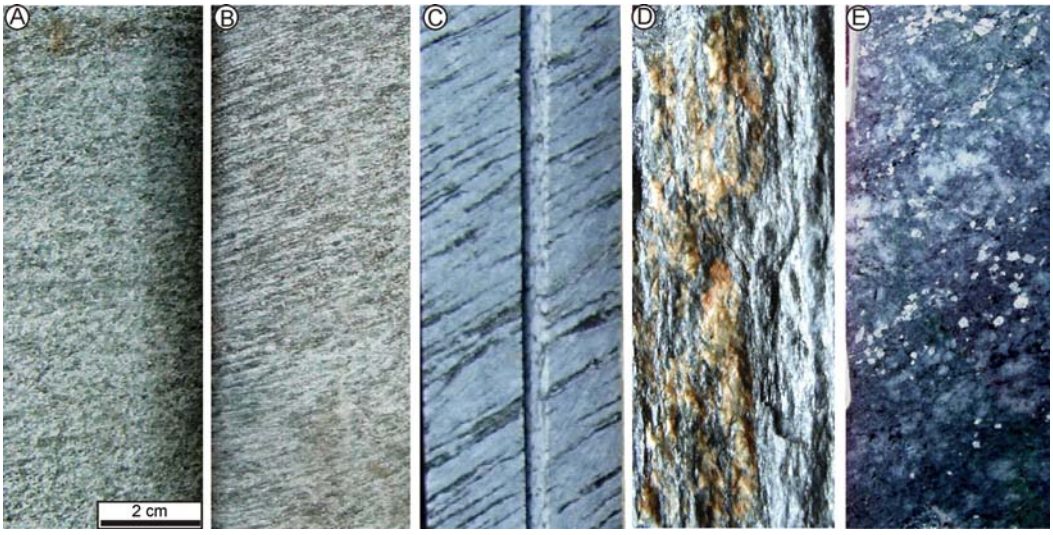

Figure 4 – Drill-cores that show the increasing hydrothermal alteration sequence from the gabbro to the sodic episyenite. A – Gabbro. B - Outer alteration zone. C – Intermediate alteration zone. D – Inner alteration zone. E – Sodic episyenite.

Sample	Depth (m)	Rock
	62,05	Carbonaceous phyllite
1	62,40-62,50	Gabbro
2	63,10-63,20	
3	64,10-64,20	
4	64,80-64,90	
5	65,95-66,05	
6	66,60-66,70	
7	67,50-67,60	
8	68,80-68,90	
9	69,80-69,90	
10	71,20-71,30	
11	72,50-72,60	
12	73,40-73,50	Outer zone
13	74,90-75,00	
14	76,50-76,60	
15	77,80-77,90	
16	79,60-79,70	
17	80,80-80,90	
18	81,80+81,90	Intermediate zone
19	82,95-83,15	
20	84,30-84,40	
21	86,25-86,35	
22	87,70-87,85	
23	89,15-89,30	
24	91,50-91,70	
25	93,80-94,00	
26	95,80-95,95	
27	97,70-97,90	
28	99,50-99,70	
29	100,20-100,35	Outer z.
30	101,30-101,40	Interm. z.
	102,00-105,60	
31	105,70-105,85	Interm. z.
32	110,50-110,75	Outer z.
33	112,40-112,60	
34	115,20-115,40	
35	123,80-124,00	Interm. z.
	124,65-139,55	
36	140,15-140,35	Interm. z.
37	141,50-141,70	Inner zone
38	143,30-143,35	
39	144,50-144,70	
40	145,50-145,70	
41	146,10-146,30	
	146,38-147,68	**Episyenite**
42	147,95-148,20	Inner zone
43	149,10-149,30	
44	150,50-150,70	
45	151,40-151,55	
	152,20	Metapelite

Drill-hole Sample	Depth (m)
CA-081	
81A	62,25-62,45
81B	74,30-74,45
81C	75,50-75,75
81D	76,55-76,75
81E	77,50-77,70
81F	80,90-81,10
81G	83,30-83,50
81H	97,70-97,90
CA-081C	
81CA	5,90-6,10
81CB	7,00-7,20
81CC	8,50-8,70
81CD	9,50-9,70
81CE	10,50-10,70
81CF	11,70-11,90
81CG	19,50-19,70
81CH	22,60-22,80
81CI	27,30-27,50
CAB	Stock-pile
CAC	
CAX	

Figure 5 – List of samples from the CA-87, CA-81 and CA-81C drill-holes of the Caiamar deposit used for petrographic and whole-rock chemical analysis with indication of the mesoscopically interpreted rock sequence and depth of sampling. See Figure 3 for location of the drill-holes.

collected, in additon to three samples from the ore stock-pile (Figure 5).

Petrography

Gabbro

The parallel position of the gabbro within sheared supracrustal rocks indicates that the structural control of the intrusion was a North-South trending fault. The presence of carbonaceous phyllites xenoliths and roof pendants suggest that the intrusion regime was probably by magmatic stoping. Thermal effects on the enclosing metasedimentary rocks have only been detected in drill-cores by the silicification and mica recristallization in the xenoliths. Reciprocal effects of the carbonaceous phyllites onto the gabbro occur within a few centimeters from

the contact and comprise a loss of cohesion and change of colour from dark-green to yellowish due to the alteration of hornblende into actinolite and plagioclase into white mica and clinozoisite.

In hand sample the gabro is dark-green, massive, locally with a faint foliation, fine to medium-grained and locally contains late quartz-carbonate or amphibole-rich veinlets. Undeformed samples (Figure 6A) have an idiomorphic to hypidiomorphic intergranular to subophitic texture, and deformed specimens have nematoblastic to granoblastic, lepidoblastic, porphyroblastic or porphyroclastic textures. On the average, major minerals comprise 45% plagioclase, 25% hornblende, 10% quartz, 15% ilmenite + magnetite, 5% garnet and traces of apatite, zircon and epidote. Mg-chlorite, white mica, biotite and carbonate are rare secondary phases.

Plagioclase occurs as anedral to subhedral, clean and untwined albite intergrown with tiny white mica, clinozoisite, carbonate, and locally garnet. The amphibole crystals are subhedral to anedral, with olive-green to green and yellowish-green pleocroism, extinction angle of 18°, typical of hornblende, probably hastingsite, partially

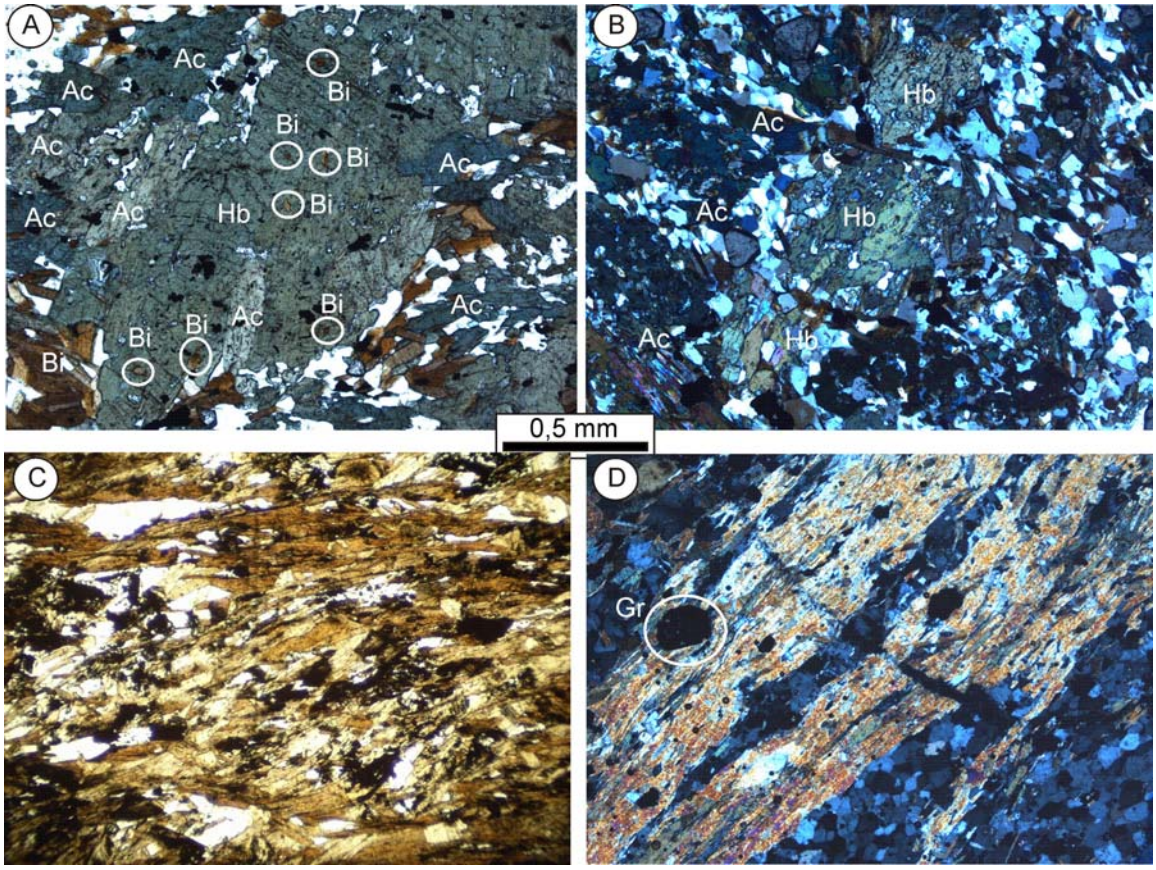

Figure 6 – Photomicrographs of the Caiamar deposit gabbro and hydrothermal alteration zones. A – Undeformed gabbro with hornblende (Hb) containing poikilitic inclusions of quartz and overgown biotite (Bi), in a finner matrix of albite, quartz and actinolite (AC). Plane-polarized light. B – Specimen of the outer hydrothermal alteration zone that shows hornblende (Hb) porphyroclast with pull-apart fractures and partialy re-requilibrate to actinolite (AC) in a very fine-grained quartz, albite and biotite matrix. Plane-polarized light. C - Specimen of the intermediate hydrothermal alteration zone dominated by biotite with a quartz + albite interstitial matrix. Plane-polarized light. D – Specimen of the inner hydrothermal alteration zone that shows the common sericitic alteration. Cross-polarized light. Hb = hornblende, Ac = actinolite, Bi = biotite, Gr = garnet.

replaced by biotite and, in deformed specimens, by Fe-actinolite. Quartz occurs as two textural varieties. One as rounded poikilitic inclusions in amphibole and the other as millimetric grains intergown with albite. The poikilitic quartz inclusions suggest that the amphibole may have derived by uralitization of a former pyroxene. Ilmenite and magnetite commonly occur as euhedral inclusions in hornblende and in rare biotite. Garnet is euhedral, clean and seldom zoned given by a clean core surrounded by a rim with submilimetric quartz and ilmenite/magnetite inclusions. Scaning electronic microscope EDS data indicate that the mineral is andradite, interpreted as resulting from a contact metamorphism event of the gabbro before its incipient hydrothermal alteration represented by biotite and carbonate. We estimate that the garnet formed by a thermal reaction between plagioclase and the original pyroxene. Mg-chlorite is an alteration product of hornblende and biotite, whereas carbonate formed through the alteration of albite and hornblende. Apatite, zircon and epidote are interstitial phases. The presence of biotite formed after hornblende and the prevalence of albite instead of labradorite indicate that even the freshest gabbro samples where affected by an incipient potassic-sodic hydrothermal alteration. The occurrence of andradite in the gabbro, as well in alteration zones and the episyenite, suggests that the rock-sequence underwent a late thermal metamorphism.

Outer hydrothermal alteration zone

Rocks of the outer zone vary from green to light-green, fine to medium-grained and contain a pervasive foliation that gradually increases in intensity from the gabbro inwards and given by trails of amphibole in a white quartz-feldspar matrix (see Figure 4B). This zone is locally cut by quartz or quartz-carbonate veinlets. The gradual increase of the foliation intensity is followed by significant textural changes as well as reactions that reduced the modal proportions of amphibole and increased those of plagioclase, quartz and biotite, without relevant modal changes of other minor minerals of the gabbro. The general texture is nematoblastic and granoblastic, subordinately porphyroclastic and porphyroblastic. Visually determined modal proportions from the 18 samples yielded 30-60% albite, 10-20% quartz, 4-20% biotite, 5-15% hornblende, 15% ilomenite + magnetite, about 5% garnet and traces of apatite, epidote, zircon, Mg-chlorite and carbonate.

Amphibole occurs in two textural varieties. The most abundant is part of the matrix and consists of bluish-green to light-green and yellowish-green pleocroic Fe-actinolite formed after hornblende porphiroclasts (Figure 6B). Both varieties contain rounded to platy inclusions of opaque minerals. Quartz occurs only as inclusions in hornblende. Plagioclase is the main component of the interstitial matrix and occurs as submilimetric, clean and untwined albite crystals intergrown with quartz and biotite, which, in turn, also derived from hornblende. Garnet is milimetric, euhedral, clean, white, unzoned and free of inclusions and, as in the gabbro, it also consists of andradite as determined by SEM EDS data.Chlorite is a rare alteration of biotite and its optical properties suggest that it consists of a Mg-rich variety. Opaque minerals occur either as part of the matrix or as inclusions in hornblende and biotite. They vary from platy, suggestive of ilmenite, to rounded crystals of magnetite. Zoisite and zircon are rare and interstitial in the matrix.

Intermediate zone

The contact between the outer and the intermediate zones is gradual and given by an increase in the amount of biotite, albite and quartz. Rocks of this zone are whitish, fine to medium-grained and contain a prominent pervasive foliation given by the orientation of biotite (see Figure 4C). The texture is granoblastic to lepidoblastic (Figure 6C), locally porphyroblastic. Visually determined modal proportions from the 14 samples yielded 25-45% albite, 14-34% quartz, 3-12% biotite, about 10% ilmenite + magnetite, 5% garnet and traces of apatite, epidote, zircon, Mg-chlorite and carbonate.

Albite is the main constituent of this zone and occurs as milimetric, anhedral to suhedral untwined crystals. Quartz occurs in three textural varieties. The most abundant consists of anhedral grains intergrown with albite, followed by tiny inclusions in biotite and within pressure shadows associated to garnet phenoclasts. Biotite is subhedral to anhedral, in general well oriented, is frequently choritized and overgrown on albite and garnet. Garnet occurs in two textural varieties distinguishable by size and internal deformation. Larger crystals have pressure shadows, are anhedral to subhedral, fractured and zoned with a core containing inclusions of albite, quartz, biotite and opaque minerals, an intermediate narrow rim with abundant tiny opaque inclusions, and a clean external rim. The smaller and less abundant variety is euhedral, does not have pressure shadows and fractures and is internally homogeneous. Both varieties consist of andradite, as determined by SEM-EDS.

Opaque minerals comprise ilmenite and magnetite, both occurring as inclusions in biotite or as disseminate phases. Apatite is rare, submillimetric and occurs either as isolated crystals or as trails along the foliation. Chlorite is of the Mg-rich variety and formed after biotite. Carbonate formed at the expenses of albite or is a component of pressure shadows.

Inner zone

The transition from the intermediate to the inner zone is gradual across a few centimeters and is marked by an increase in the proportions of quartz and by the first appearance of ankerite (see Figure 4D), white mica, as well as coarse-grained arsenopyrite, pyrrhotite and pyrite disseminated along the foliation (Figure 7A), followed by a decrease in the amount of biotite. This zone is also characterized by the occurrence of discontinous and centimetric fractures transversal to the foliation, which suggests the overprinting of an open fracture system (Figure 7B). Common features are millimetric to centimetric quartz-carbonate veinlets, locally folded and delaminated, and quartz, albite and siderite pegmatoid pods with discontinuous millimetric biotite-rich rims (Figure 7C). Where the inner zone contains gold, it is considered part of the ore.

The texture of samples from this zone is granoblastic to lepidoblastic, locally porphyroblastic. Visually determined modal proportions from 10 samples show that they contain 40-50% albite, 20-25% quartz, 5-15% biotite, about 10% ilmenite + magnetite, 5% garnet, 5% white mica, 8% carbonate, about 5% arsenopyrite and traces of apatite, epidote, zircon and Mg-chlorite.

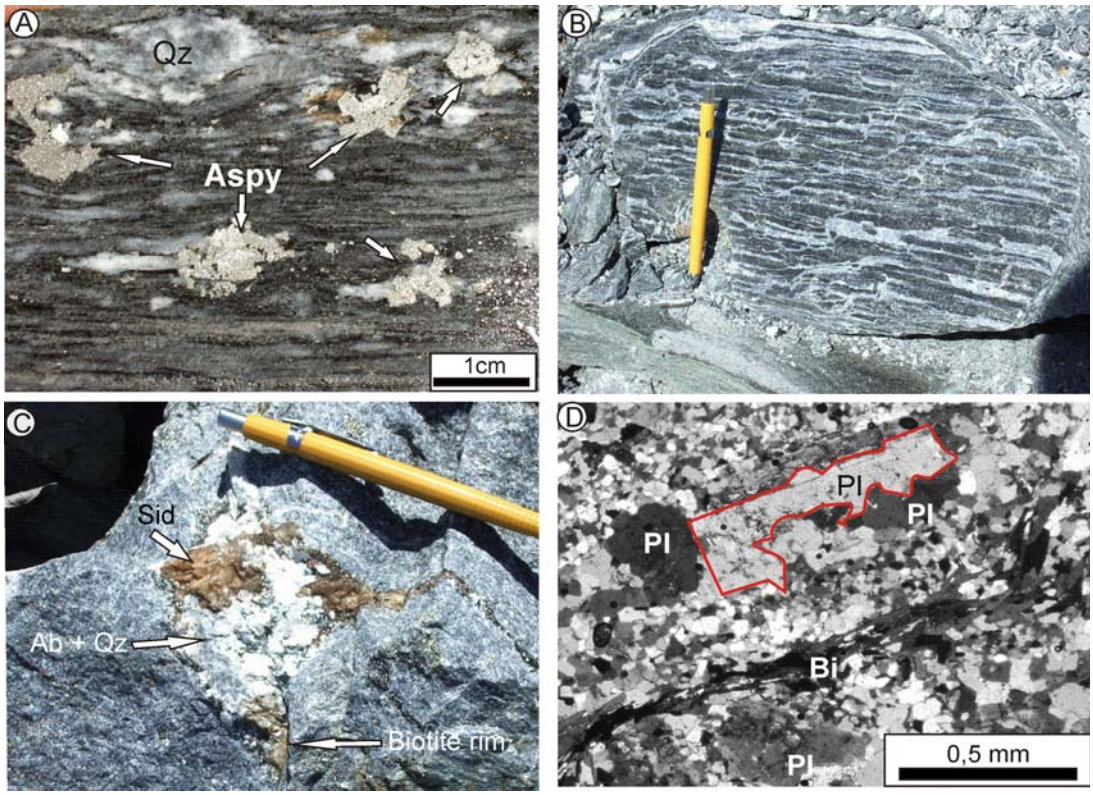

Figure 7 – Features of the inner hydrothermal alteration zone of the Caiamar deposit. A – Hand-sample that shows coarse-grained arsenopyrite disseminated along the foliation. B – Foliated hand sample overprinted by open, transversal and discontinous fractures. C – Hand-sample with a coarse-grained quartz + albite + siderite pod rimed by a discontinuous and tiny biotite-rich zone. D – Photomicrograph of a specimen that shows an irregular albite porphiroblast in the fine-grained albite + quartz matrix. Cross-polarized light. Pl = albite, Bi = biotite.

Albite occurs in two textural varieties. The most abundant is a component of the matriz and similar to that in the outer and intermediate zones. Another variety consists of euhedral to subhedral, up to 1.5-mm long, partially twinned phenoblasts with inclusions of quartz, albite and opaque minerals from the matrix, which indicates neoformation by late metasomatic blastesis (Figure 7D).

Quartz occurs as anhedral to subhedral grains intergrown with or as inclusions in albite. Biotite is commonly disposed in trails along the foliation, apparently formed beopre the albite porphyrobasts. Garnet is euhedral, millimetric andradite, free of internal structure, as determined by SEM-EDS. Arsenopyrite is a coarse-grained, up to 2 cm long, secondary phase either as isolated crystals or as aggregates along the foliation (see Figure 7A). Carbonate formed after albite and Fe-chlorite, and white mica after biotite. Epidote, apatite and zircon are rare.

Sodic episyenite

The sodic episyenite host the main gold mineralization and occurs as decimeter- to meter-wide dike-shaped body in sharp contact with the inner zone. It is dark- to light-gray, fine-grained, homogeneous, massive (see Figure 4E) and only locally foliated, which contrasts with the strongly foliated inner zone. Albite-quartz-white mica

with a biotite-rich rim pegmatoid pods are a common feature of the episyenite (Figure 8A).

Its texture is microporphyritic (Figure 8B) given by albite phenocrysts in a very fine-grained albite-quartz matrix. Modal data of 20 samples indicate that the albite content varies from 60% to 90%, while quartz, when present, may reach up to 15%. Minor minerals comprise garnet, arsenopyrite, ilmenite, magnetite, biotite and apatite. White mica, probably paragonite, carbonate and Fe-chlorite are minor secondary phases.

Albite occurs in two textural varieties. The most abundant consists of euhedral to suhedral, millimetric, and chess-board or Albite-law twinned phenocrysts (Figure 8B), either isolated or in glomeroporphyritic aggregates. X-Ray difratoctometry and SEM-EDS data of phenocrysts showed that they are low-albite. Locally, the phenocrysts underwent cominution, which may correspond to the mesoscopic narrow and episodic foliated zones seen in the galeries. The less abundant variety occurs as submillimetric, anhedral and untwinned crystals of the interstitial matrix.

Quartz, when present, is subhedral to anhedral, often ameboid, and intergrown with albite of the matrix. Biotite, also when present, is light- to dark-greenish yellow, either randomly oriented or as local undulated trails.

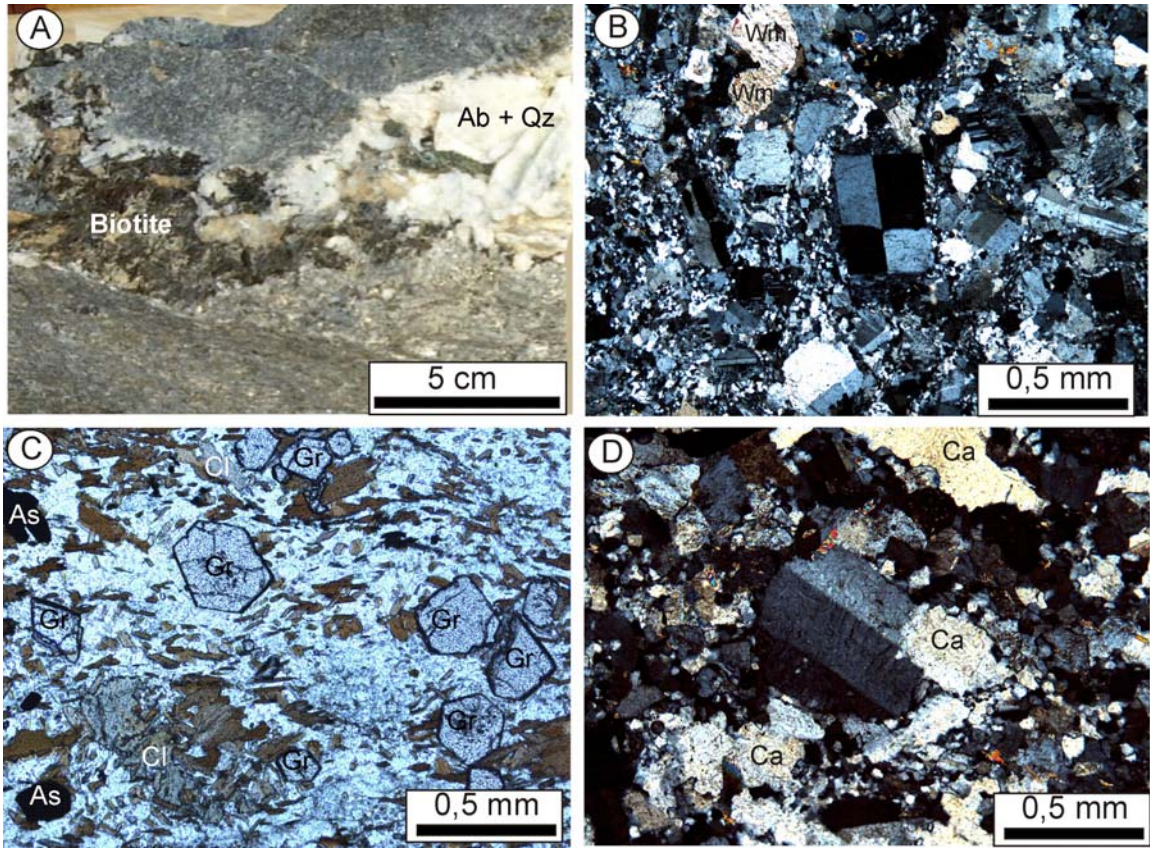

Figure 8 – Episyenite of the Caiamar deposit. A – Hand-sample that contains a quartz + albite + biotite pegmatoid pod. B – Photomicrograph that shows its microporphyritic texture given by twinned albite crystals, including chess-board twins (center of the image) in a very fine-grained albite + quartz matrix. Wm = white mica. Cross polarized light. C – Photomicrograph of a specimen with clean euhedral andradite crystals. Cl = chlorite; As = arsenopyrite. Plane-polarized light. D – Photomicrograph that shows partial replacement of albite by carbonate (Ca). Cross-polarized light.

Garnet is euhedral to suhedral, clean andradite (Figure 8C). Zircon occurs as tiny euhedral interstitial crystals or as inclusions in biotite. Opaque minerals are euhedral and consist of up to 5-mm long arsenopyrite and tiny ilmenite and magnetite crystals. Amongst the secondary phases, carbonate (Figure 8D), Fe-chlorite and paragonite (?) formed after albite and biotite. Paragonite (?), in particular, is frequent at the rims of the mineralized stockwork that crosscuts the episyenite.

Mineral paragenesis variation and metasomatic fronts

Textural and mineral proportions variations across the studied section allowed to recognize the mineral paragenesis for each hydrothermal alteration zone (Figure 9). The amount of hornblende of the gabbro decreases rapidly and does not belong to the paragenesis of the further alteration zones after about the middle of the outer zone. Labradorite is consumed still within most part of the section of the gabbro and was replaced by albite and andradite. The amount of quartz increases continuoulsy from the gabbro to the intermediate zone and from where it decreases towards the inner zone and the episyenite, almost followed by the variation of biotite, which attains maximum proportions in the intermediate zone. The amount of albite increases steadily until the intermediate zone from where it increases rapidly towards the episyenite. The combined variation of biotite and quartz suggests that maximum potassic alteration and silicification occurred in the intermediate zone and was replaced by sodium metassomatism towards the episyenite. Magnetite and ilmenite remain constant in less than 3% across the entire section. Carbonate is a rare phase in the outer and intermediate zones where it occurs as calcite/dolomite, which is replaced by ankerite in the inner zone, but is rare in the episyenite. The partial alteration of biotite into chlorite already occurs in the gabbro and extends towards the intermediate zone as the Mg-rich variety, and as Fe-chlorite from the inner zone to the episyenite. Pyrrhotite and pyrite are occasional phases only in the inner zone, with pyrrhotite occurring in the outermost portions and pyrite near the episyenite. This suggests that the outer portion of

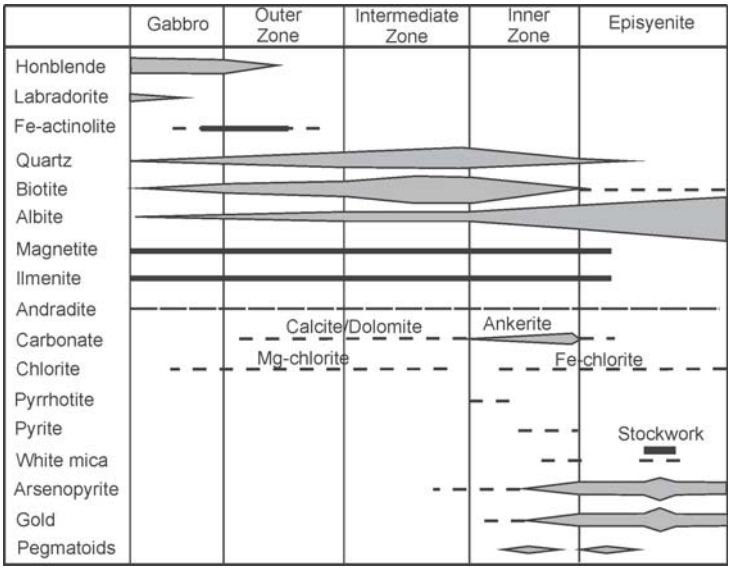

Figure 9 – Diagram of mineral compositional variation from the gabbro to the episyenite of the Caimar deposit.

the inner zone was hotter and sulfur defficient, in contrast with the inner portion, cooler and sulfur saturated. However, we did not determine whether pyrrhotite is hexagonal or monoclinic, which would better restrain the thermal conditions. White mica occurs only as an alteration phase at the margins of veins of the stockwork indicating phyllic alteration during the latest mineralization stages. Arsenopyrite + gold extend from the inner zone to the episyenite, either as dissemination or as part of the stockwork, where they attain maximum proportions. Disseminated arsenopyrite of the episyenite is considered as a phase that crystalllized during the formation of its host-rock. Quartz-albite ± arsenopyrite pegmatoid lenses are late phases of the hydrothermal alteration process. They are rare in the inner zone and may be abundant in the episyenite and predate the stockwork.

Bulk-rock Geochemistry

After the petrographic description, the 65 samples were sent for preparation and bulk-rock chemical analisys at the ALS Mineral Division Laboratory Group, Vancouver, Canadá, by means of the ME-ICP06 routine. Each sample had about 150 g from which a slab about 0.5-cm thick was cut for thin section, the remaining sent for chemical analysis. The average analitycal results for the gabbro, the outer, intermediate, inner alteration zones and the episyenite are in Table 1.

During the mesoscopic description and sampling of the CA-87 drill-cores and before receiving the whole-rock chemical data, we intepreted that the gabbro was exposed approximatelly along 20-m of core, represented by 11 samples lacking the conspicuous foliation taken as a typical feature of the outer alteration zone. The whole-rock chemical data allowed us to recognize that the composition of the 11 samples, in a TAS - Total Alkalis *versus* SiO_2 diagram (Figure 10), varied from gabbro to dioritic gabbro and diorite in response to the increase of alkalies due to progressive hydrothermal alteration. Considering that the Na_2O and K_2O contents of a normal gabbro are around 2,4% and 0,95%, respectively, we considered that only the first four samples of the section, farthest away from the outer zone, had Na_2O = 2.11% to 2.69% and K_2O = 0.33% to 1.7%, at 49.99% to 51.4% SiO_2 and, thus, could be considered as representing the freshest gabbro to support bulk-rock geochemistry and mass balance investigation. The remaining 7 samples were then interpreted as belonging to the external portion of the outer hydrothermal alteration zone because their Na_2O and K_2O contents are compatible with that zone, where Na_2O ranges from 3.2% to 4.51% and K_2O from 0.47% to 2.32%. However, for practical purposes during the description of the drill-cores, we recommend that the beginning of outer zone should be considered when the gabbro acquires a conspicuous and pervasive foliation.Therefore, in figure 5 only samples 1 to 4 are representative of the freshest gabbro and samples 5 to 11 of the external portion of the outer zone.

The SiO_2 proportions of the four freshest gabbro samples vary from 49.98% to 51.40%, Al_2O_3 from 14.53% to 14.77%, MgO from 5.33% to 6.56%, CaO from 6.52% to 9.19%, Fe_2O_3T from 14.30% to 16.70%, Na_2O from 2.11% to 2.69%, K_2O from 0.33% to 1.70%. The TiO_2 content lies between 1.43% and 1.54%, indicative that the gabbro belongs to the low-Ti mafic intrusion type. The mg# ([MgO/(MgO+Fe_2O_3)] is low and varies between 0.35 and 0.48, which, combined with the very low content of Ni (18 to 48 ppm) is uncompatible with a mafic magma

Table 1 – Whole rock average chemical results for the gabbro, the outer, intermediary, inner alteration zones and the episyenite of the Caiamar gold deposit. Major and minor element oxides in weight % and trace elements in ppm.

	Gabbro	Outer zone	Intermediate zone	Inner zone	Episyenite 1	Episyenite 2
n. samples	4	18	15	8	10	10
SiO_2	50.50	52.70	58.16	58.19	60.87	60.02
TiO_2	1.49	1.25	1.00	1.03	0.57	0.56
Al_2O_3	14.65	14.88	15.13	15.33	17.82	18.09
Fe_2O_3	15.65	13.53	10.64	10.08	6.15	5.97
MnO	0.22	0.28	0.28	0.18	0.09	0.09
MgO	5.79	4.85	2.61	2.22	0.67	0.75
CaO	7.60	6.48	4.18	4.85	1.84	1.92
Na_2O	2.44	3.76	4.00	5.17	8.87	9.08
K_2O	1.07	1.18	2.14	1.22	0.79	0.86
P_2O_5	0.20	0.22	0.33	0.39	0.09	0.14
LOI	0.42	0.87	1.53	1.34	2.33	2.39
Ba	561	512	741	500	266	293
Cs	2.94	3	26.31	3.48	0.59	0.70
Co	59	40	25	19	3	5
Cu	17	11	10	5	6	6
Ga	21	80	174	19	73	89
Hf	2.28	4	5.35	4.34	0.93	1.04
Nb	4	7	27	7	8.1	9
Ni	33	12	134	140	48	45
Pb	20	17	20	20	13	14
Rb	38	38	52	31	15	17
Sr	279	308	199	272	155	189
Ta	0.23	5	15	0.34	5	6
Th	1.94	8	21.53	3.24	9.92	11.13
U	0.83	1.5	5.08	1.18	1.92	2.15
V	483	190	10	4	7	8
W	4	3	50	9	3	4
Y	28	32	68	44	55	59
Zn	169	69	30	118	9	12
Zr	91.5	103	134	153	271	285
La	11.15	14.29	20.04	20.46	34.80	37.08
Ce	25.85	32.69	45.75	44.78	73.51	79.09
Pr	3.34	4.13	5.80	6.18	9.24	10.06
Nd	14.53	17.34	24.23	24.33	37.66	41.60
Sm	3.90	4.53	6.03	6.06	8.39	9.29
Eu	1.21	1.45	1.78	1.72	2.22	2.50
Gd	4.25	4.90	6.71	6.22	8.83	9.66
Tb	0.75	0.83	1.14	1.10	1.60	1.75
Dy	4.89	5.19	7.09	6.85	9.85	10.93
Ho	1.07	1.15	1.56	1.49	2.09	2.22
Er	3.14	3.45	4.67	4.32	5.93	6.40
Tm	0.48	0.56	0.75	0.66	0.94	0.99
Yb	3.14	3.69	4.99	4.30	6.28	6.41
Lu	0.47	0.56	0.74	0.65	0.96	0.96
CIPW norm						
Q	11.08	13.4113	19.92	18.29	11.28	-
C	-	-	2.48	1.67	0.15	-
Or	-	2.5	7.67	2.64	3.25	3.03
Ab	20.67	30	35.10	36.00	64.36	77.72
An	26.2	20	14.23	17.14	5.05	4.62
Bi	9.03	10	7.67	8.22	2.35	2.21
Hb	13.01	8	-	-	-	-
Ne	-	-	-	-	-	0.91
Wo	1.73	1.5	1.07	2.25	1.20	1.57
Il	0.47	0.5	0.57	0.49	0.23	0.14
He	15.7	13	9.93	11.23	6.65	5.54
Ap	0.47	0.5	0.83	0.86	0.30	0.23

derived from the mantle, which should have a mg# higher then 0,68 and Ni contentent between 300 ppm and 500 ppm. This suggests that the gabbro liquid may not be mantle derived, possibly representing a differentiate from a more primitive liquid.

Loss of ignition of the gabbro is low (0.27% to 0.66%) suggesting reduced hydration of the intrusion, despite its possible uralitic nature. Considering that the loss of ignition of 34 (90%) of the 41 samples from the outer to the inner hydrothermal zones the loss lies between 0.01% and 2.23%, and that only 7 samples (10%), of random occurrence in the three zones, it lies between 2.41% and 4.16%, we suggests that the hydrothermal system was fairly dry.

As shown in the $Na_2O + K_2O$ *versus* SiO_2 (Figure 10) from the four freshest gabbro samples there is a continous compositional variation that is due to hydrothermal alteration. On a chemical basis, that does not reflect a magmatic diferentiation, samples from the outer zones, which include those from the unsheared gabbro, plot as gabbroic diorite, along with two samples of the intermediate zone. Increasing alcalies content in the outer zones derive samples of monzo-diorite composition. The transition from the outer zone to the majority of the samples from the intermediate zone results of increasing SiO_2 and alcali, thus leading to diorite and granodiorite composition and, with increasing alcali, monzo-gabbro and monzonite. The transition from the intermediate to the inner zone resulted in a decrease of SiO_2 thus ploting as diorite and with increasing alcali derives samples of monzonite composition. Some samples of the episyenite plot as quartz-monzonite, while the majority as syenite, but at a SiO_2 content similar to the silica-rich samples of the intermediate zone, and as a result from the massive Na_2O metasomatism.

As shown in figure 11A to 11I, from the gabbro to all hydrothermal alteration zones the Al_2O_3 and Na_2O values increase with SiO_2, but the sodic episyenite plots as separate high Al and Na clusters, which indicates a

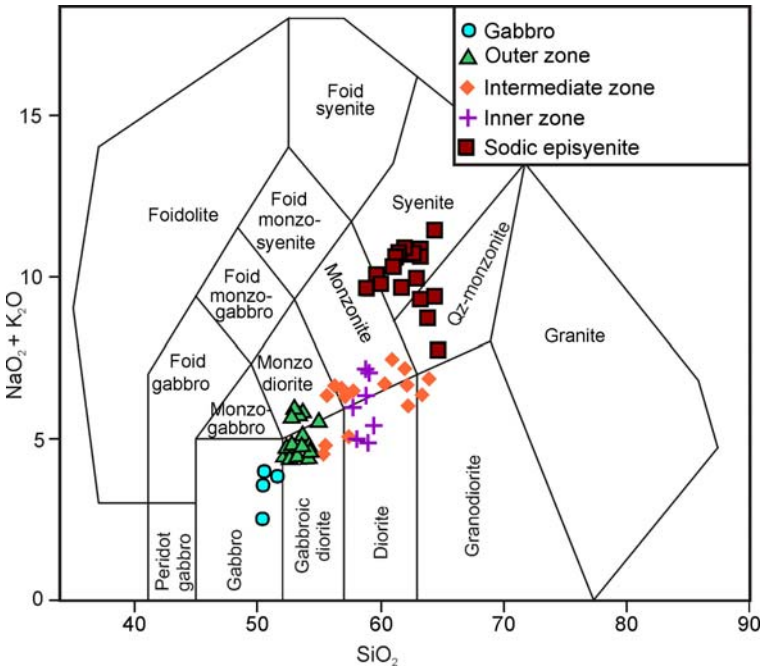

Figura 10 – $Na_2O + K_2O$ versus SiO_2 plot of Middlemost (1985) that shows the continuous variation due to hydrothermal alteration of the gabbro.

substantial depletion of other oxides during maximum sodium metassomatism. In contrast, MgO, CaO, Fe_2O_3 and TiO_2 decrease with increasing SiO_2, the lowest values corresponding to the sodic episyenite, but all samples plot along a continuous compositional trend that indicates progressive depletion of these oxides during the formation of each zone. In the case of TiO_2, some samples of the intermediate zone and the episyenite plot as an almost separate cluster that indicates substantial retention of Ti in these zones, as petrograhically suggested by the abundance of ilmenite. Observe that the inner zone samples always plot between two clusters of the intermediate zone in all diagrams for major element oxides, suggesting a SiO_2 loss.

Although these major oxides show a correlation with SiO_2, there is an overlap between the four samples of the freshest gabbro and some of the external portion of the outer zone, which correpond to samples lacking the typical foliation of the outer zone. Overlap also occurs between samples of the outer and intermediate zones, as

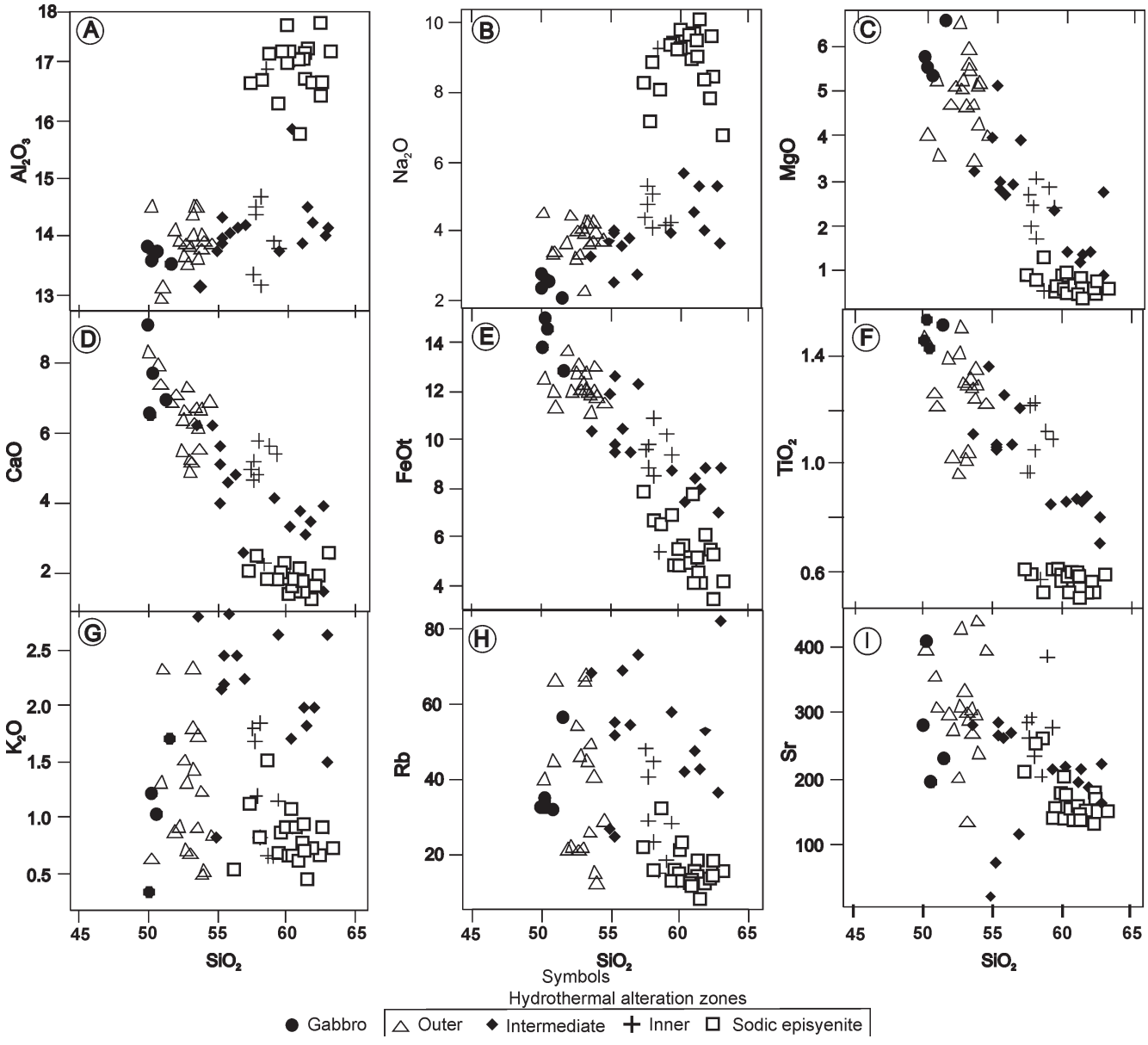

Figure 11 – Plots of major element oxides (in weight %) and Rb and Sr (in ppm) versus SiO_2 for samples from the Caiamar deposit.

well as between the inner and the intermediate zones. The samples from the inner zone have in general less SiO_2 than those from the intermediate zone, indicating that the former formed at the expense of the dissolution of silica. In the Al_2O_3 x SiO_2 diagram (Figure 11A), one sample from the intermediate zone plots within the episyenite cluster, suggesting a local more prominent concentration of Al_2O_3 due to depletion of the major oxides within this zone. One sample from the inner zone plots in all diagrams within the episyenite cluster, but it was collected at 30-cm from the episyenite foot-wall, which suggests that close to the ore-zone the inner zone underwent more aggressive hydrothermal alteration, as typical for the episyenite.

The plot of K_2O x SiO_2 (Figure 11G) shows a random behavior of potassium with increasing SiO_2. However, in detail, a negative correlation exist among the samples from the outer zone as well as amongst those from the intermediate to the inner zones and the episyenite. Despite the low number of gabbro samples, it seems that K_2O does not vary with SiO_2. The maximum potassium alteration correspsonds to some of the samples from the intermediate zone. The Rb x SiO_2 plot (Figure 11H) has a similar behavior as K_2O, as expected. The Sr x SiO_2 (Figure 11I) shows that Sr of the gabbro and the outer zone samples does not vary significantly with SiO_2, but has a negative correlation in samples from the intermediate and inner zone and the episyenite, as a response to a more aggressive metasomatism in the proximities of the ore zone. The Zr x Y plot (Figure 12) shows that these elements mantained a constant ratio from the gabbro to the inner zone, thus suggesting that they remained immobile during the hydrothermal alteration. The same plot shows that at the episyenite, albitization resulted in an increase in the content of Zr relatively to Y, but but raising the ratio from about 3:1, oif the alteration envelope, to about 5:1.

From these data we conclude that the hydrothermal alteration zones derived from the gabbro, without the interference of other rock types. The compositional overlap among samples from the several alteration zones suggest that the hydrothermal system percolated accross an heterogeneously permeable rock package responsible for a variation of the alteration sequence.

The variation of chalcophile elements Cu, Pb, Zn, Ni and Co was investigated along the CA-87 drilled section by determining minimum, maximum, average and the 0.95 percentil values, the later representing the

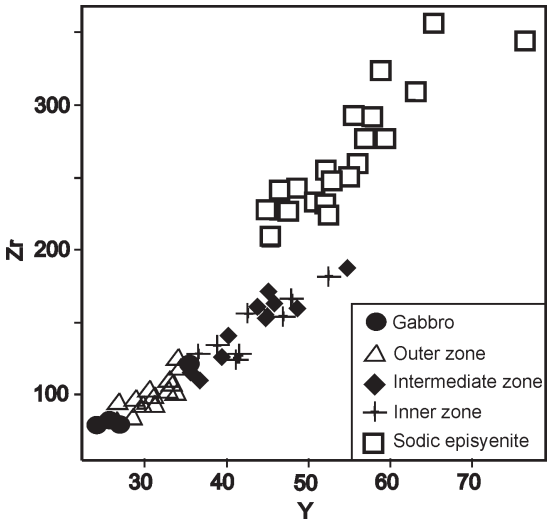

Figure 12 – Zirconium versus Ytrium plot for samples from the Caiamar deposit.

lower limit of anomalous samples of the analysed population (Table 2). Copper content of the section is very low, and only three samples contain more than 31 ppm, one of gabbro (62 ppm), one of the outer zone (38 ppm) and another of the intermediate zone (41 ppm), the later two collected near a carbonaceous schist interval within the alteration zones. Lead content of the section is also very low, and only three samples contain more than 23 ppm, two of gabbro (30 and 32 ppm) and one of a remain of the outer zone within the intermediate zone. Zinc has a larger variation than Cu and Pb, and four samples contain more than 161 ppm, two of gabbro (163 and 214 ppm) and two of the intermediate zone, which were also collected near an intercalation of carbonaceous schist. However, more than 100 ppm occur in all samples of the gabbro and randomly across the outer zone, a few in the interemediary zone and in almost all samples of the inner zone, with a sharp decrease to the episyenite, where most samples contain around 5 ppm. Nickel also has a more wide variation. In the four samples of gabbro its content is below 48 ppm and decreases towards a few samples at the beginning of the outer zone, and increases above 257 ppm in three samples near carbonaceous schist intercalations. The Nickel content of the inner zone samples is, in general, higher than the average content of the entire section and drops in the episyenite. Cobalt occurs in anomalous values only in the four samples of gabbro and in one of the outer zone, collected near an intercalation of carbonaceous schist. Accross the drilled section, its content is above average in the outer zone, below in the intermediate and inner zones and drops below 6 ppm in the episyenite, except for one sample with 24 ppm.

These data indicate that, except for the gabbro where the chalcophyle element contents are considered

Table 2 – Minimum, maximum, average and 0.95 percentil values for the chalcophile elements, in ppm, of the Caiamar deposit CA-87 drill-hole core.

	minimum	maximum	average	95%
Cu	5	52	9	31
Pb	6	32	17	23
Zn	5	214	54	161
Ni	5	357	68	257
Co	1	68	23	55

normal, the anomalous samples are all more or less related to the vicinity of carbonaceous schist intercalations, which is interpreted as a result of the extraction of these elements into the alteration zones by the percolating hydrothermal solutions.

Epysienites are, in general, targets for Uranium or Tin deposits, but the average content of U in the Caiamar deposit is of 2 ppm, with a maximum of 24 ppm within the intermediate zone, but not in the episyenite, and Sn occurs under detection limits in all samples. Therefore, U and Sn do not belong to the resources of this deposit.

The average ETR (Table 3) of the studied section increases from the gabbro throughout to the sodic episyenite. The later consists of quartz and another nepheline normative varieties, the former containing the highest ETR content. Figure 13 shows the REE paterns normalized to the chondrite data of Boynton (1984) for the individual sample sets from the gabbro to the sodic episyenite. The normalized patterns of all zones are fractionated, with increasing La_N/Yb_N from the gabbro to the episyenite, due to incresing fractionation of the LREE given by the

Table 3 - Sum of REE, Eu/Eu, La_N/Yb_N, La_N/Sm_N and Eu_N/Yb_N average values for the gabbro, outer, intermediary, inner hydrothermal alteration zones and for the sodic episyenite divided into quartz (Q) and nepheline (Ne) normative varieties (see below for discussion of CIPW norms).*

	∑REE	La_N/Yb_N	La_N/Sm_N	Eu_N/Yb_N	Eu/Eu*
Gabbro	78.2	2.4	1.8	1.1	0.91
Outer zone	94.8	2.9	2	1.2	0.95
Intermediate zone	131.3	2.9	2.1	1.1	0.86
Inner zone	129.1	3.2	2.1	1.1	0.86
Q sienyte	221.6	3.6	2.6	1	0.79
Ne sienyte	218.9	3.8	2.5	1.1	0.81

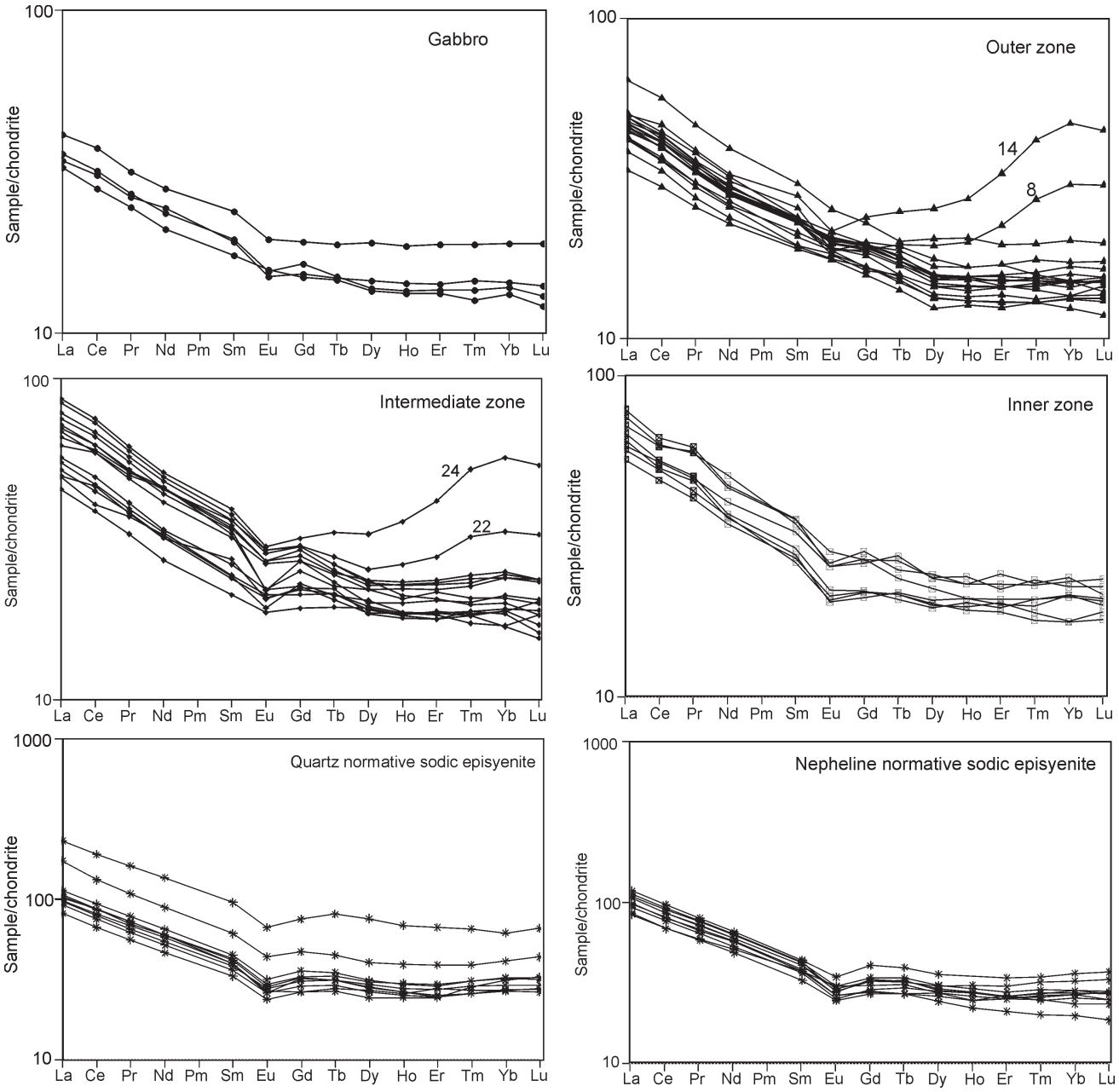

Figure 13 – REE patterns normalized to chondrite (Boynton 1984) for the gabbro and the outer, intermediary, inner hyrothermal zones and the sodic episyenite subdivided into the quartz and nepheline normative varieties.

La_N/Sm_N ratio, but with almost constant non fractionated HREE given by an Eu_N/Yb_N near unit. The majority of the samples have slight to pronounced negative Eu anomaly, but, on the average, the samples from the outer alteration zone are the least anomalous. Four samples have anomalous patterns characterized by concave pattern, two of the outer alteration zone and two of the intermediate zone. The anomalous pattern may possibly be explained by the higher U and Th concentration as compared to the average value for the samples of each zone, excluded the anomalous samples. The higher U and Th may be possibly due to the higher amout of zircon, but this interpretation in not petrographicaly supported. The behavior of the REE shows that progressive hydrothermal alteration resulted in increasing concentration of REE and fractionation of LREE and of LREE/HREE, but without significant fractionation from Eu to Yb. The increasing average Eu anomaly is in general followed by decreasing amount of Sr.

Bulk-rock geochemistry and CIPW normative minerals

Calculations of normative minerals are used to produce an idealised mineralogy of a crystallized magmatic melt. In the present case, CIPW normative minerals were calculated to follow the idealised mineral variation that resulted by the hydrothermal alteration of the gabbro to the episyenite. The norm was calculated by means of the Geochemical Data Toolkit for Windows package – GCDkit, version 2.3 (Janousek and Farrow, 2008), which includes the CIPW norm calculation of Hutchison (1974) as well as its modification with biotite and hornblende (Hutchison, 1975). Considering that the gabbro contains hornblende and biotite as a hydrothermal alteration phase, we preferred the modified version. Table 4 shows the average normative mineral composition of the four freshest gabbro samples and of the hydrothermal alteration zones. Norm calculation of the episyenite samples yielded one quartz normative group (episyenite 1) and another nepheline normative (episyenite 2).

The average normative quartz content slightly increases from the gabbro to the intermediate zone, due to

Table 4 - Average CIPW normative minerals for the gabbro, outer, intermediary, inner and episyenite alteration zones, the later devided into quartz (1) and nepheline normative (2).

		Hydrothermal alteration halos				
	Gabbro	Outer	Intermediate	Inner	Episyenite 1	Episyenite 2
Quartz	13.5	12.0	19.6	15.6	5.6	0
Corundum			0.7		0.5	0
Orthoclase		0.4	7.1	2.6	3.4	3.2
Albite	21.0	32.5	34.6	44.5	73.2	81.1
Anortite	26.3	20.7	15.4	15.4	6.8	4.7
Biotite	9.2	9.6	8.4	6.6	2.5	2.3
Hornblende	12.2	7.6	0.5	1.1		
Nefeline						1.2
Wollastonite	0.9	2.3	1.4	2.5	0.5	2.0
Ilmenite	0.5	0.6	0.6	0.4	0.2	0.2
Hematite	15.9	13.8	10.9	10.3	7.0	5.3
Apatite	0.5	0.5	0.8	1.0	0.3	0.1
Total	100	100	100	100	100	100

increasing SiO_2, from where it decreases towards the episyenite. The variation of normative quartz is accompanied by a gradual increase in albite towards the inner zone, with considerable increase in the episyenite, and a maximum in the nepheline normative group. The first appearance of normative orthoclase occurs in the outer zone and attains maximum content in the intermediate zone, followed by its decrease to the inner zone and a slight increase in episyenite1. This indicates that sodium metasomatism, petrographicaly represented by albite, and potassium metassomatism by biotite, started within the gabbro and increased in intensity across the alteration zones. However, while albite increases towards the episyenite, the amount of orthoclase increases and overlaps albitization only until the intermediate zone. Normative hornblende decreases significantly from the gabbro to the intermediate zone. The formation of normative hornblende and the increase in normative wollastonite and hematite, and part of biotite in the inner zone may reflect the abundance of hydrothermal ankerite and arsenopyrite in the actual rock.

The excess of Al_2O_3 is represented by normative corundum of the intermediate zone and in episyenite 1. This suggests progressive leaching of MgO, CaO, FeOt, whilst SiO_2 and Al_2O_3 remained immobile. Wollastonite has a random behavior. Ilmenite is almost constant from the gabbro to the intermediate zone, from where it decreases to the episyenite. Apatite increases from the gabbro to the inner zone and decreases towards the episyenite.

The two sodic episyenite varieties are intimatelly mingled in the analysed core-samples, both represented by 10 out of the 20 samples. The saturated variety has normative quartz between 0.02% and 15.5%, averaging 11,88%, is corundum normative and the albite content is around 73%. In the undersaturated samples, normative nepheline is between 0.067% and 2.1%, averaging 1.06%, is not corundum normative and the albite content raises up to about 81%. This indicates that the undersaturated variety represents a more intense sodium metassomatism than the saturated variety and the adjacent alteration zones. Normative wollastonite probably reflects the occurrence of carbonate and andradite throughout the section.

Bulk-rock geochemistry and mass balance

Alteration mass balance calculation was performed based on the average bulk-rock geochemical composition of the four least altered gabbro samples and of all samples of each hydrothermal alteration zones. Element concentrations in corresponding pairs of altered versus unaltered rocks were plotted in isocon diagrams by means of the GCDkit software (Janousek and Farrow, 2008), which follows Grant (1986) calculations approach according to the formula:

$$DC = (CF_{immobile}/CA_{immobile}) \cdot CA - CF$$

where CF and CA are the concentrations in the fresh (F) and altered (A) sample, respectively, and DC denotes the gain or loss in grams per 100 g of rock for major elements or in ppm for trace elements.

Calculations were initially performed considering the average composition of the gabbro as the unaltered rock and the average composition of the outer zone as the altered rock. In the further

steps we considered each alteration zone as unaltered rock and compared to the inmediate inward zone as altered rock, thus following the increasing alteration intensity. The calculations included the major and minor elements oxides and selected trace elements (Ba, Rb, Sr, Y, Zr, Ni, V, Co, La, Yb). The gains and losses for each pairs are shown graphically in Figure 14. This allowed recognizing the least immobile element whose concentration ratio remained unchanged during alteration. For the first three pairs, Al_2O_3 was chosen as the immobile oxide. A test using the averaged composition of the inner zone as unaltered rock versus the average composition of the quartz and the nepheline normative episyenite samples showed that the result of their mass balance did not differ. Therefore, the averaged composition of all samples of the episyenite was compared against the inner zone, and SiO_2 was considered as imobile and less than Al_2O_3. A mass variation during alteration was recognized by the the change of the measured average density from the gabbro (3.4 g/cm^2) to the outer (2.8 g/cm^3) and the intermediate (2.4 g/cm^3) alteration zones, indicating loss of mass, and a gain of mass from the intermediate to the inner zone and the episyenite (3.0 g/cm^3) due to the presence of arsenopyrite.

The isocon of Figure 14A indicates that the transformation of the gabbro into the outer zone resulted in major gains of Na, Mn, minor of Si, K, P, Sr, Zr, and loss of Fe, Ca, Mg, Ti, Co, V, Ni and Ba, while Rb, Y and the REE may be considered as almost immobile. The alteration of the outer to the intemediary zone (Figure 14B) resulted in gains of K, P, Ba, Zr, Rb, Y, La and minor Na, and losses of Fe, Ca, Mg, Sr, V, Co, minor Ni, while Yb remained immobile. The isocon of the inner zone as altered rock compared to the intermediate zone as fresh rock (Figure 14C) indicates that alteration resulted in main gains of Ca, Fe, Mg, Ti, V and Sr, minor Na, P and Co, with Y, La, Ni and Yb remained immobile. During the formation of the episyenite, as compared to the inner zone and considering SiO_2 as immobile (Figure 14D), a considerable gain of Na took place, along with minor Al, Y, Zr and La, and a major loss of Fe, K, Ca, Ti, Sr, Ba, Mn, Mg, Rb, V, P and CO, with Yb remaining immobile.

Major losses from the gabbro to the outer alteration zone reflect the breakdown of plagioclase and hornblende, Ca and probably Sr, as well as Mg, Fe, Ti, V. Co and Ni were removed, but part of Mg and Fe must have been preserved to justify the replacement of hornblende by biotite as a result of potassic alteration, a petrographically minor alteration also present in most of the gabbro samples. These reactions probably resulted in the enrichment in Si, Ba, Rb, Zr and Y in the outer zone, which was accompanied by a decrease in density from the gabbro (2.85 g/cm^3) to the outer zone (2.85 g/cm^3), which would correspond to about 10% increase in volume. Increasing alteration from the outer to the intermediate zone and complete consumption of hornblende resulted in additional loss of Fe, Mg and Ca, as well as Mn, Ti, Sr, Co and V. The removal of Ca, Mg and Fe from the intermediate and their increase in the inner zone may be explained by the formation of ankerite, and part of Fe by disseminated arsenopyrite. Therefore, the isocons also show that the intermediate zone represents the strongest potassium alteration, in contrast with the almost continuous sodic alteration that attained maximum intesity at the episyenite.

Characteristics of the gold ore

The most important gold mineralization occurs as a quartz-carbonate-arsenopyrite-(± albite) stockwork

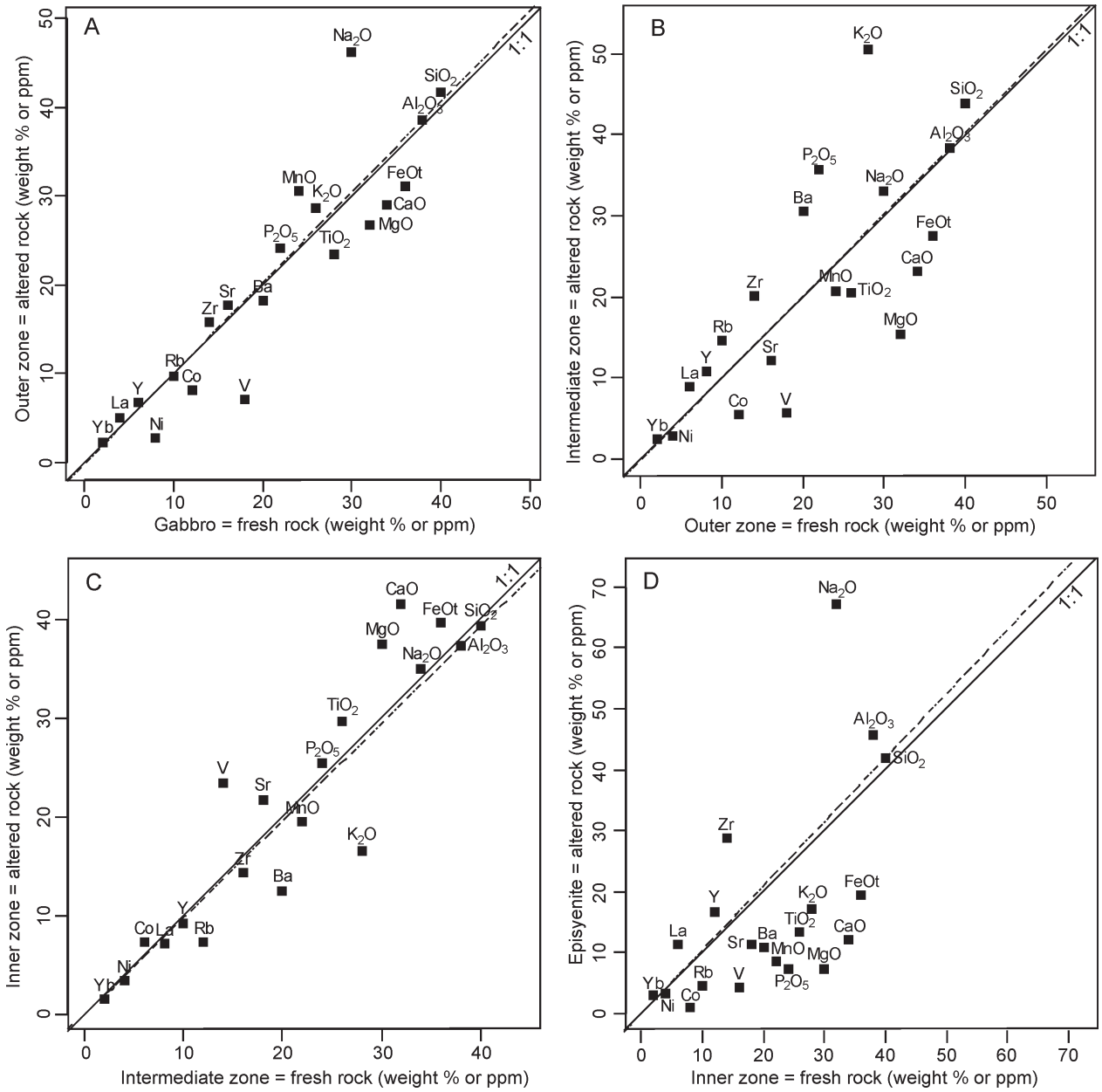

Figure 14 – Isocons for the alteration steps from the gabbro to the episyenite of the Caiamar deposit.

(Figure 15) and as disseminated arsenopyrite (see Figure 4E) within and following the strike of the episyenite. Subsidiary ore reserve occurs in the inner hydrothermal zone where it contains disseminated arsenopyrite (see Figure 7A). As gold is associated with arsenopyrite, it appears that the addition of the metal probably took place in three phases, one earlier during the formation of the inner zone, followed by its disssemination during the formation of the episyenite and a later represented by the its deposition in the open fracture system as a stockwork.

Ore petrography

Petrographic studies of ore-samples were performed only on polished sections of specimens from the stockwork and the disseminated phases in episyenite. These studies showed that the paragenesis of the ore is simple and given by arsenopyrite + gold. Pyrrhotite and pyrite are rare and occur as disseminations or in quartz

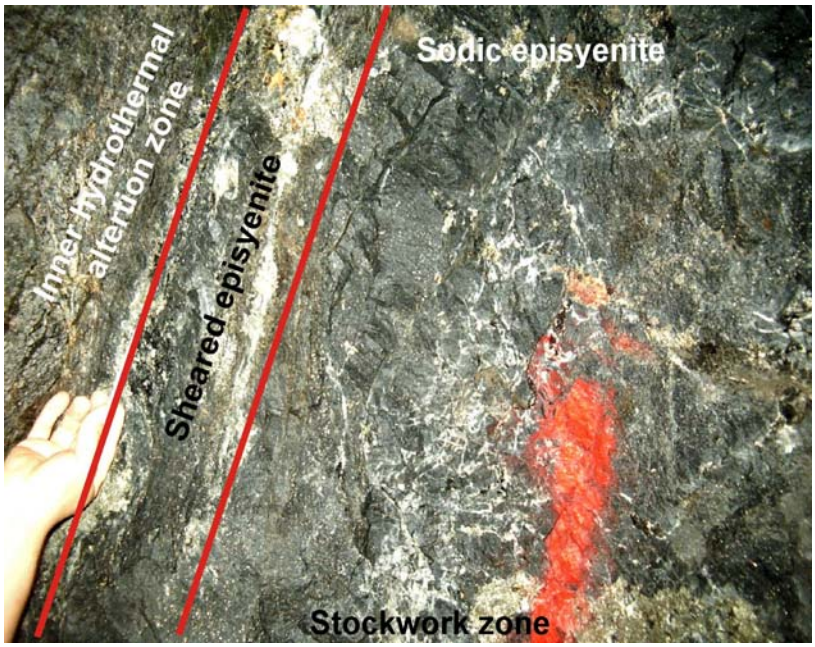

Figure 15 – Gallery roof of the Caiamar deposit that exposes the quartz-arsenopyrite-gold stockwork in the sodic episyenite, separated from the inner hydrothermal alteration zone by sheared episyenite. The right side of the inner zone is, in this case, marked by intense quartz + ankerite ± albite veining rich in arsenopyrite and parallel to the contact.

pods only in the inner zone. Pyrrhotite occurs only along the outer portion of the inner zone, before the first occurrente of disseminated arsenopyrite, where pyrite starts to occur. Arsenopyrite occurs as aggregates 5-cm to 10-cm long in the stockwork and of 2-3-mm up to 2-cm in diameter isolated crystals when disseminated.

Under the microscope, arsenopyrite aggregates formed as two textural varieties. One consists of clean anhedral to suhedral crystals with limits marked by the silicate matrix, which also occurs as rare and tiny inclusions (Figure 16A). The other variety differs from the former by the presence of abundant inclusions of the matrix (Figure 16B). This suggest that the first grew in open spaces, whilst the other probably formed under more confined conditions by dissolution of the matrix during sulfidation. Due to the grain-size size of the single crystals of both varieties, they may have formed under conditions of low nucleation.

Disseminated arsenopyrite occurs as isolated crystals in three textural varieties. One comprises clean, euhedral crystals (Figure 16C), which coexist with skeletal clean forms (Figure 16D) and with anhedral crystals containing abundant inclusions of the silicate matrix (Figure 16E). These varieties may also be intrepreted as having grown under similar conditions as the aggregates.

Pyrrhotite and pyrite are occasional phases and occur as millimetric irregular grains disseminated in the foliation of the inner zone (Figure 16G). In general, pyrrhotite is an isolated phase in the outermost portions and pyrite near the episyenite and associated with arsenopyrite (Figure 16H).

Gold grain-size is in general below 0.1 mm (Figures 16I and 16J) and seldom occurs as visible grains up 1-mm in the ore zone. Polished sections so far investigated show that the metal is interstitial to arsenopyrite aggregates or isolated in the disseminated ores.

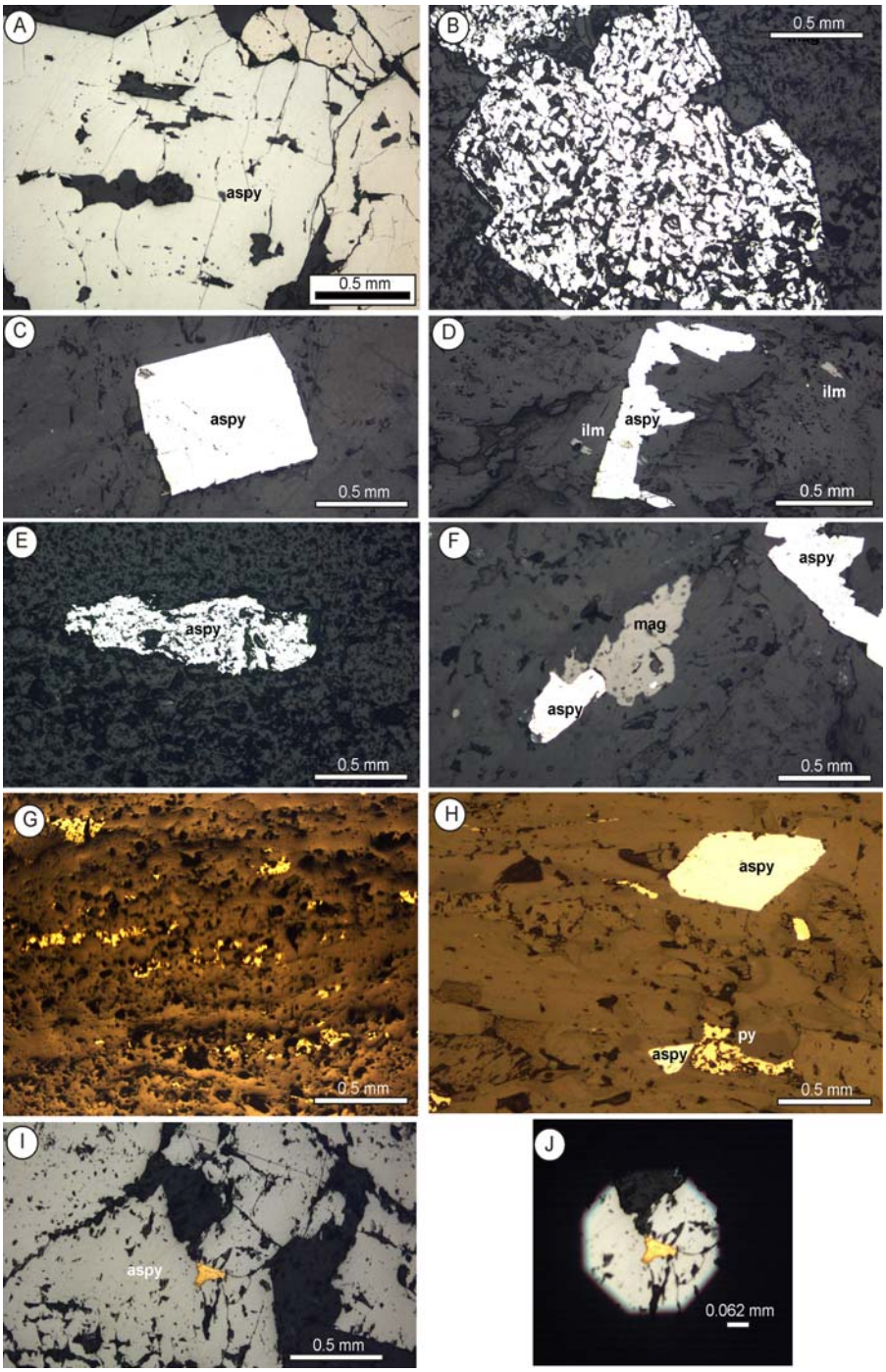

Figure 16 – Plane-polarized photomicrographs of polished sections of ore-samples from the Caiamar deposit. (A) – Clean arsenopyrite aggregate from the stockwork. B – Arsenopyrite aggregate from the outer hydrothermal alteration zone with abundant inclusions of the silicate matrix. C – Isolated euhedral arsenopyrite crystal from the disseminated type in the episyenite. D – Skeletal arsenopyrite from the disseminated ore in the apisyenite. E – Elongated arsenopyrite crystal from the outer zone with abundant inclusions of the silicate matrix. F – Disseminated arsenopyrite in the episyenite that shows corrosion relationship with a magnetite crystal. NL. G – Irregular grains of pyrite (yellow) disseminated along the foliation of the inner zone. H – Irregular grains of pyrite in lose association with arsenopyrite of the inner zone. I - Arsenopyrite aggregate with an interstitial gold. G – Detail of figure 14H to show the common dimension of Gold. Legend: aspy – arsenopyrite, il = ilmenite, mag = magnetite, py = pyrite.

Geochemical Signature

The geochemical signature of the Caiamar deposit was obtained by factor analysis as a tree-diagram (dendrogram) using the Pearson´s correlation coeficient matrix and weighted-pair group analysis (Figure 17). Calculations were performed with the Statistica for WINDOWS©, of Stasoft Inc. The analitycal data were obtained by ICP-MS of 52 elements from 200 channel-samples of ore from the galleries, totalizing 10,400 results, kindly made available by Yamana Gold Inc. Amongs these, only the data in ppm of Au, Ag, As, B, Ba, Bi, Cd, Cu, Hg, In, Mo, Pb, Pt, Re, S, Sb, Se, Te and Zn, and the % of sulfur were selected as metallogenetically sensitive elements. Bismuth, Cd, In and Pd were excluded because the results of 98% of the samples were below the detection limits. Therefore, the geochemical signature of the deposit was obtained for 16 metallogenetic representative elements after 3,200 analytical results.

The dendrogram suggests that the geochemical signature of the deposits is given by the association Au-S-Se-Sb-Ag-Te-As, in decreasing order of correlation, and is considered as the best regional geochemical pathfinders, besides gold concentration in active sediments and soil followup. A subsidiary group of elements that show less correlation with the above association comprises Ba-Zn-Pb-Mo.

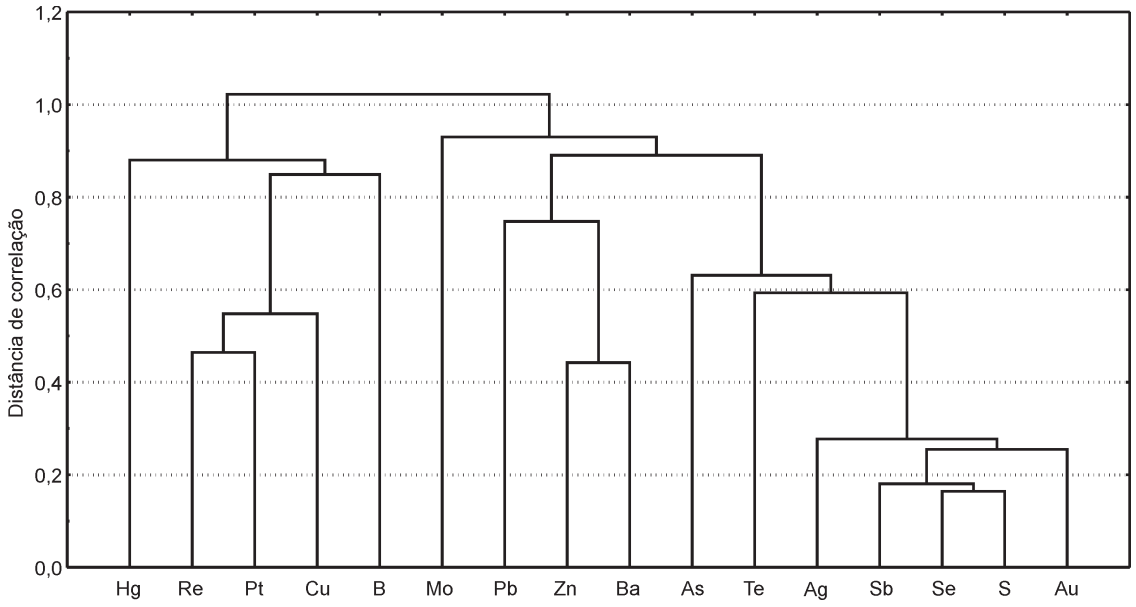

Figure 17 – Dendrogram for metallogeneticaly sensitive elements of the Caiamar deposit.

Sulphur Isotopes

Preliminary Sulfur isotope composition from concentrate sulfide samples was obtained at the Geochronological Laboratory of the University of Brasília by MC-ICP-MS. The samples were analized by comparison with a local pyrite standard. The analysed spots were about 100 μm. Nine samples of sulfides were analysed, amongst which four of disseminated arsenopyrite in the episyenite and one from the stockwork, one of pyrite from a quartz-carbonate vein, and the remaining three of arsenopyrite disseminated in the outer hydrothermal alteration zone.

The $\delta^{34}S$ most closer to 0‰ lies between 2,67‰ and -3,25‰ and correspond to arsenopyrite disseminated in the episyenite, which suggests that sulfur was provided by an igneous source. The $\delta^{34}S$ of the other samples varies from -5,20‰ to -8,82‰, indicating a sedimentary source, such as the local carbonaceous phyllites, which in general contain disseminated pyrite and/or pyrrhotite. The magmatic source for Sulfur is still an open question, considering the lack of exposures of intrusions, except the gabbro, which was already crystallized when the hydrothermal alteration and mineralization events took place. However, these data suggest that the hydrothermal solutions derived from a late magmatic fluid mixed with convecting fluids through the supracrustal rocks.

Geophysical signature

For the geophysical analysis of the Caiamar deposit area, we used the data colected by the Geophysycal Project of the State of Goiás, performed during 2004 and 2006 in three phases (Hildebrand, 2004, 2006), as a joint venture of Lasa Engenharia e Prospecção Ltda. and the Brazilian Geological Survey - CPRM, Brasilian Ministry of Mines and Energy - MME, Industry and Commerce Secretary of the State of Goiás and Fundo de Fomento a Mineração – FUNMINERAL.

The magnetic survey was undertaken with a Cesium vapour optical bombardment sensor, model CS-2 of CINTREX, with a 0,001 nT resolution. Readings were taken at each 0.1 seconds, at airplane speeds of 292 km/h and 287 km/h, which corresponds to ground measures at each 8.0-m (Hildebrand, 2004, 2006). The gamaspectrometric equipment consisted of a 256 spectral channels EXPLORANIUM, model GR-820, with readings at each second, which corresponds to ground measure at each 80-m. Accoding to Ataíde (2010), the flight direction was N-S, with 500-m line spacings, control flight direction E-W and 5.0-km line spacings, and flight height of 100-m.

The detailed aeromagnetometric map of the study area (Figure 18A) shows that the Caiamar deposit lies at the eastern edge of a negative circular dipole, which constrasts with the magnetic signature of the sorrounding supracrustal rocks of the greenstone belt. The pseudogravimetric map (Figure 18B) indicates the presence of a low density body underneath the supracrustal rocks slightly deviate to the south from the magmetic dipole. On the other hand, the radiometric potassium channel map (Figure 18C) shows difuse moderate to low positive with small negative anomalies within the domain of the magnetic dipole and surroundings, but a small and narrow positive anomaly occurs just south from the drilling sites, possibly reflecting the biotite-rich intermediate hydrothermal alteration zone.

After the net aerogeophysical products, geophysicist Bob Ellis, from Ellis Geophysical Consulting Inc., Reno, Nevada, obtained a aeromagnetic total field 3D inverson model by means of the UBC software for the Guarinos greenstone belt, as an exploration support for Yamana Gold Inc. during 2009. Description of the software may be obtained from the site www.eos.ubc.ca. Inversion is an interative process by which the model area is divided into small cells that contains a starting magnetic susceptibility distribution. This distribution is systematically changed, a forward model computed, and compared to the observed data until a specified fit to the observed data is obtained.

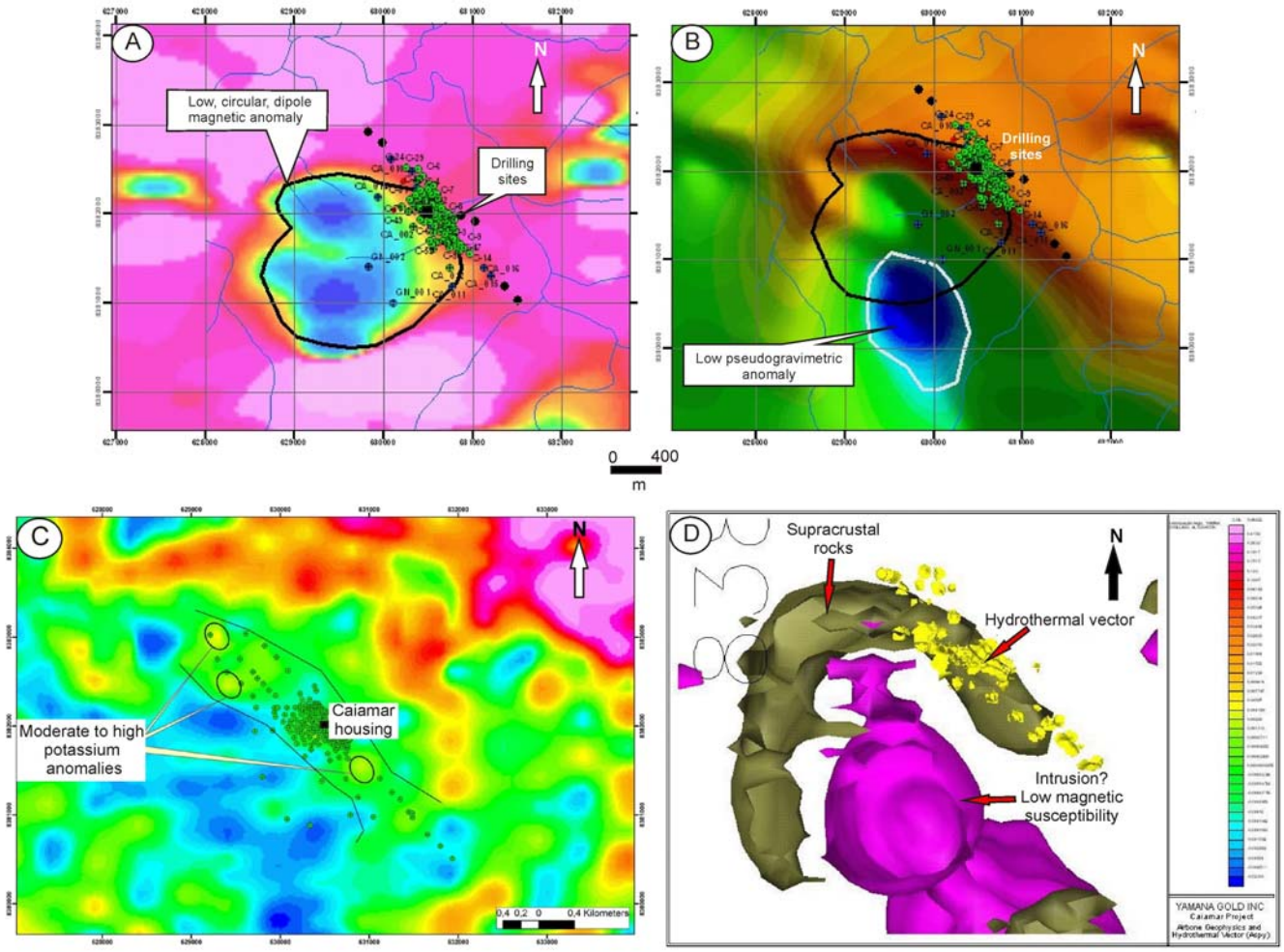

Figure 18 – Geophysical maps and 3D model of the area around the Caiamar deposit that constrain the occurrence of a possible hidden intrusion intepreted as plausible source for the hydrothermal solutions. A - Magnetic map that shows an about 1,600 m in diameter circular magnetic dipole anomaly adjacent to the drilling sites. B - Pseudogravimetric map that shows a low anomaly near the magnetic dipole. C - Radiometric map of the potassium channel with diffuse anomalies in and around the mgnetic anomaly, but that shows a narrow jpositive anomaly just souht of the drill-sites that may respond to the intermediate biotite-rich alteration zone. D - 3D model for the magnetic low anomaly and the orientation of the hydrothermal vector. Dots are drilling sites of several programs. Courtesy of Yamana Gold Inc.

The product is a magnetic susceptibility solid or voxel in SI units. The magnetic susceptibility is often quoted in CGS units. Figure 18D shows the SW-NE view of the 3D model for the magnetic data obtained via Target, of Geosoft, near the Caiamar deposit. This leads to the interpretation that, in depth, the magnetic anomaly possibly reflects a near surface semi-oval cilinder-shape body conected to a more voluminous body in depth. It also shows that the main hydrothermal vector, obtained after the LA-ICP-MS Arsenic content variation in all drill-holes, is clearly directed towards the 3D model body. This also suggests that the magnetic dipole could reflect the magmatic source for the hydrothermal fluids and the gold mineralization, but its nature is still unknown and is a subject for future investigation by deep drilling.

Age of mineralization

In situ U–Pb zircon dating of crystal fractions from the gabro and the episyenite via LA-ICPMS (Jackson et al., 2004) was performed to determine the age of the intrusion and hydrothermal alteration. The gabbro zircon crystals were analysed at the Geochronological Laboratory of the University of Brasília, and of the episyenite at the Geochronological Laboratory of the Federal University of Rio Grande do Sul.

In the LA-MC-ICPMS technique, all zircon grains and a sample of the GJ-1 (GEMOC ARC Nat. Key Center) standard zircon were mounted in 2.5 cm-diameter circular epoxy mounts and polished until the zircons were revealed. Images of zircons were obtained using a Leica MZ 125 microscope and in back-scattered electron images using a Jeol JSM 5800 electron microscope. The grains were analysed with a New Wave UP213 laser ablation microprobe coupled to a Neptune MC-ICPMS, with collector configuration for simultaneous measurements of Th, U, Pb and Hg isotopes. The isotope ratios and inter-element fractionation data were evaluated in comparison with the GJ-1 standard at every set of 4 to 10 zircon spots, and used to estimate the necessary corrections and internal instrumental fractionation. The laser spot size was 25 ìm. For each standard and spot run, a blank sample was also run and its values subtracted from all individual cycle measurements. The ^{204}Pb value was corrected for ^{204}Hg, assuming the ^{202}Hg/^{204}Hg ratio to be 4.355. The necessary correction for common ^{204}Pb, after Hg correction based on the simultaneously measured ^{202}Hg was insignificant in most cases and the Pb isotopic composition assumed to follow the isotopic evolution proposed by Stacey and Kramers (1975), which is required to attribute an initial estimated age. After the blank and common Pb corrections, the ratios and their absolute errors (1ó) of ^{206}Pb*/^{238}U, ^{232}Th/^{238}U and ^{206}Pb*/^{207}Pb* were calculated in an Excel spreadsheet and the intercepts determined as proposed by Youden (1951).

The episyenite sample was collected from the ore stock-pile and consisted of 10 kg fine-grained, massive specimen with disseminated arsenopyrite. The analytical results are in Table 5. The sample contained three populations of zircon grains, 30 to 100 ìm in length. One rare population consisted of rounded detrital grains, which in CL images display homogeneous internal structure (Figure 19A). The other population consisted of 6 prismatic, euhedral grains, which in CL images display a faint internal growth zoning surfaces (Figure 19B). Theze grains in general contain a white, narrow rim of possible xenotime. The Th/U ratio of these grains was between 0.41 and 0.82. The third population also consisted of 6 grains, some showing part of the grain with growth zoning surfaces in CL images, but the other part with a spongy texture (Figure 19C), interpreted as inherited grains partially replaced by a new generation of zircon, whereas other grains are intirely spongy and without growth zoning surfaces (Figure 19D). The Th/U ratio of the analyzed sites of the later two populations was between 0.01 and 0.14 and yielded the same age. According to Corfu et al. (2003), these two population could be interpreted as representing hydrothermal zircon crystals grown and/or overgrown from aqueous fluids at low pressure (<2 kbar) and low temperature (<500 °C) and high water/rock ratios. To definitively interpret these zircon crystals as having been formed under hydrothermal conditions they should have high contents of HFSE, ETR, non radiogenic Pb and fluorine (Corfu et

Table 5 - In situ U–Pb LA-ICP-MS analytical results for zircon crystals of the Caiamar deposit episyenite sample, Guarinos greenstone belt, Central Brazil.

Spot	Ratios										Age (Ma)						
number	$^{206}Pb/^{234}U$	$^{207}Pb/Pb^{206}$	1σ(%)	$^{207}Pb/^{235}U$	1σ(%)	$^{206}Pb/^{238}U$	1σ(%)	f(206)	Th/U	Rho	$^{207}Pb/^{206}Pb$	1s(%)	$^{207}Pb/^{235}U$	1s(%)	$^{206}Pb/^{238}U$	1s(%)	Conc (%)
MT19_21B	56141	0.06314	1.13	0.85201	1.80	0.09787	1.40	0.03	0.02	0.77	712.97	23.93	625.75	8.41	601.90	8.07	84.42
MT19_21N	38398	0.06257	1.14	0.86457	2.30	0.10021	2.00	0.07	0.06	0.87	693.77	24.29	632.61	10.83	615.63	11.74	88.74
MT19_8N	45667	0.06380	1.63	0.72032	2.67	0.08188	2.11	0.04	0.06	0.79	735.15	34.46	550.85	11.34	507.33	10.32	69.01
MT19_6B	31098	0.06329	1.04	1.08430	2.16	0.12426	1.89	0.06	0.14	0.87	717.95	22.14	745.73	11.40	755.02	13.46	105.16
MT19_6N	21505	0.06436	1.18	1.01972	2.16	0.11491	1.81	0.09	0.08	0.83	753.48	24.82	713.77	11.05	701.21	12.01	93.06
MT19_8B	28826	0.06438	1.40	1.11366	2.39	0.12546	1.94	0.06	0.10	0.81	754.09	29.46	759.93	12.76	761.92	13.91	101.04
MT19_sn2B	30279	0.06562	1.55	0.88830	2.26	0.09819	1.64	0.06	0.01	0.72	794.15	32.40	645.45	10.77	603.77	9.47	76.03
MT19_06B2	47062	0.06319	0.95	1.02536	1.30	0.11768	0.88	0.04	0.12	0.66	714.70	20.11	716.61	6.66	717.22	6.00	100.35
MT19_07B	27540	0.06464	1.16	1.03585	1.73	0.11622	1.28	0.06	0.10	0.73	762.62	24.41	721.85	8.92	708.80	8.60	92.94
MT19_9	112978	0.06222	1.49	1.13079	2.14	0.13182	1.53	0.02	0.09	0.71	681.53	31.86	768.13	11.51	798.24	11.49	117.13
MT19_07	19086	0.06330	1.12	0.88198	1.61	0.10105	1.16	0.09	0.11	0.71	718.35	23.84	642.05	7.68	620.57	6.86	86.39
MT19_sn2	39424	0.06511	1.96	0.74445	2.49	0.08292	1.53	0.05	0.03	0.70	778.03	41.19	565.00	10.77	513.53	7.55	66.00
MT19_4	3529	0.14584	1.74	7.94371	4.23	0.39505	3.85	0.42	0.41	0.91	2297.67	29.87	2224.65	38.12	2146.22	70.33	93.41
MT19_4B	2873	0.13795	1.06	5.73967	2.13	0.30176	1.84	1.22	0.82	0.86	2201.66	18.38	1937.36	18.38	1700.01	27.55	77.22
MT19_5	4666	0.15133	1.65	8.49470	3.76	0.40711	3.38	0.32	0.62	0.90	2361.03	28.13	2285.36	34.12	2201.72	62.95	93.25
MT19_5B	4764	0.13147	2.85	4.49079	3.66	0.24773	2.30	0.34	0.62	0.78	2117.76	50.03	1729.27	30.43	1426.76	29.41	67.37

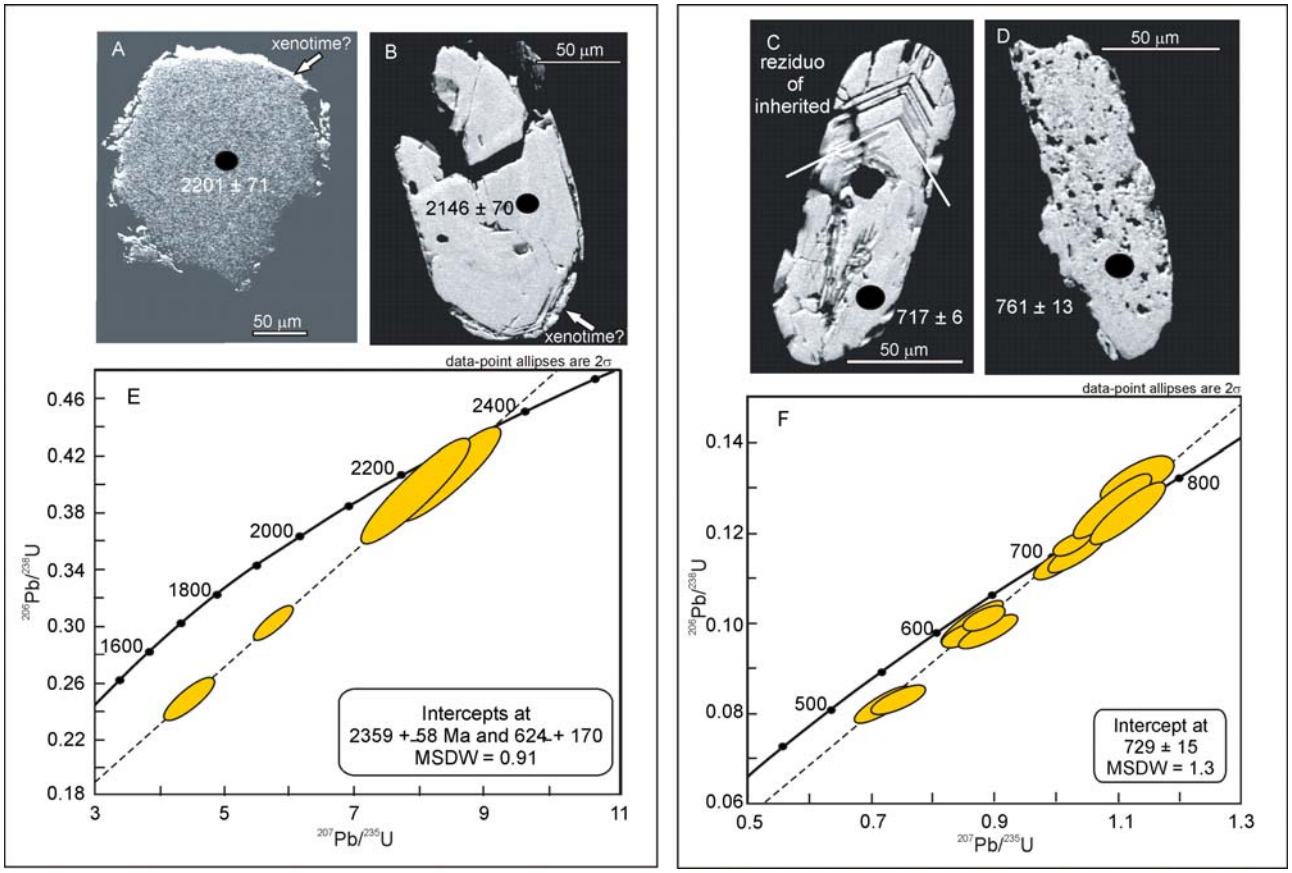

Figure 19 – A to D - CL images of zircon crystals from the episyenite. Crystals in A and B are interpreted as inherited detrital grains, with possible xenotime clear rims. C - This grain is intepreted as an inherited detrital grain with preserved growth zoning (upper partion), partially replaced by spongy hydrothermal zircon (lower portion). D - Zircon grain with a spongy teexture interpreted as resulting from hydrothermal alterarion. E - Concordia diagram for the inherited zircon crystals. F - Concordia diagram for the hydrothemal zircon grains. Black spots indicate the position of in situ dating and correponding ages.

al., 2003), but we have not performed mineral chemistry of these crystals to assure that they are hydrothermal products. However, as stated by Williams (1998) the expected Th/U ratios of hydrothermal zircon should be much less than 0.1, as found in the more abundant population of the episyenite sample, thus supporting that it formed under hydrothermal alteration.

The U–Pb analyses were undertaken on four sites of the first population (Table 5). The sites yielded a discordia line with an upper intercept of 2.359 ± 58 Ma and a lower intercept at 624 ± 170 Ma (Figure 19C). The results indicate a Paleoproterozoic zircon growth that agrees with the age of detrital grains from metagraywackes of the Guarinos greenstone belt obtained by Jost et al. (2008, 2010) and reflects the age of crystallization in the source area. Therefore, these grains are interpreted as inherited from the local metasedimentary sequence where the gabbro intruded. The U–Pb analyses undertaken on the 12 grains of the two other populations (Table 5) yielded a discordia line with an upper intercept of 729 ± 15 Ma (Figure 19D), indicating that the hydrothermal alteration represented by the episyenite took place during the Neoproterozoic.

Discussion and conclusions

The Neoproterozoic geochrological data of the episyenite and the Paleoproterozoic age of the low-grade metamorphic sequence of the Guarinos greenstone belt indicate that the metassomatic process responsible for the gold mineralization is not related to the evolution of the supracrustal rocks but possibly to the beginning of the tectonic event that resulted in the formation of the Brasília thrust-and-fold belt. The predominant massive structure of the preserved gabbro in constrast with the pervasive foliation typical from the outer to the inner hydrothermal alteration zones indicates that only part of the intrusion underwent deformation within a corridor possibly by reactivation of the fault that host the intrusion and that channeled the main volume of the hydrothermal solutions. The lack of pervasive foliation of the episyenite in contrast with the adjacent alteration zones suggests that episyenitization resulted in replacing the mineral assemblage of the inner zone and destructed its fabric features by a ponded magmatic fluid mixed with convective fluids within the supracrustal rocks and channaled towards a narrow microfractured dilatancy zone developed by hydraulic pressure. The volume loss during episyenitization favored a late open fracture system that hosted the stockwork, but not a stage of vug-infilling by late low-temperture minerals, such as is found in potassic episyenites formed after granites and with Sn and U mineralization (e.g. Cathelineau, 1986; Poty *et al*., 1986; Palomba, 2001; Costi *et al*., 2005).

Since Leroy (1978) defined episyenitization as a process that resulted in gradual leaching of quartz during Na and/or K metassomatism of a granite, several articles refer to similar processes in other granitoids (Thorette *et al*., 1990; Petersson & Eliasson, 1997;Jébrak & Doucet, 2002; Rossi *et al*., 2005, among others). As a rule, episyenitization of granitoids has been interpreted as a process characterized by a systematic depletion of SiO_2 and elements associated with mafic minerals (Fe, Mg, Mn, Ca), with enrichment in Na_2O and other minor elements. Episyenitization of mafic rocks has rarely been described (Witt, 1997), where mass balance calculations indicate that SiO_2 and Na_2O have been added during episyenitization, with loss of FeO, MgO and in some cases

K_2O and CaO, and gain in others. Mass balance calculations of the alteration zone of the Caiamar deposit episyenite, which derives from a gabbro, shows a gain in SiO_2 and loss of all major element oxides and trace elements that are typical of a gabbro, which is opposite to the behavior observed in granitoid alteration. However, the data presented here lead to our interpretation that the increase of SiO_2 is mostly due to its immobility during the hydrothermal alteration rather then addition of the oxide, as a result of leaching of mobile elements from the gabbro.

The field, petrographic, geochemical, geochronological and geophysical data suggest that the studied gold deposit can be possibly interpreted as an intrusion-related type. The definition of this class is recent (Newberry et al., 1995; McCoy et al., 1997; Thompson et al., 1999; Lang et al., 2000) and its difference with other systems related to intrusions such as the Cu-Au poprhyry deposits lies in the significant economic concentration of Gold, low content of Cu, Mo, Sn and W, and relative high concentrations of Bi, As, Sb and Te (Thompson & Newberry, 2000). Intrusion related deposits occur in distinct tectonic environments, such as volcanic arcs, back-arc basins and continental settings (Thompson & Newberry, 2000). Groves *et. al* (2003) state that they occur in cratons adjacent to subduction zones in association with Sn and W provinces, but lack, amongst other features, a definite link beween the hydrothermal fluids and an intrusion. On the other hand, Lang *et al.* (2000) and Thompson & Newberry (2000) suggest that these deposits have, amongst other features, a good correlation between Au-Bi-Te-As (W,Mo,Sb), a wide temperature range for the hydrothermal alteration and mineralization events (<300°C to >500°C) and pressures above 1.5 kbar and are not laterally extensive (<2km). In addition, they have narrow hydrothermal alteration zones and low concentration of base metals, a consistent pattern of early potassic or sodic alteration followed by a later sericite and carbonate alteration, as well as evidence for an early pyrite-pyrrhotite assemblage followed by a late pyrite-arsenopyrite. Deposits within the plutons have the Au-Bi-W±Te±Mo±As association, in the peripheral deposits the Au-As-Sb±Hg assemblage and late veins with a Ag-Zn-Pb±Cu±Au association. The main Au-S-Se-Sb-Ag ± (Te-As-Ba-Zn-Pb-Mo) association of the Caiamar deposit in much resembles some of the associations of the intrusion-related deposits, between the peripheral and late-veins systems. This is also suggested by the position of the deposit at the eastern edge of superposed geophysical anomalies, which contrast with the positive geophysical signtures of the surrounding supracrustal rocks. We therefore conclude that the hydrothermal fluids were probably derived from a hidden intrusion underneath the greenstone belt, from which the gabbro may be a shallow part, as illustrated in Figure 20.

We interpret that the deposit formed by hydrothermal activity of an early meteoric or formational convective water stage driven by the intrusion thermal effect, followed by a higher temperature stage when significant orthomagmatic fluids were introduced into the system. The early fluids contained significant sodium and potassium to convert the gabbro into the outer, intermediate and inner alteration zones, with increasing fCO_2, followed by a sodium-rich fluid responsible for explain the episyenite zone and quartz-As-Au-rich later fluids. Fluid-rock ratios were initially low with the system becoming fluid-dominated during the later stages. Based on studies of episyenites in the French Massif Central, the albitization could have occurred in the temperature range between 250°C and 400°C (Cathelineau, 1986; Poty *et al.*, 1986).

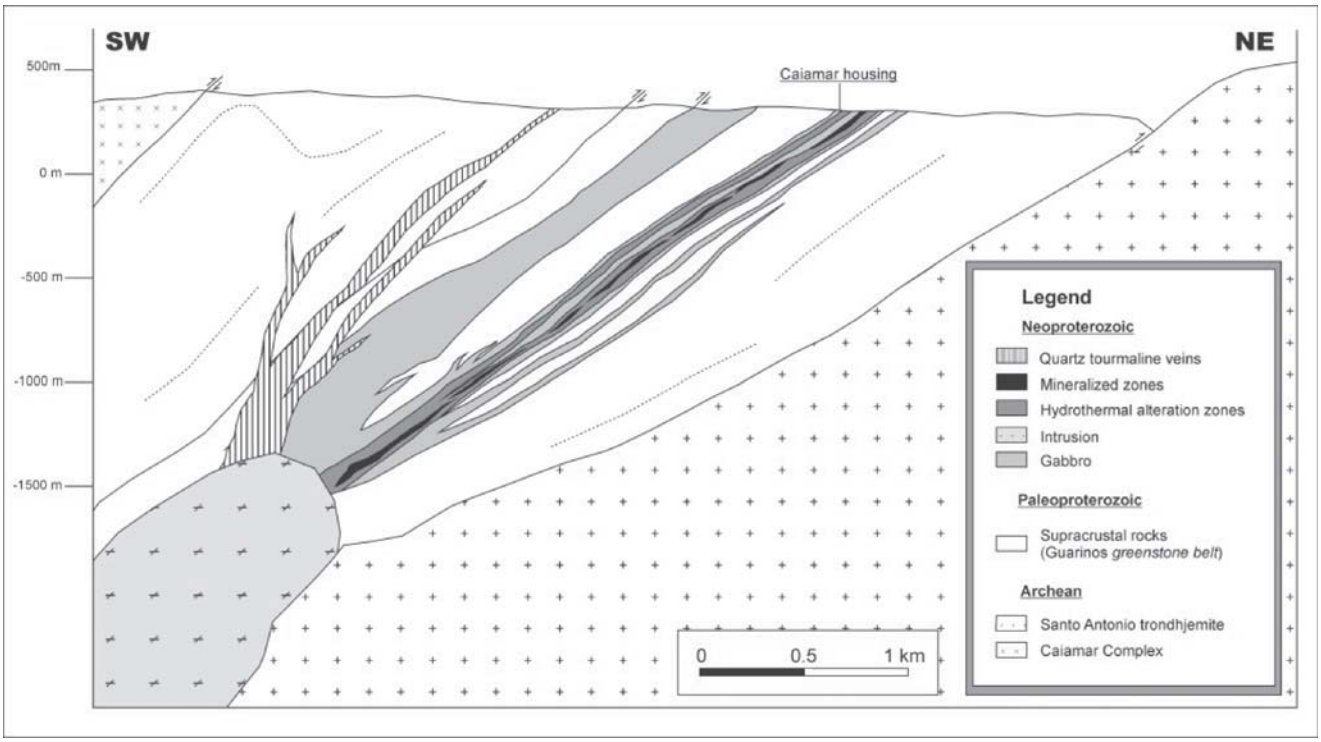

Figure 20 – Sketch that ilustrates the estimated relationships between the gabbro, Gold mineralization and a possible hidden intrusion of the Caiamar deposit.

Acknowledgements To Yamana Gold Inc. for field and laboratory support as well as access to the deposit data. Partial financial support provided by the National Council for Scientific and Technological Development of Brazil (grant # 304764/2007-6) is gratefully acknowledged. To the Area of Forensis Balistic of the Criminalistic National Institute of the Brazilian Federal Police Department for the data on garnet by SEM-EDS was much appreciated. Prof. Bernard Buhm kindly assisted with Sulphur isotope analysis, and Juliana Charão Marques with the geochronological data. To Profs. José Affonso Brod and Nilson Francisquini Botelho for their valuable comments and constructive revisions of the manuscript. Anonimous journal reviewers greatly improved the final manuscript.

References

Ataíde K.L.P., 2010. *Integração de dados de sensoriamento remoto e aerogeofísicos aplicados a cartografia geológica e no controle das mineralizações auríferas dos greenstone belts de Guarinos e Pilar de Goiás*. Unpublished MSc Dissertation, Geoscience Institute, University of Brasília.

Borges R.M.K., Villas R.N.N., Fuzikawa K., Dall'Agnol R., Pimenta M.A. 2009. Phase separation, fluid mixing, and origin of the greisens and potassic episyenite associated with the Água Boa pluton, Pitinga tin province, Amazonian Craton, Brazil. *J. South Am. Earth Sci*., 27:161-183

Boynton W.V. 1984. Cosmochemistry of rare earth elements: meteorite studies. In: HENDERSON, P. (Ed.) *Rare Earth Element Geochemistry*. Amsterdam/ New York: Elsevier, 1984. p. 63-114.

Cathelineau M. 1986. The hydrothermal alkali metassomatism effects on granitic rocks: Quartz dissolution and related subsolidus changes. *J. Petrol*., **27**:945-965.

Corfu F., Hanchar J.M., Hoskin P.W.O., Kinny P. 2003. Zircon. In: Hanchar, J.M., Hoskin, P.W.O. (Eds.) Atlas of zircon textures: Reviews in Mineralogy and Geochemistry, **53**:469–499.

Costi H.T., Borges R.M.K., Dall´Agnol R. 2005. Depósitos de Estanho da Mina Pitinga, Estado do Amazonas. In: O.J. Marini, W.B. Ramos, E.T. Queiroz (Eds.) *Caracterização de depósitos minerais em distritos mineiros da Amazônia.* ADIMB – Agência para o Desenvolvimento Científico e Tecnológico da Indústria Mineira Brasileira, pp.: 395-471.

Costi H.T., R. Dall'Agnol R., Borges R.M.K., Minuzzi O.R.R., Teixeira J.T. 2002. Tin-Bearing Sodic Episyenites Associated with the Proterozoic, A-Type Água Boa Granite, Pitinga Mine, Amazonian Craton, Brazil. Gond. Res., 5:435-451

Dahlkamp F.J. 2009. Uranium Deposits of the World: Asia. Springer-Verlag, Berlim-Heidelberg, 493 pgs.

Danni J.C.M. & Ribeiro C.C. 1978. Caracterização estratigráfica da seqüência vulcano-sedimentar de Pilar de Goiás e de Guarinos, Goiás. In: SBG, Congesso Brasileiro de Geologia, 30. Recife, 1978. Anais.., vol. 2, p. 252-269.

Danni J.C.M., Fuck R.A., Leonardos O.H. 1982. Archean and Lower Proterozoic units in central Brazil. Geologisches Rundschau, 71(1):291-317.

Danni J.C.M., Jost H., Winge M., Andrade G.F. 1986. Aspectos da evolução de terrenos granito-greenstone: exemplo da região de Hidrolina, GO. In: SBG, Congresso Brasileiro de Geologia, 36, Goiânia, Anais..., v. 2, p. 570-584.

De Wit M. & Ashwall L.D. 1997. Greenstone Belts. Oxford Monographs on Geology and Geophysics, 35, 809 p.

De Wit M.J, Hart R. A., Hart R.J. 1987. The Jamestown ophiolite complex, Barberton Mountain land: a composite section through 3.5 Ga oceanic crust Journ. African EarthSci.,6:681-730

Dunn E.J. 1929. Geology of Gold. Charles Griffin & Co., London, 303p.

Emmons W.H. 1937. Gold Deposits of the World. McGraw-Hill, New York, 562p.

Folinsbee R.E, Baadsgaard H., Cumming G.L, Green D.C. 1968. A very ancient island are: the crust and upper mantle of the Pacific área. Am. Geoph. Union, Geoph. Mon., 12:441-448

Foster M.D. 1960. Interpretation of the composition of trioctrahedral mica. USGS Prof. Paper, 354B:11-48

Gomes C.H. 2006. Caracterização das rochas vulcânica e plutônicas félsicas e intermediárias do Alvo Estrela (Cu-Au), Serra dos Carajás, Pará. Dissertação de Mestrado, UNISSINOS, 126 pgs.

Grant J.A. 1986. The isocon eiagram a simple solution to Gresens' Equation for metasomatic alteration. Econ. Geol., 81:1976-1982

Groves D.I., Goldfarb R.J., Robert F., Hart J.R.C. 2003. Gold deposits in metamorphic belts: overview of current understanding, outstanding problems, future research and exploration significance. Econ. Geol., 98:1-29.

Henderson J.B. 1981. Archaean basin evolution in the Slave Province, Canada. In: A. Krõner (ed.) Plate tectonics in the Precambrian. Elsevier, Amsterdam, pg. 213-235

Herzig P.M., Petersen S., Hannington M.D. 1998. Geochemistry and sulfur-isotopic composition of the TAG hydrothermal mound, Mid-Atlantic Ridge 26 °N. Proc ODP, Sci. Results, 158:47-70

Hildebrand J.D. 2004. Relatório final do levantamento e processamento dos dados magnetométricos e gamaespectométricos. Levantamento Aerogeofísico do Estado de Goiás, Área 2. Projeto Arco Magmático de Mara Rosa, Texto Técnico. Lasa Engenharia e Prospecções S.A., 151p.

Hildebrand J.D. 2006. Relatório final do levantamento e processamento dos dados magnetométricos e gamaespectométricos. Levantamento Aerogeofísico do Estado de Goiás, Área 2. Projeto Paleo-Neoproterozóico do Nordeste de Goiás, Texto Técnico. Lasa Engenharia e Prospecções S.A., 128 p.

Hutchison C.S. 1974. Laboratory Handbook of Petrographic Techniques. JohnWiley & Sons, New York, p. 1-527

Hutchison C.S. 1975. The norm, its variations, their calculation and relationships. Schweiz Mineral Petrogr Mitt, 55:243-256

Irvine T.M. & Baragar W.R. 1971. A guide to the chemical classification of common volcanic rocks. Canad. J. Earth Sci., 8:523-548

Jackson, S.E., Pearson, N.J., Griffin, W.L., Belousova, E.A., 2004. The application of laser ablation-inductively coupled plasma-mass spectrometry to in situ U–Pb zircon geochronology. Chemical Geology 211, 47–69.

Janousek V. & Farrow C. 2008. Geochemical Data Toolkit for Windows. Downloaded from http://www.gla.ac.uk/gcdkit on December 2010.

Jébrak M. & Doucet P. 2002. Geology and gold–molybdenum porphyry mineralisation of the Archean Taschereau–Launay plutons, Abitibi, Quebec. Prec. Res., 115:329–348

Jébrak M. 1992. Les gisements d'Or des tonalites archeénnes (Abitibi, Québec). Min. Depos., 27:1-9

Jost H. & Fortes P.T.F.O . 2001. Gold deposits and occurrences of the Crixás Gold Field, central Brazil. *Mineralium Deposita*, 36:358-376

Jost H. & Oliveira, A.M. 1991. Stratigraphy of the greenstone belts, Crixás region, Goiás, central Brazil. *Jour. South Am. Earth Science,* **4**:201-214.

Jost H., Chemale Jr. F., Dussin I.A., Tassinari C.C.G. 2010. Gpoiás greenstone belts: Archean or Paleoproterozoic events?. In: SBG, Congresso Brasileiro de Geologia, 45, Belém, Boletim de Resumos em CD, PAP 33, 1 pg.

Jost H., Dussin I.A., Chemale Jr. F., Tassinari C.C.G., Jungues S. 2008. U-Pb AND Sm-Nd constraints for the Paleoproterozoic age of the metasedimentary sequences of the Goiás Archean greenstone belts. *South American Symposium on Isotope Geology, 6,* San Carlos de Bariloche, Argentina, Resumos Expandidos em CD, 4 pgs.

Jost H., Rodrigues V.G., Jost H., Campos D.S., Oliveira M.C.B, Marques R.L., Carvalho M.J., Rangerangel T. Carvalho Costa R.T.C. 2011. Redefinição estratigráfica do greenstone belt de Guarinos, Goiás. (submitted).

Lacerda H. 1991. Gold in Central Brazil. In: E.A. Ladeira (ed.) *Brazil Gold´91*. Belo Horizonte, Balkena, p. 195-202.

Lang, J.R., Baker, T., Hart, C.J.R., Mortensen, J.K.2000. An exploration model for intrusion-related gold systems. SEG Newsletter, No. 40, p. 1, 6-15

Langford F.F. & Morin J.A. 1976. The development of the Superior Province of northwestern Ontarioby merging island ares. *Am. Jour. Sei.,* **276**:1023-1034

LASA Engenharia e Prospecções S.A. 2006. Projeto Levantamento Aerogeofísico do Estado de Goiás – 3ªEtapa – Paleo-Neoproterozóico do Nordeste de Goiás - Relatório Final do Levantamento e Processamento dos Dados Magnetométricos e Gamaespectrométricos. SGM/MME/CPRM and SIC/SGM/FUNMINERAL/State of Goiás, Rio de Janeiro, Final Report, 22 vol.

Leroy J. 1978. The Margnac and Fanay Uranium Deposits of the La Crouzille District (Western Massif Central, France): Geologic and Fluid Inclusion Studies. *Econ. Geol*., **73**:1611-1634

McCoy, D., Newberry, R.J., Layer, P., DiMarchi, J.J., Bakke, A., Masterman, S., Minehane, D.L. 1997. Plutonic-related gold deposits of Interior Alaska. Economic Geology Monograph, 9, p. 191-241.

Newberry, R.J., McCoy, D.T., and Brew, D.A. 1995. Plutonic-hosted gold ores in Alaska: Igneous versus metamorphic origins. Resource Geology, Special Issue 18, p. 57-100.

Palomba M. 2001. Geological, mineralogical, geochemical features and genesis of the albitite deposits of Central Sardinia (Italy). *Rendiconti Seminario Facoltà Scienze Università Cagliari Supplemento,* **71**(2):35-57.

Petersson J. and Eliasson T. 1997. Mineral evolution and element mobility during episyenitization (dequartzification) and albitization in the postkinematic Bohus granite, southwest Sweden. *Lithos*, **42**:123-146

Poty B., Leroy J., Cathelineau M., Cuney M., Friedrich M., Lespinasse M., Turpin L. 1986. Uranium deposits spatially related to granites in the French part of the Hercynian orogen. *In*: H.D. Fuchs (Ed.), Vein Type Uranium Deposits. TECDOC-361, IAEA, Vienna, pp. 215-246.

Queiroz C.L., Jost H., Silva L.C., McNaughton N.J. 2008. U–Pb SHRIMP and Sm–Nd geochronology of granite–gneiss complexes and implications for the evolution of the Central Brazil Archean Terrain. Journal of South American Earth Sciences, 26:100–124.

Rossi M., Rolland Y., Vidal O., Cox S.F. 2005. Geochemical variations and element transfer during shear-zone development and related episyenites at middle crust depths: insights from the Mont Blanc granite (French — Italian Alps) *Geological Society, London, Special Publications, 245*:373-396.

Ruzicka V. 1993. Vein uranium deposits. *Ore Geol. Rev.,* **8**:247-276.

Stacey J.S. and Kramers J.D., 1975. Approximation of terrestrial lead isotope evolution by a two-stage model. Earth and Planetary Science Letters 26, 207–221.

Theodore T.G., Blair W.N., Nash J.T. 1987. *Geology and Gold mineralization of the Gold Basin-Lost Basin mining district, Mohave County, Arizona*. USGS Prof. Paper 1361, 134 pp.

Thompson J.F.H. and Newberry R.J. 2000. Gold deposits related to reduced granitic intrusions. *Soc. Econ. Geol. Reviews*, **13**:377-400.

Thompson J.F.H., Sillitoe R.H., Baker T., Lang J.R., Mortensen J.K. 1999. Intrusion-related gold deposits associated with tungsten-tin provinces: *Mineralium Deposita*, 34:323-334.

Thorette J., Jebrak M., Guha J. 1990. Gold in episyenite: an atypical gold mineralization in the Abitibi greenstone belt. *In*: F. Robert, P.A. Sheahan, S.B. Green (eds.) *Greenstone Gold and Crustal Evolution.* NUNA Conference Volume, Geological Association of Canada, *Proc. Workshop held at Val d'Or, Québec,* pg. 221

Williams, I.S., 1998. U–Th–Pb geochronology by ion microprobe. In: McKibben, M.A., Shanks III, W.C., Ridley, W.I. (Eds.), Applications of microanalytical techniques to understanding mineralizing processes: Reviews in Economic Geology, vol. 7, pp. 1–35.

Witt W.K. 1997. Some atypical styles of gold mineralization and alteration in the Yilgarn Craton Kalgoorlie. In: An International Conference on Crustal Evolution, Metallogeny and Exploration of the Yilgarn Craton - An Update, *Extended Abstracts, Record 1997141,* pp.151-152.

Yamaoka W.N. & Araújo E.M. 1988. Depósito de ouro Mina III, Crixás, Goiás. In: DNPM/CVRD, Brasília, DF: *Principais Depósitos Minerais do Brasil*, Vol. III, Capítulo XXXIV, pp. 491-498.

Youden, W.J., 1951. Statistical methods for chemists. National Bureau of Standards. Washington, D. C., John Wiley and Sons, Inc., New York, 126 pp.

ANEXOS

TABELAS COMPLETAS DE ANÁLISE QUÍMICA DE ROCHA TOTAL DO DEPÓSITO CAIAMAR

	Gabbro				Outer hydrothermal zone							
Sample	1	2	3	4	5	6	7	8	9	10	11	12
SiO_2	51.4	49.98	50.4	50.2	51.8	52.6	52.9	53.79	53.1	50.8	52.7	53.7
TiO_2	1.52	1.46	1.43	1.54	1.39	1.41	1.3	1.35	1.29	1.26	1.51	1.24
Al_2O_3	14.53	14.77	14.7	14.6	15.1	14.85	14.8	15.01	15.35	13.9	14.5	14.75
Fe_2O_3	14.3	15.4	16.2	16.7	15.15	14.5	13.65	14.4	13.4	13.25	13.35	13.27
MnO	0.23	0.22	0.22	0.2	0.19	0.24	0.2	0.59	0.25	0.27	0.25	0.18
MgO	6.56	5.73	5.33	5.52	4.66	5.01	4.65	4.23	5.55	5.2	5.2	5.1
CaO	6.97	9.19	7.7	6.52	6.84	6.36	7.29	5.51	4.9	7.92	6.6	6.15
Na_2O	2.11	2.41	2.56	2.69	3.64	3.98	4.04	4.25	3.96	3.33	3.31	3.69
K_2O	1.7	0.33	1.03	1.2	0.86	0.7	0.66	0.47	1.78	1.3	1.3	1.22
P_2O_5	0.22	0.21	0.16	0.2	0.27	0.23	0.2	0.2	0.22	0.23	0.24	0.22
LOI	0.46	0.3	0.27	0.66	0.1	0.13	0.31	0.2	0.2	2.54	1.04	0.48
TOTAL	100	100	100	100.03	100	100.01	100	100	100	100	100	100
Ba	940	473	444	386	246	223	348	178	893	571	571	526
Rb	56.4	32.5	32.2	34.3	21.2	20.6	21.4	14.8	65.8	44.9	46.3	40.4
Sr	231	281	194	408	297	307	332	294	298	353	427	444
Y	25.6	24.4	27.3	35.7	31.2	34.1	29.6	33.8	29.3	28.4	30.9	32
Zr	83	80	79	124	97	125	93	102	98	84	94	103
Nb	4.7	3.5	2.6	5.2	3.1	5.5	2.9	29.2	3.1	2.3	3.05	3.2
Ta	0.3	0.1	0.1	0.4	0.2	0.5	0.1	27.2	2.23	0.1	0.2	2.13
Th	2.33	1.22	1.44	2.75	1.83	2.25	1.93	11	6	1.82	1.9	5
Pb	32	30	10	11	6	7	9	22.3	23	7	8	21.6
Ga	18.8	20.6	21.8	23.2	22.4	22.5	22.1	127	126	19.9	22.5	122
Zn	214	154	163	148	116	134	111	5	12	104	152	5
Cu	5	7	52	5	16	5	5	6	6	8	5	11
Ni	48	46	18	21	10	11	7	6	6	5	11	11
V	264	578	550	542	482	468	408	19.6	2.3	364	390	2.5
Hf	3	2.1	1.9	2.1	2.1	4.4	2.2	2.07	11.05	2.1	2.3	6.28
Cs	3.56	2.54	2.5	3.16	3.01	2.58	2.97	4.2	0.2	7.54	7.21	0.2
Co	52	68	56	61	45	47	40	37.8	41.1	36	39	37.15
U	1.44	0.58	0.55	0.75	0.65	1.34	0.71	5.68	0.75	0.66	0.69	0.76
W	7	3	4	2	2	1	3	2	2	3	2	1
La	10.6	10.1	11.1	12.8	14.3	14.2	13.9	13.7	15.2	13.1	14.5	15.2
Ce	24.9	22.6	25.7	30.2	31.7	32.01	32.01	32.2	33.9	29.2	33.2	34.9
Pr	3.22	2.99	3.3	3.85	4.06	4.01	4.06	4.03	4.3	3.74	4.22	4.38
Nd	14.6	12.6	14.1	16.8	16.9	17.1	17.2	16.8	18.1	15.6	17.7	18.6
Sm	3.74	3.4	3.8	4.65	4.52	4.51	4.5	4.47	4.49	4.18	4.65	4.98
Eu	1.1	1.15	1.14	1.43	1.52	1.34	1.41	1.38	1.46	1.41	1.45	1.38
Gd	3.95	3.85	4.25	4.95	5.08	4.21	4.81	4.89	4.97	4.69	4.9	5.1
Tb	0.7	0.69	0.71	0.89	0.83	0.75	0.8	0.93	0.83	0.75	0.81	0.86
Dy	4.67	4.35	4.42	6.12	5.09	4.67	4.79	6.27	5.01	4.66	4.93	5.02
Ho	1.02	0.95	0.97	1.33	1.12	1.01	1.05	1.43	1.1	1.04	1.11	1.12
Er	2.98	2.78	2.85	3.95	3.32	3.02	3.05	4.74	3.07	3.02	3.16	3.28
Tm	0.47	0.41	0.44	0.61	0.52	0.48	0.47	0.88	0.46	0.48	0.5	0.5
Yb	2.99	2.75	2.88	3.95	3.51	3.01	3.14	6.32	2.84	3.12	3.17	3.31
Lu	0.45	0.39	0.42	0.61	0.53	0.49	0.48	0.97	0.47	0.48	0.48	0.5
Norm												
Q	16.10	10.26	13.21	13.66	11.18	10.09	9.67	12.12	12.49	10.83	13.90	13.43
C	0	0	0	0	0	0	0	0	0	0	0	0
Or	0	0	0	0	0	0	0	0	0	0	0	0
Ab	17.85	20.39	21.66	22.76	30.80	33.68	34.18	35.96	33.51	28.18	28.01	31.22
An	25.15	28.51	25.58	24.22	22.32	20.59	20.30	20.49	18.85	19.14	20.87	20.08
Ho	8.66	19.25	10.59	9.62	9.67	12.66	11.65	7.91	3.86	7.34	7.34	7.76
Wo	0.80	0.93	1.74	0.04	1.29	0.25	2.67	0	0.55	5.64	2.16	1.49
Bi	14.41	2.80	8.73	10.17	7.29	5.93	5.60	3.98	15.09	11.02	11.02	10.34
Ne	0	0	0	0	0	0	0	0	0	0	0	0
Hm	14.30	15.40	16.20	16.70	15.15	14.50	13.65	14.40	13.40	13.25	13.35	13.27
Il	0.49	0.47	0.47	0.43	0.41	0.51	0.43	1.26	0.54	0.58	0.54	0.39
Ap	0.52	0.50	0.38	0.47	0.64	0.55	0.47	0.47	0.52	0.55	0.57	0.52
Sum	98.29	98.5	98.56	98.07	98.74	98.75	98.63	96.60	98.80	96.52	97.74	98.49

	Outer hydrothermal zone									
Sample	13	14	15	16	17	29	32	33	34	37
SiO_2	53.4	53.9	54.5	50.1	50.95	53.09	52.5	53.2	52.1	53.5
TiO_2	1.31	1.29	1.22	1.47	1.21	1.01	0.96	1.04	1.02	1.28
Al_2O_3	15.5	14.9	14.84	15.5	14.10	15	14.65	15.5	14.9	14.6
Fe_2O_3	13.15	13.05	12.75	13.9	12.59	14.1	14.15	13.3	13.3	12.3
MnO	0.27	0.27	0.19	0.3	0.2	0.41	0.34	0.35	0.35	0.22
MgO	4.66	5.15	3.98	4.01	3.54	5.91	6.48	5.44	5.06	3.44
CaO	6.24	6.65	6.88	8.29	7.35	5.22	5.48	5.15	7.07	6.7
Na_2O	4.22	3.93	3.71	4.51	3.38	2.26	3.2	4.22	4.43	3.61
K_2O	0.89	0.51	0.82	0.61	2.31	2.32	1.5	1.42	0.91	1.72
P_2O_5	0.25	0.25	0.17	0.28	0.2	0.2	0.2	0.18	0.19	0.22
LOI	0.11	0.1	0.94	1.02	4.16	0.48	0.54	0.2	0.67	2.41
TOTAL	100	100	100	99.99	99.99	100.00	100.00	100.00	100.00	100.00
Ba	401	138	409	250	1075	709	660	741	495	787
Rb	25.6	11.9	28.7	39.8	66.4	67.6	54.1	44.8	21.9	49.1
Sr	305	237	393	394	306	132	200	286	272	267
Y	33.4	44.7	30.6	40	34.5	26.6	26.6	25.6	24.2	33.2
Zr	105	156	101	138	120	85	92	82	69	108
Nb	3.7	50.1	3.3	3.9	3.7	2.5	2.6	2.5	2.1	4.6
Ta	2.7	45.4	2.3	0.2	0.6	1.64	0.2	1.66	0.1	2.63
Th	5	14	10	3.24	2.05	39	1.98	12	1.37	21
Pb	22.6	22.2	21	15	12	19	21	20.3	22	19.9
Ga	118	86	112	25.4	21.3	280	21.2	116	20.1	153
Zn	6	6	5	151	127	5	158	15	118	9
Cu	5	5	5	5	20	30	5	26	38	5
Ni	5	5	5	5	5	30	33	26	26	5
V	2.6	34.4	2.4	369	278	2.1	266	2.05	319	3.1
Hf	3.54	1.58	3.41	3.5	2.7	4.79	2.3	4.9	1.6	7.04
Cs	0.2	7.1	0.2	3.14	6.26	0.1	4.53	0.1	2.52	0.2
Co	38.3	36.2	34.4	32	31	49.5	56	51.1	46	28.1
U	0.87	8.97	0.77	1.14	0.68	0.63	0.73	0.62	0.54	0.81
W	2	2	2	2	5	4	3	3	2	13
La	14.2	15.5	14.6	19.9	14.8	11.9	13.2	12.9	10.4	15.7
Ce	33.1	37.6	33.3	45.5	34.7	26.9	29.7	28.98	23.99	35.6
Pr	4.13	4.72	4.25	5.67	4.36	3.36	3.74	3.62	3.14	4.63
Nd	17.3	19.5	17.3	23.5	17.9	14.3	16.1	15.4	13.7	19.2
Sm	4.57	5.44	4.61	5.93	4.65	3.78	4.05	3.81	3.7	4.66
Eu	1.5	1.59	1.49	1.86	1.58	1.3	1.38	1.35	1.29	1.47
Gd	5.06	6.19	5.03	5.95	5.11	4.32	4.31	4.33	4.09	5.16
Tb	0.89	1.18	0.83	0.95	0.85	0.72	0.74	0.71	0.67	0.92
Dy	5.4	8.2	4.9	6.6	5.1	4.28	4.42	4.31	4	5.7
Ho	1.2	1.96	1.09	1.48	1.09	0.94	0.97	0.94	0.91	1.2
Er	3.57	6.89	3.17	4.12	3.19	2.74	2.87	2.71	2.62	3.57
Tm	0.57	1.35	0.49	0.64	0.49	0.42	0.43	0.42	0.42	0.51
Yb	3.62	9.82	3.11	4.23	3.15	2.78	2.83	2.77	2.59	3.17
Lu	0.56	1.44	0.49	0.64	0.45	0.43	0.44	0.42	0.38	0.5
Norm										
Q	10.39	10.88	14.67	4.30	11.30	20.58	13.55	10.61	6.76	15.04
C	0	0	0	0	0	0	0	0	0	0
Or	0	0	0	0	5.50	0.11	0	0	0	2.25
Ab	35.71	33.25	31.39	38.16	28.60	19.12	27.08	35.71	37.48	30.55
An	20.72	21.51	21.42	20.25	16.48	23.93	21.18	19.16	18.08	18.55
Ho	9.36	14.06	7.39	9.63	0	0	6.71	7.07	10.74	0
Wo	0.85	0	2.68	5.14	7.80	0.28	0	0.11	3.44	5.53
Bi	7.55	4.32	6.95	5.17	11.69	19.52	12.72	12.04	7.71	11.36
Ne	0	0	0	0	0	0	0	0	0	0
Hm	13.15	13.05	12.75	13.90	12.59	14.10	14.15	13.30	13.30	12.30
Il	0.58	0.58	0.41	0.64	0.43	0.88	0.73	0.75	0.75	0.47
Ap	0.59	0.59	0.40	0.66	0.47	0.47	0.47	0.43	0.45	0.52
Sum	98.90	98.25	98.06	97.85	94.86	98.98	96.59	99.17	98.72	96.57

	Intermediate hydrothermal zone											
Sample	18	19	20	21	22	23	24	25	26	27	28	30
SiO_2	53.55	56.32	55.30	55.29	55.79	59.25	62.77	61.06	61.37	60.23	61.80	62.8
TiO_2	1.11	1.07	1.05	1.07	1.26	0.85	0.80	0.87	0.86	0.86	0.88	0.7
Al_2O_3	14.12	15.17	14.87	15.34	15.06	14.76	15.01	14.89	15.49	16.84	15.25	15.16
Fe_2O_3	11.50	10.57	10.59	10.94	11.57	9.65	7.77	9.33	8.92	8.24	9.82	9.88
MnO	0.20	0.34	0.21	0.21	0.25	0.2	0.20	0.32	0.39	0.31	0.40	0.12
MgO	3.19	2.92	3.00	2.83	2.71	2.35	0.92	1.20	1.39	1.4	1.42	2.76
CaO	6.24	4.85	5.65	5.15	4.58	4.17	3.92	3.78	3.10	3.36	3.51	1.48
Na_2O	3.32	3.82	3.94	4.00	3.60	3.97	5.27	4.54	5.28	5.66	4.01	3.65
K_2O	2.79	2.45	2.18	2.45	2.82	2.64	1.49	1.99	1.81	1.71	1.98	2.62
P_2O_5	0.25	0.25	0.25	0.89	0.75	0.47	0.2	0.28	0.28	0.27	0.29	0.04
LOI	3.73	2.23	2.93	1.82	1.61	1.68	1.63	1.73	1.09	1.11	0.65	0.78
TOTAL	99.99	99.99	99.99	99.99	100.00	99.99	99.99	99.99	99.99	99.99	99.99	99.99
Ba	695	673	653	607	708	629	542	899	927	932	1305	1060
Rb	68	55	52	55	70	58	36	48	43	42	53	83
Sr	283	271	264	286	260	213	221	195	214	218	187	164
Y	44.7	35.8	35.5	39.4	45.3	40.2	54.6	44.1	46	45.1	43.8	48.3
Zr	154	131	117	127	156	140	188	160	164	172	161	161
Nb	71	4	5	6	21	5	54	6	6	6	6	8
Ta	74	3	2	3	22	3	53	4	4	4	4	9
Th	15	12	25	14	19	23	28	16	28	22	29	40
Pb	21	20	20	21	21	21	20	21	20	22	25	18
Ga	121	117	128	131	135	130	86	130	223	87	152	446
Zn	5	5	7	5	5	5	7	5	11	5	5	162
Cu	5	5	10	7	5	5	5	5	5	5	5	41
Ni	252	171	154	136	105	26	15	10	15	20	11	128
V	54	3	3	5	15	3	32	4	4	4	4	3
Hf	4.73	3.14	2.49	2.56	3.08	2.99	1.81	2.41	1.92	1.96	2.96	5.4
Cs	11.6	0.3	0.1	0.5	3.1	0.3	7.5	0.4	0.3	0.3	0.4	0.7
Co	29	21	21	20	21	13	8	10	10	8	10	11
U	14	1.0	0.9	0.9	4.6	1.2	10.6	1.2	1.3	1.4	1.3	6.7
W	6	4	4	4	5	3	10	4	13	36	9	2
La	15.4	17.6	17	19.2	20.4	21.7	26.8	21.2	24.3	26.1	23.2	22.3
Ce	37.3	39.8	37.7	47.5	48.3	50.1	60.6	47.7	55	58.8	53.3	50.15
Pr	4.64	5	4.8	6.1	6.26	6.35	7.5	5.97	6.95	7.25	6.71	6.3
Nd	19.1	20.3	19.9	27.4	27.1	26.2	30.6	24.7	28.7	29.6	27.3	27.5
Sm	5.34	5.14	4.76	6.79	7.04	6.57	7.64	6.23	7.07	7.34	6.68	6.4
Eu	1.51	1.62	1.56	1.98	2.15	1.61	2.2	1.95	2.1	2.15	1.98	1.62
Gd	5.76	5.82	5.5	7.26	7.82	7.01	8.22	6.99	7.76	7.77	7.58	6.49
Tb	1.05	0.97	1.01	1.18	1.32	1.1	1.57	1.16	1.25	1.25	1.2	1.07
Dy	5.95	5.98	6.13	7.55	8.19	6.44	10.55	7.1	7.55	7.44	7.29	7.1
Ho	1.29	1.33	1.31	1.51	1.89	1.43	2.57	1.59	1.67	1.63	1.64	1.48
Er	3.75	3.89	3.73	4.32	5.84	4.28	8.72	4.63	4.94	4.8	4.85	4.55
Tm	0.59	0.61	0.61	0.64	1.04	0.65	1.69	0.73	0.79	0.75	0.77	0.67
Yb	3.95	4.01	3.87	4.17	6.97	4.41	11.85	5	5.22	5.12	5.01	4.32
Lu	0.55	0.61	0.52	0.59	1.05	0.66	1.73	0.76	0.76	0.76	0.75	0.64
Norm												
Q	13.90	16.21	14.78	14.78	16.62	19.08	19.71	20.28	17.95	14.32	24.19	28.48
C	0	0	0	0	0	0	0	0	0	0.22	0.82	3.72
Or	9.14	7.76	5.98	7.96	10.43	10.19	6.69	9.00	7.50	6.88	8.43	9.13
Ab	28.09	32.32	33.34	33.85	30.46	33.59	44.59	38.41	44.68	47.89	33.93	30.88
An	15.38	17.01	16.45	16.67	16.60	14.66	12.90	14.37	13.22	14.91	15.52	7.08
Ho	0	0	0	0	0	0	0	0	0	0	0	0
Wo	5.82	2.26	4.15	1.28	0.51	1.24	2.19	1.07	0.14	0	0	0
Bi	10.53	9.64	9.91	9.35	8.95	7.76	3.04	3.96	4.59	4.62	4.69	9.11
Ne	0	0	0	0	0	0	0	0	0	0	0	0
Hm	11.50	10.57	10.59	10.94	11.57	9.65	7.77	9.33	8.92	8.24	9.82	9.88
Il	0.43	0.73	0.45	0.45	0.54	0.43	0.43	0.69	0.83	0.66	0.86	0.26
Ap	0.59	0.59	0.59	2.11	1.78	1.11	0.47	0.66	0.66	0.64	0.69	0.10
Sum	95.40	97.09	96.24	97.38	97.45	97.71	97.78	97.76	98.48	98.38	98.95	98.64

	Intermediate hydrothermal zone			Inner hydrothermal zone							
Sample	31	35	36	38	39	40	41	42	43	44	45
SiO_2	56.9	55.2	54.8	59.3	57.7	58.00	57.64	58.45	57.48	58.9	58.01
TiO_2	1.21	1.06	1.36	1.09	1.22	1.05	0.97	0.57	0.97	1.12	1.23
Al_2O_3	15.2	14.98	14.75	14.8	15.5	15.68	15.39	17.87	14.34	14.91	14.15
Fe_2O_3	13.65	13.99	13.25	10.45	10.85	9.46	9.81	6.00	10.61	11.35	12.1
MnO	0.27	0.49	0.21	0.21	0.19	0.19	0.19	0.08	0.19	0.2	0.21
MgO	3.88	5.13	3.98	2.42	2.44	1.74	1.98	0.57	2.70	2.84	3.06
CaO	2.59	4.02	6.26	5.43	5.23	4.81	4.67	2.28	4.98	5.63	5.8
Na_2O	2.77	2.54	3.7	4.24	4.78	5.06	5.32	9.25	4.38	4.2	4.13
K_2O	2.23	2.15	0.81	1.15	1.19	1.84	1.67	0.65	1.80	0.64	0.82
P_2O_5	0.22	0.21	0.26	0.69	0.77	0.42	0.34	0.26	0.23	0.2	0.25
LOI	1.08	0.22	0.62	0.22	0.13	1.74	2.00	4.02	2.31	0.01	0.25
TOTAL	100.00	99.99	100.00	100.00	100.00	99.99	99.99	100.00	100.00	100.00	100.01
Ba	919	290	283	560	502	748	647	211	698	319	315
Rb	74	25	27	29	29	45	41	15	48	18	23
Sr	117	71	21	277	292	233	262	204	286	386	233
Y	36.7	218	247	39	47	43	48	53	41	42	37
Zr	110	28	36	135	155	157	167	224	126	128	129
Nb	12	94	113	5	5	13	7	8	5	5	5
Ta	4	31	7	0	0.1	1.1	0.1	0.7	0.1	0.1	0.2
Th	43	4	5	3	3	4	3	5	3	3	3
Pb	22	20	20	21	20	22	22	20	21	19	18
Ga	723	3	3	21	20	22	22	13	20	21	19
Zn	173	37	13	119	133	142	117	93	123	113	111
Cu	31	24	6	5	5	7	5	5	5	6	6
Ni	332	292	357	95	96	53	49	184	197	258	195
V	4	4	3	4	4	5	5	4	4	4	4
Hf	4.99	19.7	20.1	4.05	3.6	5.1	4.8	6.4	3.5	3.6	3.7
Cs	1.1	237	131	5.54	5.09	2.54	3.03	0.89	4.28	2.84	3.59
Co	38	38	31	17	19	13	13	21	23	25	21
U	1.2	24	6	0.8	1.1	1.5	1.3	1.8	1.1	1.0	1.0
W	3	292	357	1	2	27	24	10	5	1	2
La	15.3	14	16.1	18.8	21.8	23.2	24.4	20.6	19.6	17	18.3
Ce	32.8	31.2	36.01	43.5	48.6	49.2	51.8	44.1	41.6	38.2	41.2
Pr	4.54	4.00	4.67	5.85	7.11	7.02	7.32	5.95	5.75	5.07	5.34
Nd	19.5	16.3	19.2	24.3	26.9	29.4	27.4	22.3	21.7	20.7	21.9
Sm	4.73	4.13	4.65	6.37	6.94	6.75	6.99	5.65	5.4	5.28	5.11
Eu	1.42	1.37	1.52	1.87	2.08	1.92	1.87	1.58	1.45	1.51	1.47
Gd	5.93	4.98	5.71	6.96	6.92	7.34	6.73	5.54	5.28	5.48	5.47
Tb	1	0.92	1.01	1.11	1.26	1.18	1.3	0.95	1	0.99	0.99
Dy	6.55	6.2	6.27	6.98	7.57	7.74	7.52	6.09	6.45	6.27	6.2
Ho	1.34	1.32	1.33	1.45	1.7	1.61	1.61	1.41	1.45	1.33	1.37
Er	3.9	3.95	3.86	4.22	4.54	5.07	4.71	3.97	4.08	3.86	4.12
Tm	0.59	0.6	0.56	0.65	0.75	0.73	0.72	0.65	0.62	0.56	0.59
Yb	3.52	3.92	3.55	4.33	4.6	4.92	4.77	4.27	4.32	3.57	3.58
Lu	0.50	0.65	0.59	0.62	0.71	0.67	0.75	0.64	0.65	0.56	0.59
Norm											
Q	27.32	24.17	15.85	21.51	17.08	13.80	12.93	0	17.05	19.82	19.47
C	4.05	1.67	0	0	0	0	0	0	0	0	0
Or	4.25	0.90	0	1.23	1.42	6.87	5.31	2.53	4.42	0	0
Ab	23.44	21.49	31.31	35.88	40.45	42.81	45.01	75.94	37.06	35.54	34.95
An	11.41	18.57	21.25	17.95	17.32	14.64	13.18	5.32	14.15	19.94	17.65
Ho	0	0	7.49	0	0	0	0	0	0	4.72	3.76
Wo	0	0	1.20	1.87	1.50	2.71	3.24	1.79	3.78	1.41	2.86
Bi	12.81	16.94	6.87	7.99	8.06	5.75	6.54	1.88	8.92	5.43	6.95
Ne	0	0	0	0	0	0	0	1.26	0	0	0
Hm	13.65	13.99	13.25	10.45	10.85	9.46	9.81	6.00	10.61	11.35	12.10
Il	0.58	1.05	0.45	0.45	0.41	0.41	0.41	0.17	0.41	0.43	0.45
Ap	0.52	0.50	0.62	1.63	1.82	1.00	0.81	0.62	0.55	0.47	0.59
Sum	98.03	99.28	98.27	98.96	98.90	97.43	97.24	95.51	96.93	99.10	98.78

	Quartz normative episyenite									
Sample	81B	81D	81G	81H	81CA	81CC	81CD	81CF	CAB	CAC
SiO_2	61.18	60.80	61.72	58.61	62.21	60.15	57.30	63.14	62.27	59.34
TiO_2	0.54	0.60	0.52	0.52	0.53	0.58	0.61	0.59	0.56	0.61
Al_2O_3	17.71	16.78	17.64	18.15	17.66	18.02	17.65	18.21	17.42	17.31
Fe_2O_3	5.79	8.67	6.76	7.29	6.15	6.22	8.72	4.71	5.80	7.67
MnO	0.06	0.06	0.12	0.13	0.10	0.06	0.23	0.10	0.06	0.08
MgO	0.72	0.50	0.61	1.32	0.48	0.99	0.90	0.61	0.61	0.55
CaO	1.65	1.51	1.29	1.91	1.62	1.40	2.08	2.59	1.67	1.85
Na_2O	8.98	8.91	8.31	8.08	7.84	9.20	8.29	6.81	8.43	9.29
K_2O	0.70	0.60	0.73	1.51	0.66	1.08	1.11	0.73	0.65	0.67
P_2O_5	0.06	0.03	0.07	0.23	0.13	0.21	0.26	0.11	0.13	0.02
LOI	2.61	2.50	2.21	2.25	2.59	2.08	2.86	2.40	2.39	2.60
TOTAL	100.00	100.96	99.99	100.00	99.99	100.00	100.00	100.00	100.00	100.00
Ba	259	193	225	537	280	360	393	268	238	211
Rb	14.6	11.4	12	32.6	13.6	23.3	22.2	15.7	14.2	12.7
Sr	139	134.5	152.5	263	180	138	210	150	131	140
Y	51.1	52.9	45.1	92.5	46.6	55.2	76.6	46.9	48.7	57
Zr	232	250	208	475	241	293	344	231	247	278
Nb	6.7	7.1	6.9	18.4	7.9	8.7	10.7	8.3	8.1	7.6
Ta	5.39	4.72	4.22	10.65	4.68	5.54	7.38	4.77	5.2	5.03
Th	10	10	8	14	10	8	14	9	8	10
Pb	13	11	13	17	15	14	16	15	13	12
Ga	86	57	63	161	60	105	95	70	68	61
Zn	5	5	45	5	24	5	5	27	11	5
Cu	10	5	5	6	5	5	5	5	5	5
Ni	10	104	22	47	49	56	109	13	50	19
V	6.7	7.1	5.8	12.9	6.5	8.2	9.6	6.4	7	7.8
Hf	0.84	0.64	0.76	2.13	0.82	1.43	1.2	1.05	0.94	0.74
Cs	0.7	0.6	0.4	1.4	0.5	0.6	0.7	0.5	0.5	0.6
Co	2.2	2.9	3.4	24.1	4.1	1.5	6.2	3.7	3.8	1.9
U	1.71	1.85	1.46	4.09	1.61	1.99	2.58	1.69	1.76	1.9
W	6	2	1	2	6	2	2	6	3	2
La	31.4	30	25.1	71.3	28.4	34.8	53.6	32.1	30.1	32.9
Ce	69.6	63.6	53.5	152.5	60.4	74.7	106	69.2	64.8	69.4
Pr	8.53	7.89	6.76	19.55	7.54	9.46	13.1	8.83	8.31	8.77
Nd	35.7	32.5	27.6	81.2	30.8	38.6	52.8	35.6	34.2	35.8
Sm	7.64	7.41	6.38	18.45	7	8.7	11.8	8.03	7.71	8.28
Eu	1.95	2.02	1.73	4.85	1.9	2.3	3.19	2.06	1.89	2.14
Gd	6.79	7.94	6.77	19.3	7.38	9.17	12.1	8.33	8.17	8.39
Tb	1.3	1.46	1.25	3.43	1.36	1.64	2.1	1.47	1.47	1.55
Dy	8.61	9.35	7.78	20.1	8.37	9.94	12.9	8.91	9.02	9.78
Ho	1.83	1.98	1.73	3.32	1.78	2.09	2.78	1.87	1.88	2.13
Er	5.78	5.71	5.06	9.45	5.09	5.97	7.51	5.13	5.25	6.13
Tm	0.87	0.92	0.79	1.38	0.83	0.99	1.21	0.83	0.83	0.99
Yb	5.6	6.02	5.33	8.85	5.58	6.65	8.2	5.66	5.51	6.73
Lu	0.88	0.93	0.75	1.32	0.88	1.01	1.21	0.87	0.84	1.03
Norm										
Q	3.30	4.23	8.02	2.39	10.98	0.29	1.31	15.49	7.54	0.02
C	0	0	1.00	0.30	1.41	0	0	1.77	0.12	0
Or	2.48	2.40	2.91	5.89	2.80	4.10	4.49	2.91	2.44	2.69
Ab	75.98	75.39	70.31	68.37	66.34	77.84	70.14	57.62	71.33	78.61
An	5.95	4.02	5.94	7.97	7.19	4.68	7.67	12.13	7.44	3.55
Ho	0	0	0	0	0	0	0	0	0	0
Wo	0.77	1.37	0	0	0	0.37	0.40	0	0	2.29
Bi	2.38	1.65	2.01	4.36	1.59	3.27	2.97	2.01	2.01	1.82
Ne	0	0	0	0	0	0	0	0	0	0
Hm	5.79	8.67	6.76	7.29	6.15	6.22	8.72	4.71	5.80	7.67
Il	0.13	0.13	0.26	0.28	0.21	0.13	0.49	0.21	0.13	0.17
Ap	0.14	0.07	0.17	0.55	0.31	0.50	0.62	0.26	0.31	0.05
Sum	96.92	97.93	97.39	97.39	96.97	97.40	96.81	97.13	97.11	96.86

	Nepheline normative episyenite									
Sample	81A	81C	81E	81F	81CB	81CE	81CG	81CH	CAX	81CI
SiO_2	59.93	59.89	59.54	61.20	62.37	60.13	60.55	60.98	57.95	61.33
TiO_2	0.57	0.59	0.61	0.59	0.52	0.58	0.52	0.60	0.59	0.50
Al_2O_3	18.02	18.62	18.19	18.17	18.69	18.21	18.06	18.08	17.70	18.26
Fe_2O_3	6.04	5.40	5.34	5.02	3.83	6.18	5.45	4.55	7.40	4.48
MnO	0.08	0.06	0.07	0.06	0.06	0.04	0.16	0.08	0.11	0.04
MgO	0.58	0.89	0.63	0.83	0.77	0.51	0.75	0.69	0.78	0.39
CaO	2.29	2.01	1.94	1.80	1.94	1.88	1.65	2.20	2.56	1.53
Na_2O	9.32	9.22	9.38	9.46	9.59	9.72	9.67	9.70	8.85	10.06
K_2O	0.66	0.92	0.87	0.93	0.92	0.65	0.91	0.77	0.81	0.45
P_2O_5	0.26	0.11	0.01	0.01	0.02	0.04	0.03	0.02	0.42	0.02
LOI	2.24	2.29	2.42	1.91	1.28	2.07	2.25	2.33	2.85	2.93
TOTAL	99.99	100.00	99.00	100.00	100.00	100.01	100.00	100.00	100.00	100.00
Ba	211	338	301	283	318	240	202	229	288	159
Rb	15.3	21	15.6	18.7	18.4	13.1	12.3	15.5	15.5	8.1
Sr	204	178	156.5	159	166	175	156	143	255	147
Y	52.5	52.7	63.3	58.1	45.2	65.7	56	55.4	51.5	56.3
Zr	224	252	309	321	228	358	292	253	228	259
Nb	7.6	8.2	9	9.2	6.7	9.9	6.8	8.6	7.7	6
Ta	5.23	5.19	6.04	6.62	4.78	7.4	5.56	5.68	4.46	5.3
Th	11	11	11	10	10	10	11	9	15	9
Pb	13	15	14	14	15	15	14	14	16	14
Ga	93	104	70	83	83	69	57	74	86	50
Zn	19	5	5	5	5	5	5	5	5	5
Cu	8	8	5	5	5	5	8	5	5	5
Ni	42	5	48	28	22	55	48	41	118	47
V	6.4	7.2	8.7	8.8	6.5	10.2	8.1	7.1	6.3	7.3
Hf	0.89	1.19	0.88	1.17	1.07	0.73	0.75	1	0.92	0.41
Cs	0.7	0.7	0.7	0.7	0.5	0.8	0.5	0.6	0.5	0.5
Co	2.2	2.4	2	1.7	1.8	3.9	2.8	1.3	3.3	1.8
U	1.81	1.72	2.15	2.3	1.54	2.55	1.93	1.96	1.8	1.88
W	10	5	3	1	2	2	1	2	10	1
La	33.5	33.1	36.1	37.1	29.2	40.3	36.2	38.6	28.5	31.9
Ce	70.9	71.4	76	79.6	60.8	85.8	76.1	81.7	61	67.8
Pr	9.09	8.92	9.55	10.15	7.78	10.7	9.63	10.35	7.9	8.54
Nd	38	37.2	39.1	41.2	31.8	43.1	39.2	41.8	33.6	34.9
Sm	8.13	7.98	8.68	8.94	6.96	9.34	8.68	9.1	7.96	7.76
Eu	2.11	2.11	2.34	2.41	1.96	2.76	2.26	2.23	2.42	2.01
Gd	7.93	7.79	9.14	9.61	7.63	11.5	9.17	9.35	8.66	8.09
Tb	1.4	1.39	1.66	1.75	1.39	2.04	1.69	1.67	1.59	1.52
Dy	9.13	9.63	10.65	10.75	8.48	12.6	10	10.2	9.57	9.79
Ho	1.93	1.93	2.4	2.27	1.73	2.72	2.15	2.16	2.04	2.14
Er	6.02	5.75	6.89	6.36	4.81	7.8	5.97	5.99	5.75	5.92
Tm	0.87	0.88	1.13	1.01	0.71	1.21	0.97	0.96	0.93	0.91
Yb	5.78	5.33	7.42	6.44	4.48	8.25	6.22	6.45	6.08	6.06
Lu	0.87	0.82	1.16	0.95	0.65	1.3	0.95	0.98	0.97	0.87
Norm	81A	81C	81E	81F	81CB	81CE	81CG	81CH	CAX	81CI
Q	0	0	0	0	0	0	0	0	0	0
C	0	0	0	0	0	0	0	0	0	0
Or	2.57	3.39	3.69	3.59	3.66	2.67	3.65	2.96	2.99	1.76
Ab	78.74	76.47	76.13	79.51	80.90	78.43	78.35	78.85	74.64	82.42
An	5.38	6.70	4.96	4.37	5.23	4.14	3.18	3.52	6.18	3.34
Ho	0	0	0	0	0	0	0	0	0	0
Wo	1.79	1.07	1.92	1.88	1.78	2.06	2.01	3.03	1.58	1.72
Bi	1.92	2.94	2.08	2.74	2.54	1.68	2.48	2.28	2.58	1.29
Ne	0.07	0.84	1.76	0.29	0.13	2.07	1.88	1.75	0.13	1.47
Hm	6.04	5.40	5.34	5.02	3.83	6.18	5.45	4.55	7.40	4.48
Il	0.17	0.13	0.15	0.13	0.13	0.09	0.34	0.17	0.24	0.09
Ap	0.62	0.26	0.02	0.02	0.05	0.10	0.07	0.05	1.00	0.05
Sum	97.28	97.19	96.05	97.54	98.26	97.40	97.41	97.16	96.72	96.60